

*Robert Myklebust*

Electron Probe Analysis

Society of America

PROCEEDINGS

FIFTH NATIONAL CONFERENCE

ON

ELECTRON PROBE ANALYSIS

New York City, New York

July 22-24, 1970

1971 July 28, 29, 30  
Pittsburgh Hilton

1972 July 19, 20, 21  
San Francisco Hilton

Additional copies of these Proceedings  
may be obtained for \$5.00 per copy, prepaid,  
from:

D. R. Beaman  
Dow Chemical Co.  
241 Building  
Midland, Michigan, 48640

Make checks payable to EPASA. Payment  
must accompany order, we will not invoice.

FIFTH NATIONAL CONFERENCE ON ELECTRON PROBE ANALYSIS

PRESENTED BY

THE ELECTRON PROBE ANALYSIS SOCIETY OF AMERICA

JULY 22-24, 1970

WALDORF ASTORIA HOTEL  
NEW YORK, NEW YORK

THE ELECTRON PROBE ANALYSIS SOCIETY OF AMERICA

- NATIONAL OFFICERS-1970 -

PRESIDENT

R. E. Ogilvie  
Massachusetts Institute of Technology

PRESIDENT-ELECT

T. O. Ziebold  
Massachusetts Institute of Technology

SECRETARY

L. F. Vassamillet  
Carnegie Mellon Institute

TREASURER

D. R. Beaman  
Dow Chemical Co.

MEMBERS AT LARGE

H. Yakowitz  
National Bureau of Standards

J. W. Colby  
Bell Telephone Laboratories

D. Wittry  
University of Southern California



# THE ELECTRON PROBE ANALYSIS SOCIETY OF AMERICA

## SUSTAINING MEMBERS

Applied Research Laboratories  
Glendale, California

Canberra Industries  
Middletown, Connecticut

Bell and Howell  
Pasadena, California

Corning Glass Works  
Corning, New York

General Telephone & Electronics Laboratories  
Bayside, New York

JEOLCO (U.S.A.), Inc.  
Medford, Massachusetts

Kent Cambridge Scientific Inc.  
Morton Grove, Illinois

Materials Analysis Company  
Palo Alto, California

Ortec, Inc.  
Oak Ridge, Tennessee

Perkin-Elmer Corporation  
Norwalk, Connecticut

Philips Electronic Instruments  
Mount Vernon, New York

Siemens America, Inc.  
New York, New York

## PREFACE

As has been stated at previous conferences, the success of any meeting depends upon the collective efforts of many people. In the New York area we are fortunate in having an active and interested group called the "Metropolitan Section of the Electron Probe Analysis Society of America". In addition to those committee members listed on the opposite page, many members of this group contributed suggestions and participated in other ways.

I wish at this time to thank the many industrial firms listed on the opposite page, who not only paid the way of some of their people to attend committee meetings, but also allowed them to spend many working hours on the organization of this meeting. Some even supplied secretarial help and postage.

Thanks are also due to our sustaining members, our exhibitors for their financial support, and the invited speakers. Finally, we must acknowledge the help given us by the past organizers of previous conferences and in particular, Arthur Chodos.

We have endeavored to present an interesting and varied program with adequate time for discussion and informal meetings. The conviviality of electron probe scientists is legendary and will be in evidence at the social hour. We hope all attendees will find this meeting memorable.

Paul Lublin  
General Chairman

# FIFTH NATIONAL CONFERENCE ON ELECTRON PROBE ANALYSIS

## - CONFERENCE ORGANIZERS -

GENERAL CHAIRMAN	P. Lublin, General Telephone & Electronics Laboratories Incorporated
SECRETARY	M. A. Giles, Bell Telephone Laboratories
TREASURER	W. T. Kane, Corning Glass Works W. Singer, Bell & Howell
PROGRAM	J. Colby, Chairman, Bell Telephone Laboratories J. Goldstein, Lehigh University N. Koopman, International Business Machines J. Shappirio, U.S. Electronics Command Laboratories
ARRANGEMENTS	H. Schreiber, Chairman, Bell Telephone Laboratories R. Ingersoll, Anaconda American Brass Company M. J. Kornblau, General Telephone & Electronics Laboratories Incorporated
PHOTOGRAPHIC EXHIBIT	J. Solomon, International Business Machines M. A. Giles, Bell Telephone Laboratories
EXHIBIT	G. Fisher, Chairman, International Nickel Co., Inc. P. Walitsky, Westinghouse N. Anderson, Pratt & Whitney Aircraft
PUBLICITY & PRINTING	R. MacQueen, Chairman, International Business Machines T. Huebner, International Business Machines H. DeBen, Western Electric Company
REGISTRATION	J. Blaise, Chairman, Chromalloy American Corp. G. Busch, Grumman Aircraft Engineering Corp. C. Schwartz, Air Reduction Central Research R. Henry, Bethlehem Steel Corporation K. Gumz, Pratt & Whitney Aircraft
LADIES PROGRAM	I. D. Payne, Chairman, Bell Telephone Laboratories M. A. Giles, Bell Telephone Laboratories Mrs. J. Colby Mrs. H. Schreiber Mrs. W. Kane Mrs. J. Solomon Mrs. P. Lublin

FIFTH NATIONAL CONFERENCE ON ELECTRON PROBE ANALYSIS

- INVITED SPEAKERS -

P. Duncumb  
Tube Investments Research Laboratories  
Essex, England

K. F. J. Heinrich  
National Bureau of Standards  
Gaithersburg, Maryland

R. Shimizu  
Osaka University  
Japan

D. B. Brown  
Naval Research Laboratories  
Washington, D.C.

D. B. Wittry  
University of Southern California  
Los Angeles, California

R. E. Ogilvie  
Massachusetts Institute of Technology  
Cambridge, Massachusetts

A. M. Langer  
Mt. Sinai Hospital  
New York, New York

T. C. Loomis  
Bell Telephone Laboratories  
Murray Hill, New Jersey

# FIFTH NATIONAL CONFERENCE ON ELECTRON MICROPROBE ANALYSIS

## PROGRAM

### TUESDAY, JULY 21, 1970

- 1:30 PM Executive Council of the Electron Probe Analysis Society of America meets in the Pillement Suite
- 7:00 PM Registration begins in the Silver Gallery
- 7:00 PM Exhibits will open in the Basildon Room, and the Jade Room

### WEDNESDAY, JULY 22, 1970

- 8:00 AM Registration in the Silver Gallery
- All Technical Sessions Will Be Held In The Astor Gallery
- 8:45 AM Welcome by P. Lublin, Conference Chairman
- 8:50 AM Opening address by R. E. Ogilvie, President of the Electron Probe Analysis Society Of America.

### TECHNICAL SESSION

Seminar On Quantitative Electron Probe Analysis  
R. E. Ogilvie, Chairman

- 1 9:00 AM INVITED PAPER. Quantitative Microprobe Analysis;  
P. Duncumb
- 2 9:40 AM INVITED PAPER. Uncertainties in Quantitative Electron  
Probe Microanalysis; K. F. J. Heinrich
- 10:10 AM Coffee Break
- 3 10:30 AM INVITED PAPER. Monte Carlo Technique As Applied To Micro-  
probe Analysis; R. Shimizu and K. Murata
- 4 11:00 AM INVITED PAPER. Microprobe Analysis - Use of Electron  
Transport Theory - A Review; D. B. Brown
- 11:30 AM Discussion on Quantitative Microprobe Analysis.
- 12:30 PM Lunch

## TECHNICAL SESSION

## Microprobe Automation and Data Acquisition

**J. W. Colby, Chairman**

- |    |         |  |
|----|---------|--|
| 5  | 1:45 PM | An Automated Electron Microprobe Analyzer; E. Eichen, F. Kunz, and H. G. Matthews  |
| 6  | 2:05 PM | A Computerized Electron Microprobe; R. Wolf and A. Saffir  |
| 7  | 2:25 PM | A Computer Assisted Microprobe Laboratory; W. F. Chambers  |
| 8  | 2:35 PM | Computer Processing of Solid State X-Ray Detector Data; E. Lifshin   |
| 9  | 2:50 PM | Rapid Quantitative Bulk Analysis of Brasses Using The Energy Dispersion X-Ray Analyzer; J. C. Russ                             |
| 10 | 3:00 PM | Computer Evaluation of Multiple X-Ray and Electron Images from the SEM; H. Gorz, E. W. White, R. E. McMillan, and J. Lebiedzki |
|    | 3:20 PM | Coffee Break   |
|    | 3:30 PM | Business Meeting   |
|    | 6:00 PM | Reception in the Hilton Room   |

THURSDAY, JULY 23, 1970

## TECHNICAL SESSION

## Physics And Mathematics Of Microprobe Analysis

P. Duncumb, Chairman

- |    |          |   |
|----|----------|---|
| 11 | 9:00 AM  | Comments on the Continuum Fluorescence Correction;<br>R. L. Myklebust, H. Yakowitz, and K. F. J. Heinrich                                 |
| 12 | 9:20 AM  | Indirect Determination of Mass Absorption Coefficients for<br>Soft X-Rays; D. F. Kyser  |
| 13 | 9:40 AM  | The X-Ray Continuum from Thick Targets; T. S. Rao-Sahib<br>and D. B. Wittry   |
| 14 | 10:00 AM | Time Sharing Computer Programs for Data Processing and<br>Corrections in Microprobe Analysis; F. Borile                                   |
|    | 10:10 AM | Coffee Break  |
| 15 | 10:40 AM | Electron Probe Analysis of Thin Films; W. Reuter  |
| 16 | 11:00 AM | Some Problems in the Determination of the Valence State of<br>Iron Using Fe L X-Ray Emission Spectra; D. G. W. Smith<br>and R. K. O'Nions |

- 17 11:20 AM The Simultaneous Determination of Calculated Concentrations in Quantitative Electron Microprobe Analysis; D. R. Beaman and R. Klimpel
- 18 11:40 AM An Investigation of Electron Probe Microanalysis Corrections in Ni-Co Binary Alloys; G. L. Fisher
- 19 12:00 N An Evaluation of the Philibert-Tixier Atomic Number Correction for Au-Cu Binary Alloys; P. J. Walitsky and J. W. Colby
- 12:15 PM Luncheon

#### TECHNICAL SESSIONS A & B

The First Invited Paper by D. B. Wittry will be in the Astor Gallery, as will Technical Session A. Technical Session B will be in the Louis XVI Suite.

- 20 1:30 PM INVITED PAPER. Applications of Scanning Electron Microprobes to Solid State Electronics. D. B. Wittry

#### TECHNICAL SESSION A

Metallurgical Applications  
L. S. Birks, Chairman

- 21 2:05 PM INVITED PAPER. Review of Metallurgical Applications of the Electron Microanalyzer; R. E. Ogilvie
- 22 2:35 PM Quantitative Measurement of Transferred Surface Material; J. Aronstein, G. Judd, and W. E. Campbell
- 23 2:50 PM An Investigation of the Solute Distribution in the Grain Boundary Region in an Al-Zn-Mg Alloy; C. R. Shastry and G. Judd
- 3:05 PM Coffee Break
- 24 3:30 PM Diffusion Enhancement Effects in Explosion Welded Metals; L. F. Trueb
- 25 3:45 PM Techniques for the Determination of Interaction Products of Plutonia-Urania Nuclear Fuel with Sodium; T. E. Lannin, H. S. Rosenbaum, and G. F. Melde
- 26 4:00 PM Local Compositions in Dendritic Structures; H. M. Pielet, A. J. Saffir, and J. F. Elliot
- 27 4:15 PM Electron Microprobe Study of the Role of Diffusion in the Adhesion of Copper to Nickel; G. H. Walker and B. W. Lewis
- 28 4:30 PM Concentration Profiles Across Brazed Hastelloy X Joints Using Electron Microprobe Analysis; W. B. Lisagor and H. L. Bloxom

## TECHNICAL SESSION B

### Non-Metallurgical Applications

A. J. Tousimis, Chairman

- 29    2:05 PM    INVITED PAPER. Electron Microprobe Analysis of Particles in Tissue; C. Berkley, A. M. Langer, and I. Rubin
- 30    2:35 PM    Rise and Decay Time and Polarized Cathodoluminescence Emission by Special Microprobe Techniques; R. J. R. S. B. Bhalla and E. W. White
- 31    2:50 PM    Electron Microprobe Analysis of Lunar Glasses and Pyroxenes from Apollo 11; J. C. Drake, C. Klein, Jr., and M. Campot
- 3:05 PM    Coffee Break
- 32    3:30 PM    The Use of the Electron Microprobe to Analyze Very Minute Amounts of Liquid Samples; C. Lechene
- 33    3:45 PM    Electron Probe Microanalysis of Electrolytes in Kidney Slices; A. P. Von Rosenstiel, H. J. Hohling, J. Schnermann, and W. Kriz
- 34    4:00 PM    Electron Microprobe Characterization of the Stoichiometry and Homogeneity of Mixed-Crystal Semiconductor Materials; J. P. Smith and H. Kraus
- 35    4:15 PM    Application of Complex Analysis of Variance to Electron Probe Analysis; A. J. Saffir and G. E. Schwartz
- 36    4:30 PM    Analysis of Rocks by Electron Probe; J. C. Rucklidge and E. L. Gasparrini
- 6:00 PM    Reception (a la carte) in the Empire Room
- 7:00 PM    Banquet in the Empire Room

---

FRIDAY, JULY 24, 1970

---

## TECHNICAL SESSION

### New Methods and Instrumentation I

H. Yakowitz, Chairman

- 37    9:00 AM    INVITED PAPER. Non-Dispersive X-Ray Analysis; T. C. Loomis
- 38    9:30 AM    An Analytic Method for the Ion Microprobe Mass Analyzer; C. A. Andersen
- 39    10:00 AM    An Automatic Color Recording Technique for Electron Probe X-Ray Images; T. Baum and R. Lewis



- 10:10 AM Coffee Break
- 40 10:40 AM Characterization of Homoepitaxial GaAs Using the Direct Imaging Mass Analyzer; R. Lewis, R. B. Marcus, and J. DiLorenzo
- 41 11:00 AM Ion Probe Mass Spectrometer: Concentrations and Diffusion Profiling; J. M. Hollerbach
- 42 11:20 AM Expanded Wavelength Coverage with Digitally Controlled X-Ray Spectrometers; E. Davidson, A. J. Hartwick, and J. M. Taylor
- 43 11:40 AM An Improved Target Current Amplifier for the Electron Microprobe and the Scanning Electron Microscope; K. F. J. Heinrich, C. E. Fiori, and L. A. Marzetta
- 44 12:00 N A Clean Vacuum Electron Beam Column for Cathodoluminescence Investigations; H. C. Marciniak and D. B. Wittry
- 12:20 PM Luncheon

#### TECHNICAL SESSION

##### New Techniques and Instrumentation II P. Lublin, Chairman

- 45 1:30 PM Changes in the Fine Features of X-Ray Emission Spectra from Al-Cu Alloys Using the Electron Microbeam Probe; J. S. Solomon and W. L. Baun
- 46 1:50 PM The Interaction of Self-Prolonging and Non Self-Prolonging Counting Components; D. R. Beaman, J. A. Isasi, and H. K. Birnbaum
- 47 2:10 PM Improved Low Carbon Analysis of Fe-Base Alloys; E. Eichen, K. R. Kinsman, and J. Tabock
- 48 2:20 PM High Resolution Scanning Electron Microscopy with an Electron Microprobe; C. H. Anderson, J. W. Leitner, and J. M. Taylor
- 49 2:40 PM A Universal Heating Stage Module for Use in Electron Microprobe Analyzers and Scanning Electron Microscopes; W. D. Donnelly
- 2:55 PM Coffee Break
- 50 3:15 PM Enzymatic Destruction of Bone; A. J. Saffir, S. Kreitzman, and M. Fritz
- 51 3:30 PM Dispersive X-Ray Spectrometer for Scanning Electron Microscope; S. Kimoto, H. Hashimoto, and S. Tagata

- 52 3:45 PM The Use of Backscattered Electrons in High Resolution Scanning Electron Microscopy; P. S. Ong
- 53 4:00 PM The New AMR/Phillips High Resolution Scanning Electron Microscope; S. Moll, M. Shippert, R. E. Ogilvie, J. T. Norton, and D. Koffman
- 54 4:15 PM A New Scanning Electron Microscope; J. Guernet, M. Tong, and C. Conty

## MEETING

### SIXTH NATIONAL CONFERENCE ON ELECTRON PROBE ANALYSIS

This meeting is to be held at the Pittsburgh Hilton Hotel, Pittsburgh, Pennsylvania (USA) July 28, 29, 30, 1971.

The sponsor of the meeting will be the Electron Probe Analysis Society of America.

Attendance at the meeting is estimated to be between 400 and 500.

For general information pertaining to this meeting, contact:

Dr. Lawrence F. Vassamillet  
Mellon Institute  
4400 Fifth Avenue  
Pittsburgh, Pennsylvania 15213

The topics of the technical sessions will include:

Electron Microprobe X-Ray Analysis, Techniques, Methodology, and Instrumentation. Principles of Electron Scattering and X-Ray Generating, Quantitative Correction Procedures, Soft X-Ray Emission and Micro-Analysis, Computer Applications to Microprobe Data, Kossel Techniques, Scanning Electron Microscopy, New Methods and Instrumentation in Micro-Analysis, and Applications.

The number of papers to be presented is estimated to be between 50 and 100. Contributed papers will be considered and a "call for papers" will be issued through direct mailing and meeting announcements six or eight months in advance of the meeting. The deadline for papers will be April 1, 1971. Everyone is invited to contribute papers. Abstracts must be submitted in English and sent to:

Dr. Eugene White  
1119 Houserville Road  
State College, Pennsylvania 16801

Exhibitors should contact:

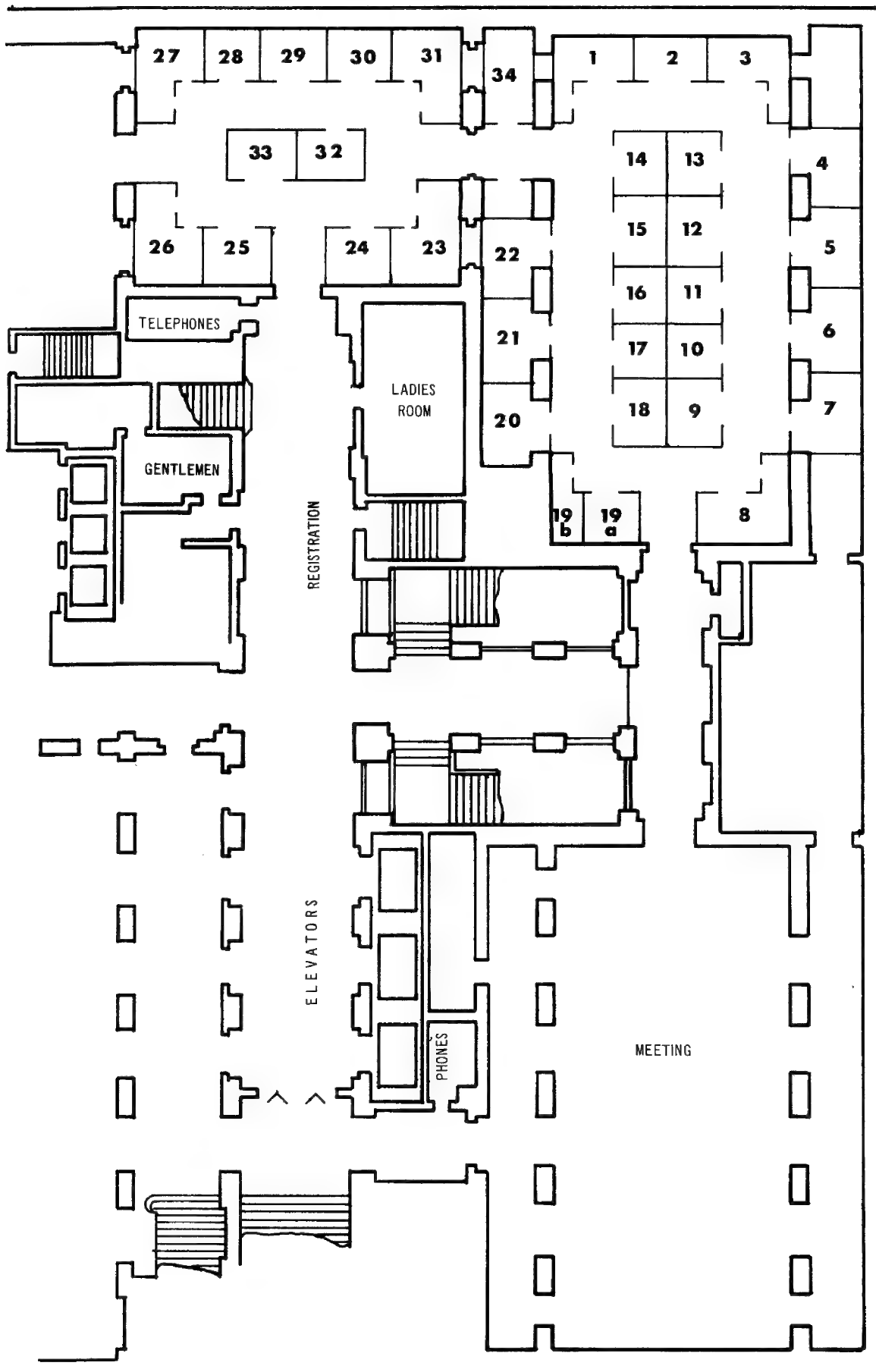
Mr. James Makosey  
Latrobe Steel Corporation  
2626 Ligonier Street  
Latrobe, Pennsylvania 15650

MANUFACTURERS EXHIBITING AT THE 5th NATIONAL  
CONFERENCE ON ELECTRON PROBE ANALYSIS

---

	<u>Booth Number</u>
Applied Research Laboratories	30, 31
Bell and Howell	25, 26
Buehler Ltd.	21
Canberra Industries	15, 16
Denton Vacuum, Inc.	17
Ernest F. Fullam, Inc.	4
Geoscience Instruments	8
Harshaw	32, 33
Isomet Corp.	14
Jeolco Inc.	12, 13
Kent Cambridge Scientific, Inc.	1
Kevex Corp.	20
Materials Analysis Co.	27, 28
McCrone Associates	11
Nuclear-Chicago Corp.	34
Nuclear Diodes, Inc.	9
Nuclear Equipment Corp.	18
On-Line Systems, Inc.	19B
Ortec	29
Perkin-Elmer Corp.	23, 24
Philips Electronic Instruments	5, 6, 7
Princeton Gamma-Tech, Inc.	22
Ultrascan Co. and Physical Electronics Industries, Inc.	2, 3
Veeco Instruments	10
Wang Laboratories	19A

JULY 20-24, 1970 THE WALDORF ASTORIA





SUMMARIES  
OF  
PAPERS

An Index of Authors and their affiliations follows these papers.





QUANTITATIVE MICROPROBE ANALYSIS

P. Duncumb  
 Tube Investments Research Laboratories,  
 Hinxton Hall, Cambridge, England.

The physical principles of quantitative microanalysis were set down in some detail by Castaing as long ago as 1951, and subsequent work (largely French) summarised by him in 1960. Since that time the rapid spread of commercial instruments has led to wide interest in quantitative work, and several excellent reviews have appeared on the subject, notably that of Philibert(1) in 1969.

Three stages can be recognised in linking the basic physics to the needs of the microprobe operator :-

- (i) The choice of a physical model to describe the complex process of electron scattering and hence of X-ray generation, absorption and fluorescence;
- (ii) rigorous testing of the model against experiment to establish its accuracy and range of application and
- (iii) preparation of a computer program for use by the average operator having no detailed knowledge of stages (i) and (ii). Several

approaches have evolved in this way and the 1% accuracy foreshadowed by Castaing can now often be realised in practice, at least for elements from sodium upwards. Below this range chemical valence effects introduce large uncertainties, and it seems unlikely that this accuracy will be achieved easily, except perhaps by direct comparison of the unknown with standards of similar composition and chemical bonding.

The most basic approach to quantitative theory is probably the Monte Carlo method (see 1) in which individual electron trajectories are simulated in the computer as a series of random scattering acts. This permits the calculation of basic data on electron back-scattering and X-ray distribution in the target, but does not easily lend itself to routine use because of the complexity of the calculation. Where this is possible, however, Pascal (2) has shown that it is capable of a high accuracy. The transport equation method, developed by Brown (3), falls into the same category, though in this approach the electron beam is treated as a flux undergoing progressive diffusion within the target. The Archard-Mulvey model (see 1) should also be classed here, though the simplifying assumption is made in this case that scattering occurs abruptly at a given depth. All three models permit the calculation of generation, absorption and fluorescence effects together, and enable more irregular geometries to be studied such as occur with the electron probe at an interface or inclined to the surface.

Probably the most widely used methods at present are those based on Philibert's (1) expression for the absorption correction. The atomic number and absorption effects are calculated separately and parameters in each have been optimised by comparison with experimental analyses of known specimens chosen to exhibit one or other effect strongly (4). Correction for fluorescence from characteristic radiation is also included, and that from the continuum may be added if the extra complication is thought worthwhile. A number of computer programs based on this theory have been prepared, and have been critically compared, together with others, by Beaman (5), both for accuracy and for convenience to the user. Present indications are that the better of these can be expected to reduce the error in uncorrected results by about one order of magnitude (4); at the same time the correction procedure can be conveniently carried out on a computer having a core store of only 8192 words (6). Sweatman and Long (7) have used such a program in the analysis of silicate minerals and have discussed the many factors influencing the final accuracy in some detail, from the choice of standards and experimental technique to the theory itself.

The increasing use of "desk-top" computers raises the question of whether an even more simplified procedure can be programmed to fit into a core store of 4096 words or less. This would have the advantage that a small computer dedicated to the on-line control of an instrument or to non-dispersive analysis could additionally be used for processing the final results. The method of "alpha coefficients" offers a way of doing this, by condensing the atomic number, absorption and fluorescence corrections for a given pair of elements into a single coefficient, as described by Ziebold and Ogilvie (see 1) some years ago. Now, however, the coefficients to enter into the program can be calculated by one of the more recently developed methods referred to above, and present indications are that a substantial saving in core storage is possible with little loss in accuracy. The method may also be used with advantage where corrections must be calculated by hand.

1. J. Philibert, 5th International Congress on X-ray Optics and Microanalysis, Tubingen 1968 (Springer: 1969), p.114
2. B. Pascal, Electricite de France, Report D120 MAT/C 011, 1969.
3. D. B. Brown, D. B. Wittry and D. F. Kyser, J.Appl.Phys, 40, 1627, (1969)
4. P. Duncumb, P. K. Shields-Mason and C. da Casa, Ref(1), p.146
5. D. R. Beaman and J. A. Isasi, Proc. 4th National Conference on Electron Microprobe Analysis, Pasadena 1969 (EPASA 1969)
6. P. Duncumb and E. M. Jones, Tube Investments Technical Report 260, 1969.
7. T. R. Sweatman and J. V. P. Long, J. Petrology, 10, 332, (1969)

## UNCERTAINTIES IN QUANTITATIVE ELECTRON PROBE MICROANALYSIS

Kurt F. J. Heinrich  
National Bureau of Standards  
Washington, D.C.

Quantitative electron probe microanalysis is a complicated process which is affected by many potential sources of error. Since these errors can originate in all steps of the analytical procedure, it is necessary to investigate each in order to attempt to minimize them. Some uncertainties which arise during the data reduction can not be eliminated, and the analyst must estimate their magnitude in order to properly assess the limits of accuracy of the analysis.

Errors in analysis can be random or systematic. Random errors, which set a limit to the precision of the measurement, should be estimated by repeating the experiment under identical procedures, and can be described by well-known statistical procedures. The laws of Poisson's statistics are frequently used to estimate random errors in photon counting. However, drift and noise also contribute to random error. Therefore, Poisson's statistics only set a lower theoretical limit to the precision which can be achieved. The estimates of precision obtained from Poisson's statistic—and the limits of detection calculated by means of this statistic—should not be considered as valid unless confirmed by experiment. This is particularly true when the operator has tried to minimize random errors by using long counting periods. The effects of drift in the beam current can be reduced, but not completely eliminated by the use of drift corrections. If monitoring of the beam current is used for these purposes, the limits of proportionality between beam current and monitor current must be experimentally established.

Systematic errors are more insidious, since they cannot be detected by repetition of the measurement. Sources of such errors can be found in the experimental measurement (dead-time effects, errors in the background correction, chemical shifts). These errors are not generally discussed in the treatment of the theory of quantitative analysis; yet they often limit the accuracy of the measurement to a significant degree. In particular, the measurement of small amounts of an element in a complex matrix (e.g. in minerals) is frequently limited by the accuracy of the estimation of the background level rather than by statistics. Yet, the technique of background measurement is rarely, if ever, discussed in detail.

Serious errors and uncertainties arise in the theoretical formulation of data reduction procedures. These errors arise from deficiencies in the theoretical foundations of the calculations, from errors and uncertainties in the numerical values of constants and parameters, and from approximations and simplifications in the

theoretical derivations of the procedure. Frequently, several important uncertainties combine in the procedure, and it is a very common mistake to only consider one source of error, neglecting other factors which may have contributed significantly. It is, for instance, quite common to attribute analytical errors to inaccuracies in the mass attenuation coefficients, ignoring the equally serious uncertainties in the distribution of depth of the x-ray generation. I suspect that in the same manner the effects of the fluorescence due to the continuum are frequently ignored, and the resulting errors are attributed to the generation calculation ("atomic number effect").

If the uncertainty in constants and parameters (mass attenuation coefficients, fluorescence yields, emergence angle of x-rays) can be estimated, the well-known techniques of error propagation can be applied to estimate their effects on the accuracy of the analytical result.<sup>1,2,3</sup> This procedure predicts the conditions under which serious uncertainties can be expected. In some cases the uncertainty can be reduced by a choice of operating conditions (proper choice of line, avoidance of high operating voltages and low x-ray emergence angles for soft radiation). In other instances (e.g. analysis with ultra-soft x-rays) the inherent and unavoidable limits of accuracy must be recognized. Such studies may also stimulate further research in the areas in which constants and parameters are insufficiently well known.

Models can be tested by analyzing known materials under conditions in which the effects of changes in the model become apparent. In such case, however, the success of the investigation depends on the quality of the analysis and the knowledge of the composition of the standards, it is more appropriate to painstakingly investigate a limited number of carefully prepared and characterized standards, than to derive conclusions from a large number of analyses performed under less controllable conditions, or using doubtful standards. Such an analytical mass effort would seem to confuse systematic errors with statistical errors.

Certain aspects of the theory must be tested in special experiments, such as the investigation of distribution in depth by means of variable emergence angle and tracers, the study of non-diffused couples and Derian's determination of backscatter losses. To these experiments we must also add investigations—such as the determination of fluorescence yields, and of the intensity of continuous radiation—which were not performed for the specific purpose of electron probe analysis. The results of these investigations are of crucial importance. Unfortunately, the investigations are frequently difficult to perform, and the results may be subject to large uncertainties. This is the case with Derian's results, and with the determination of mean excitation potentials, and, most notably, with the determinations of the absolute intensities of emission of characteristic and continuous radiation. It is quite sterile to refine the mathematical procedures without recognizing that some of the basic premises of our theoretical calculation stand on quite uncertain ground. This is not to say that the calculations should not be performed with the necessary rigor. In the past, when computational facilities were not as freely available as now, we have too frequently given in to the temptation to introduce simplifications in the calculation, without carefully considering the concomitant errors. At present, more rigorous procedures, such as the program COR

which is being developed at the National Bureau of Standards, can be employed. This will enable us to investigate which simplifications can be accepted without significant loss of accuracy.

The procedures using Monte-Carlo techniques and transport equations are promising avenues towards a check of the accuracy of more conventional procedures. It must be considered, however, that they do not eliminate the need for a better knowledge of the constants and parameters which are at present imperfectly known. I believe that all procedures of this nature used at present still require considerable empirical accommodations. Therefore, their usefulness is, in my opinion, limited at the present time by the uncertainties which also plague the more traditional procedures.

It has also been proposed to use empirical procedures, which in several cases have yielded very good results, and which eliminate the sources of error inherent in the theory. Their application is, however, limited by the quality of the standards that can be made available. While such procedures can be applied successfully in many areas such as in the analysis of silicate minerals<sup>4</sup>, I do not expect that the procedures will entirely replace the theoretical calculations.

Progress in quantitative analysis is thus dependent on an intelligent combination of theoretical knowledge and empirical procedures. While it does not seem probable that the techniques used at present will change radically in the near future, careful and patient work in the directions I have indicated above should enable us to close the gap which now exists between the precision of the measurement and the accuracy of the complete analytical procedure.

1. Yakowitz, H., and Heinrich, K. F. J., *Mikrochim. Acta* 1968, 182.
2. Heinrich, K. F. J., and Yakowitz, H., *Mikrochim. Acta* 1968, 905.
3. Heinrich, K. F. J., and Yakowitz, H., *Mikrochim. Acta* 1970, 123.
4. Bence, A. E., and Albee, A. L., *J. Geology* 76, 1968, 382.

## MONTE CARLO TECHNIQUE AS APPLIED TO MICRO PROBE ANALYSIS

by Ryuichi SHIMIZU and Kenji MURATA  
 Department of Applied Physics, Osaka University  
 Suita, Osaka, Japan

Monte Carlo technique applied to the microprobe analysis is usually based on the two theoretical precedures; the energy loss of electrons given as Bethe's formula,

$$-\frac{dE}{dx} = \frac{2\pi e^4 N Z}{E} \ln \left( \frac{2E}{J} \right) \quad (1)$$

and the angular distribution of the scattered electrons which was dervied for certain path of the scattering electron,  $x$ , by Lewis as following

$$f(\omega) = \frac{1}{4\pi} \sum_{\ell=0}^{\infty} (2\ell+1) P_{\ell}(\cos \omega) \exp - \int_0^x \kappa_{\ell} dx \quad (2)$$

and

$$\kappa_{\ell} = 2\pi N \int_0^{\pi} \sigma(\omega) [1 - P_{\ell}(\cos \omega)] \sin \omega d\omega, \quad (3)$$

where  $\sigma(\omega)$  is the single scattering cross section of the screened Rutherford type expression written by

$$\sigma(\omega) = \frac{Z^2 e^4}{p^2 v^2 (1 - \cos \omega + 2\beta)^2}. \quad (4)$$

In those formulae it is easily understood that the physical parameters, mean ionization potential  $J$  and screening parameter  $\beta$  play a very important role in the Monte Carlo procedure. How  $\beta$  influences on the angular distribution has already been studied<sup>(2)</sup> by the comparison of the angular distribution of the scattered electrons obtained by equation 2 with the experiments for thin film of copper and aluminum by Cosslett and Thomas<sup>(1)</sup>. However the study as for the mean ionization potential from the standpoint of the Monte Carlo technique has been left out and only used by introducing the conventional form given by

$$J = 11.5 Z. (eV) \quad (5)$$

whereas Duncumb and da Casa<sup>(3)</sup> pointed out from the quantitative study in electron microprobe analysis that it might be better to use another empirical formula for  $J$ . Hence it is necessary to see how the values of  $J$  given by different formulae result in the change in the net calculation for such as energy dissipation, electron back-scatter coefficient  $\eta$  and depth distribution of X-ray emission in the specimen.

The normalized energy dissipations for the electrons of 30 keV in copper were obtained by the Monte Carlo calculations by using the energy loss formulae with three different formulae of  $J$  and are plotted in figure 1 with those by Spencer<sup>(4)</sup> and Bishop<sup>(5)</sup> for incident beam energy of 25 keV. And similar results are also plotted

for aluminum in figure 2 by taking "normalized  $dE/dx$ " as ordinate in order to compare with the experiment by Hoff and Everhart<sup>(6)</sup>, with the empirical curve of Cosslett and Thomas<sup>(7)</sup> and with the Monte Carlo calculation of Bishop<sup>(8)</sup>.

The depth distributions of Al  $K\alpha$ -radiation in aluminum were plotted in figure 3 for the two different formulae of  $J$  and are compared with experimental result of Henoc<sup>(9)</sup> obtained by tracer method. The electron backscatter coefficients  $\eta$  for copper show remarkable changes for the different values of  $J$ , e. g. 0.339 for  $J=11.5Z$  and 0.374 for  $J=13.0Z$ , however those for aluminum give the same value, 0.175 within the accuracy of the calculation.

The other results from Monte Carlo procedure are the spatial distributions of the backscattered electrons on the specimen surface of copper, which are shown by histogram for angle of incidence  $\gamma = 90^\circ$  and  $45^\circ$  in figures 4 and 5 with the depth distributions of Cu  $K\alpha$  radiation for incident beam energy of 30 keV.

The more detailed investigations on the depth distribution of characteristic  $K\alpha$ -radiation and  $f(\chi)$ -curves in inclined target will be presented in comparison between the Monte Carlo calculation and the experimental results which were obtained by the rotating target method.

#### References

- (1) V. E. Cosslett and R. N. Thomas, Brit. J. Appl. Phys. 15, 235 (1964); 15, 1283 (1964).
- (2) G. Shinoda, K. Murata and R. Shimizu, "Quantitative Electron Probe Microanalysis" (ed. J. Heinrich ; N.B.S. Special Edition, 1968) p155.
- (3) P. Duncumb and da Casa, Conference on Electron Probe Microanalysis, Institute of Physics and Physical Society London (1967).
- (4) L. V. Spencer, Nat. Bur. Stand. Monograph, 1 (1959).
- (5) H. E. Bishop, Brit. J. Appl. Phys., 18, 153 (1967).
- (6) P. E. Hoff and T. E. Everhart, presented at 10th symposium on Electron, Ion and Laser Beam Technology may 21~23, (1969).
- (7) V. E. Cosslett and R. N. Thomas, Brit. J. Appl. Phys. 16, 779 (1965).
- (8) H. E. Bishop, Proc. Phys. Soc. 85, 885 (1965).
- (9) J. Henoc, J. Microscope 5, 122 (1966).

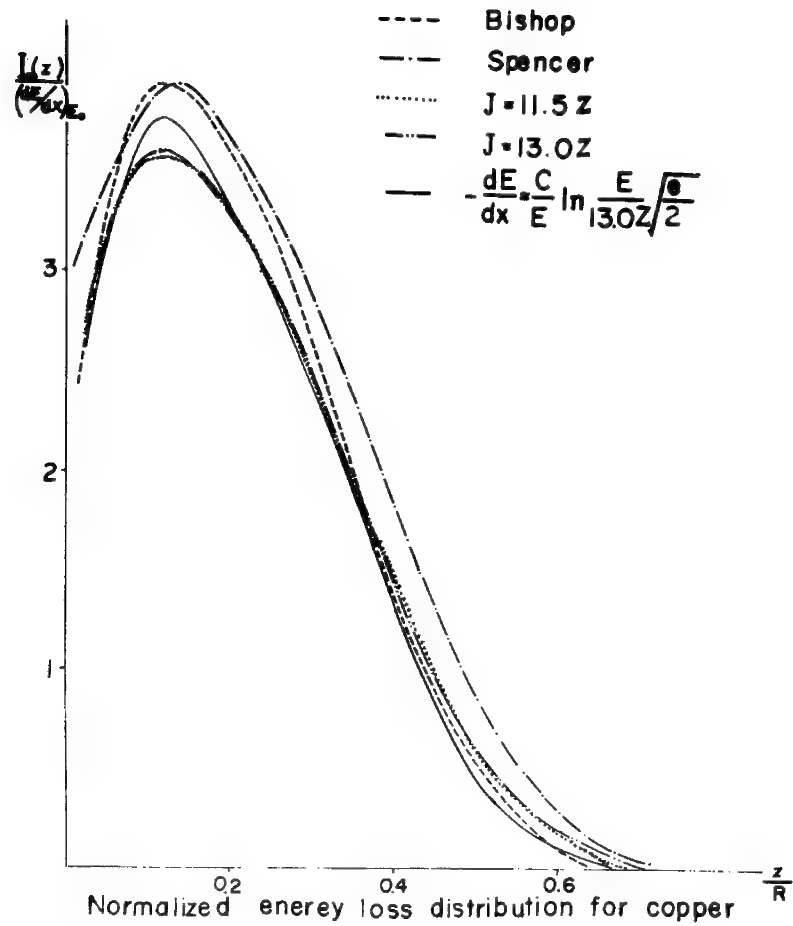


Fig. 1 Normalized energy loss distributions for copper: Curves represented by ·····, - · -, — are obtained by Monte Carlo calculation for three different expressions of Stopping power for an incident beam energy of 30 keV.  $I(z)dz$  is the energy dissipated between  $z$  and  $z+dz$ .



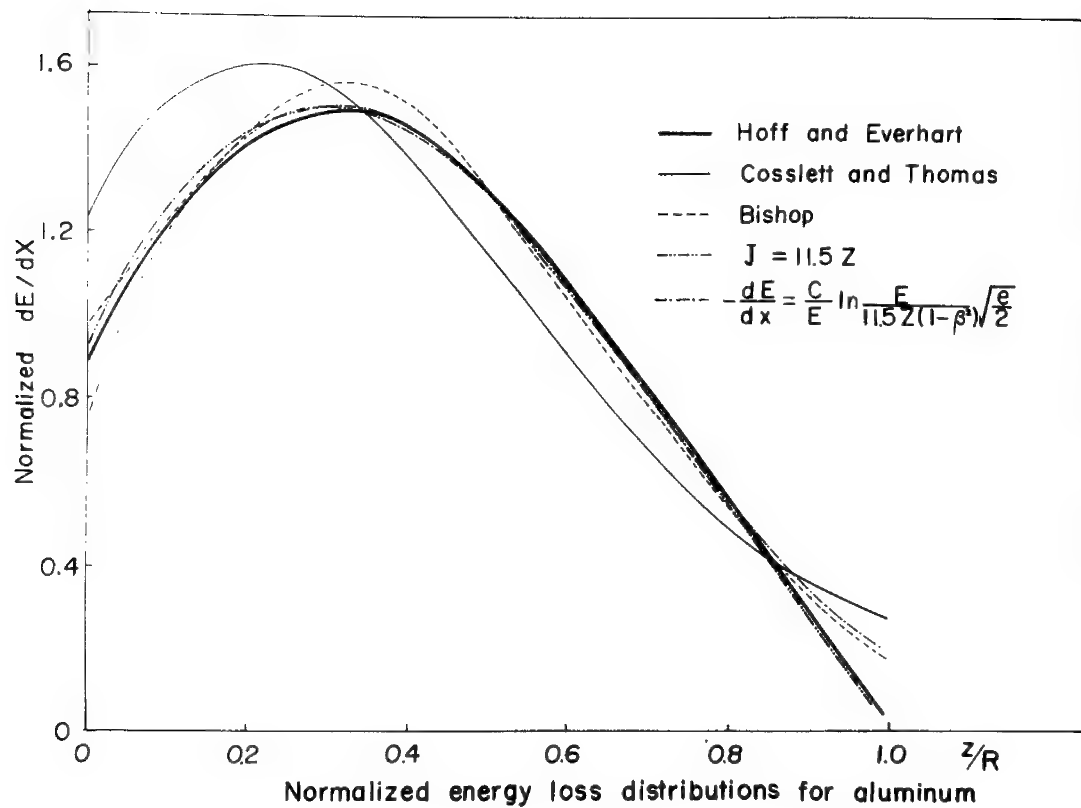


Fig. 2 Normalized energy loss distributions for aluminum plotted against  $Z/R$  obtained from Monte Carlo calculation for two expressions of stopping power — · —, — · — . The distributions according to Bishop; Cosslett and Thomas; Hoff and Everhart are also shown.

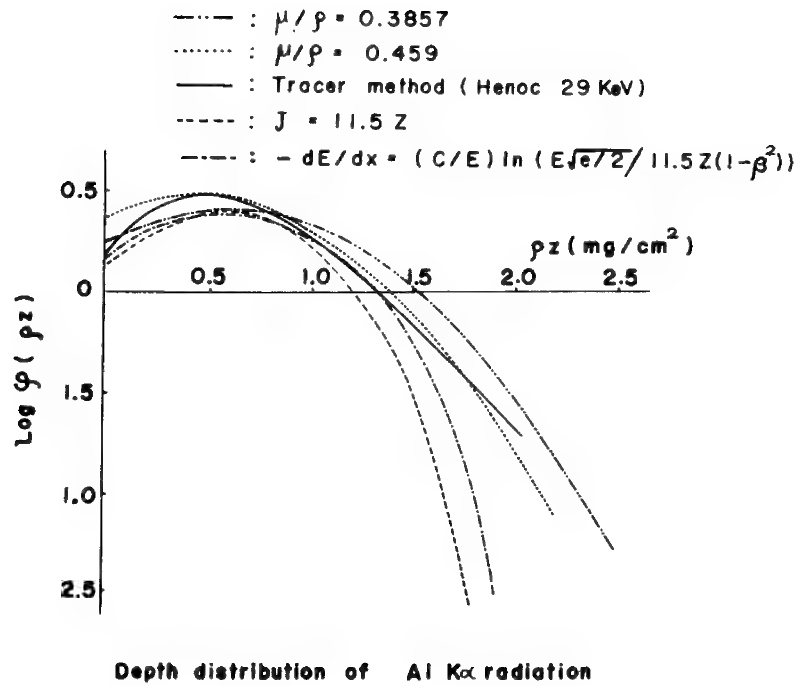


Fig. 3 Depth distribution of AlK $\alpha$ -radiation: The curves --- , ---- are present calculations by Monte Carlo method for different two expressions of stopping power at 29.3kV. The curves — ; ..... ; are obtained experimentally at 30 keV by the analysis of angular distribution for the value of absorption coefficient of aluminum for AlK $\alpha$ -radiation, 0.3857 and 0.459 cm<sup>2</sup>/mg respectively. ; obtained by Henoc from tracer method at 29kV.

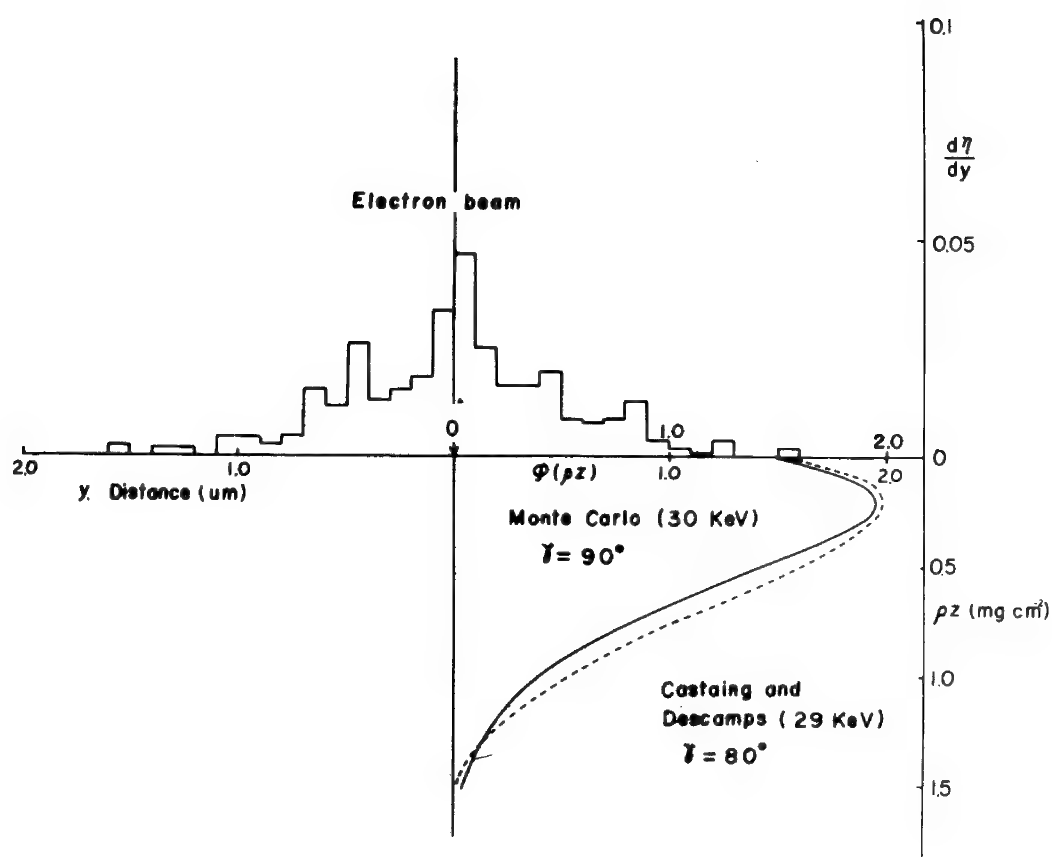


Fig. 4 The spacial distribution of the backscattered electrons on the specimen surface of copper and depth distribution of Cu  $K\alpha$ -radiation obtained from the Monte Carlo calculation for the incident beam energy of 30 keV at normal incidence,  $\gamma = 90^\circ$ .

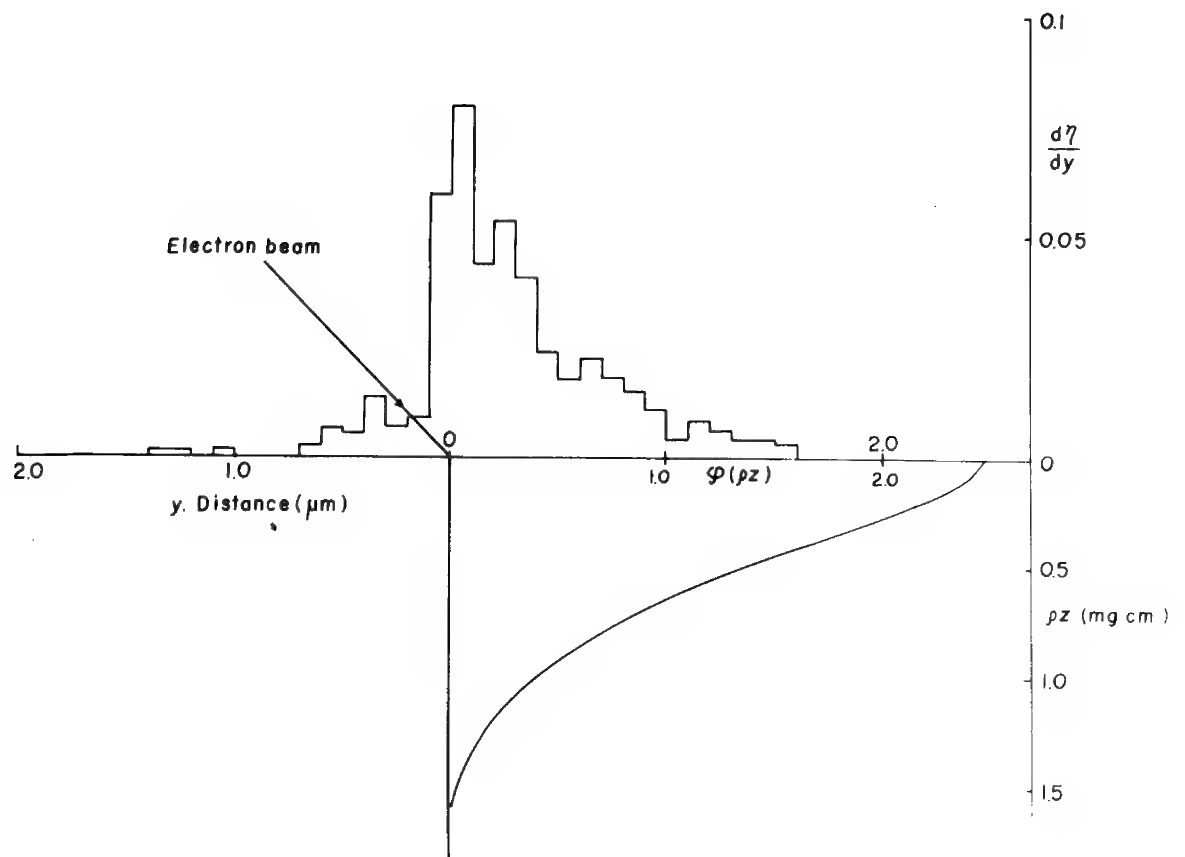


Fig. 5 The spatial distribution of the backscattered electrons on the specimen surface of copper and depth distribution of  $\text{CuK}\alpha$ -radiation obtained from Monte Carlo calculation for the incident beam energy of 30 keV at angle of incidence,  $\delta = 45^\circ$ .

# MICROPROBE ANALYSIS - USE OF ELECTRON TRANSPORT THEORY - A REVIEW

D. B. Brown  
U. S. Naval Research Laboratory  
Washington, D. C. 20390

## The TEP

The "correction" of microprobe intensity ratios developed historically in the form which is now sometimes called the ZAF technique (Z for atomic number, A for absorption, F for fluorescence) (1, 2). Two implicit assumptions underlie the ZAF technique:

- It is reasonable to split the problem into three independent parts.
- The three corrections can be most reasonably treated by using theoretical insight to extrapolate from a limited number of experimental determinations of the corrections.

The Transport Equation Program (3, 4) or TEP was also designed to do microprobe corrections. It is based on one premise:

- The best way to do microprobe correction is to begin with the distribution in depth of x-ray production.

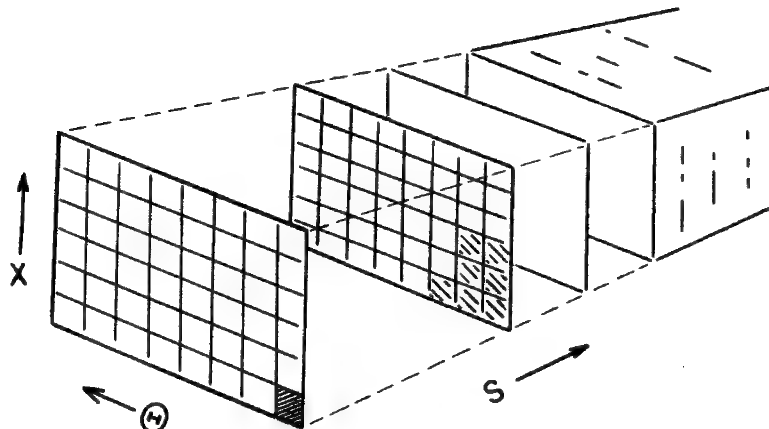
The distribution in depth of x-ray production has only been measured for a few cases. An attempt to calculate this distribution requires a fairly detailed knowledge of how the electrons travel in the specimen. This leads to the biggest difference between the TEP and the ZAF technique:

- In the TEP most of the work is devoted to the problem of electron transport.

## Numerical Solution

This problem is treated by solving a transport equation. In the TEP this equation is solved numerically. A convenient way of looking at this solution technique is given in Fig. 1.

Figure 1



Let us imagine the mathematics as represented by a series of maps. The first map represents the status of the electrons when the path length which they have traveled,  $s$ , is zero. The squares represent the number of electrons at various depths,  $x$ , and directions of travel,  $\theta$ . In the figure the square at  $x = 0$  and  $\theta = 0$  is darkened. This symbolizes the fact that  $s = 0$  the electrons are at the surface of the specimen and are traveling straight into the specimen. The second map represents the electrons after they have traveled a small distance in the specimen. The purpose of the transport equation is to supply the instructions on how to get the second map from the first. On the second map several squares are partially darkened indicating that the electrons now have a range of depths and directions. The computer continues stepping through these imaginary maps (that is, stepping along the electron path) until the electrons are calculated to have too little energy to be of interest.

### Input Parameters

A number of parameters are required as input to a TEP calculation. Three which appear to have important problems associated with them are

- the rate at which electrons lose energy
- the x-ray absorption coefficients
- the cross sections for ionization.

These parameters introduce important uncertainties into a TEP calculation. The same parameters are needed for a ZAF type calculation, and the uncertainties introduced into a ZAF calculation are of the same kind. These problems will be mentioned again in examples which follow.

### Relative Intensities from the Microprobe

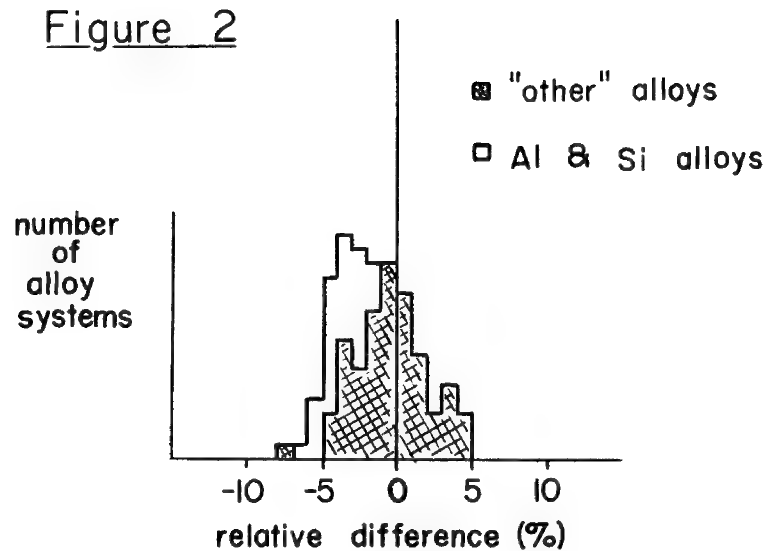
The TEP has been used to predict relative x-ray intensities as commonly measured in the microprobe. This study has served to emphasize two points:

- The well recognized difficulty of finding a substantial body of "good data" to test a procedure such as the TEP remains a serious problem.
- It is apparent that there is an important failure in our understanding of the process of electron energy loss.

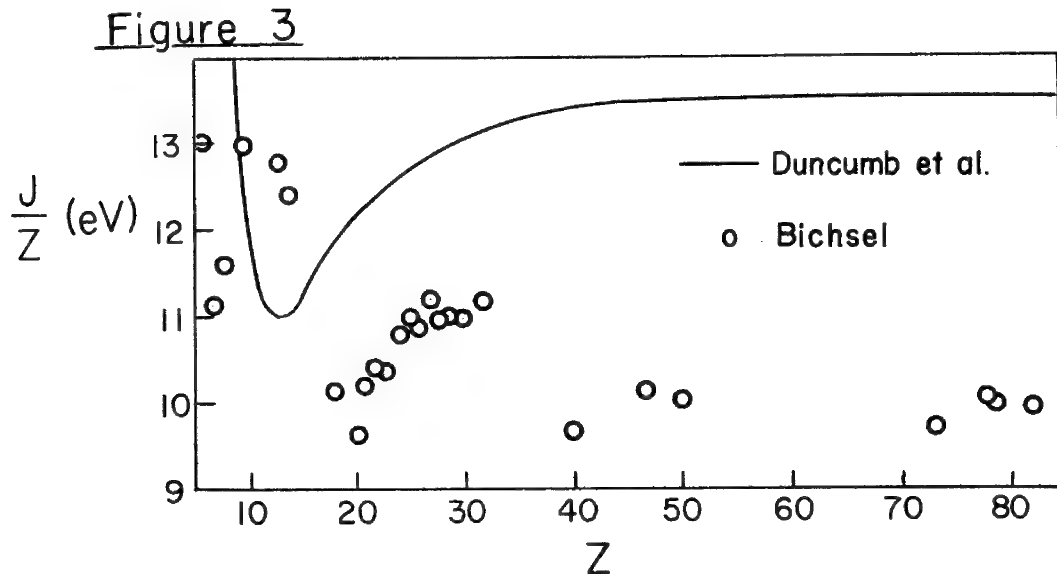
In order to minimize the first problem we have followed the lead of Heinrich (5). Beginning with the data collection of P. M. Thomas (6) of 150 sets of alloy data we have abstracted a smaller collection of 100 sets of data using the following suggestions of Heinrich.

- Data showing internal inconsistency was dropped.
- Cases where  $f(\chi)$  was less than 0.6 were dropped because uncertainties in our knowledge of  $\mu/\rho$  would invalidate the test.
- Cases for concentrations less than 5% were dropped.

The relative percent difference between the intensity ratio calculated using the TEP and that measured is shown for 100 alloys in Fig. 2. The results separate themselves clearly into two groups. First, a set of 30 alloys containing Al and Si with a heavier element which were analyzed by radiation from the heavier element. Secondly, all other alloys analyzed. The second group shows a scatter about the zero line which we attribute largely to "bad data" which we have not managed to weed out. The first group, on the other hand, shows a rather similar scatter, but centered on about -3.5%.



Recognition of this problem with Al and Si alloys is implicit in the important work of Duncumb and coworkers (7, 8). It is most likely that the source of difficulty lies in our understanding of the way that electrons lose energy to the target. Duncumb decided to make an empirical modification of the average ionization energy,  $J$ , which is used to calculate the rate of energy loss. Fig. 3 compares the Duncumb  $J$  with a recent data compilation of Bichsel (9). The absolute magnitude of  $J$  is not so important for our purposes; the thing to notice is the trends. Note in particular the way the Duncumb curve drops to a minimum in the neighborhood of Al. The empirical modification of  $J$  is unsatisfying in the sense that it does not represent the physical processes of energy loss in any way which I can understand. Unfortunately I cannot offer a more fundamentally correct solution at this time.



### Absolute Intensity from Tubes

A somewhat different problem to which we have applied the TEP is the prediction of the intensity of characteristic x-radiation emitted from an x-ray generator. The calculations were compared with a number of experimental values, in particular the recent measurement by Gilfrich of the output of OEG-50 x-ray tubes (10). We found that the principal uncertainty in the calculation was introduced by the uncertainty in the cross section for ionization. For K lines, quite good agreement was obtained using a cross section based on those calculated by Burhop multiplied by 1.2. For L lines the situation is less clear. The values calculated by Burhop appear to be low by a factor of about two as was first observed by Green (11). Recent calculations by Platzman and his collaborators (12, 13) are also in rough agreement with this factor of two. This problem of ionization cross sections will continue to receive our attention.

### Additional Applications of the TEP

Here are brief comments on two areas in which the TEP is beginning to be used.

1. The application of microprobe corrections to low atomic numbers ( $Z < 20$ ) has problems. Many workers in this atomic number region rely exclusively on empirical calibration methods such as the use of standards similar to the unknown. The TEP should be well adapted to contribute to the solution of this problem because of the way it is constructed in terms of fundamental physical processes such as electron scattering, electron energy loss, and inner shell ionization.
2. The TEP is straightforwardly applicable to the calculation of the production of continuum radiation. This work is under way.

- 
1. P. Duncumb and P. K. Shields, *Brit. J. Appl. Phys.* 14, 617 (1963).
  2. J. Philibert in Vth International Congress on X-Ray Optics and Microanalysis, G. Möllenstedt and K. H. Gaukler, Eds. (Springer-Verlag, New York, 1969), p. 114.
  3. D. B. Brown and R. E. Ogilvie, *J. Appl. Phys.* 37, 4429 (1966).
  4. D. B. Brown, D. B. Wittry and D. F. Kyser, *J. Appl. Phys.* 40, 1627 (1969).
  5. K. F. J. Heinrich in Advances in X-Ray Analysis, Vol. 11, J. B. Newkirk, G. R. Mallett and H. G. Pfeiffer, Eds. (Plenum Press, New York, 1968), p. 40.
  6. P. M. Thomas, AERE Rept. 4593 (1964), Atomic Energy Research Establishment, U. K. A. E. A., Harwell.
  7. P. Duncumb and S. J. B. Reed in Quantitative Electron Probe Microanalysis, K. F. J. Heinrich, Ed., NBS Special Pub. 298, 1968.
  8. P. Duncumb, P. K. Shields-Mason and C. da Casa in Vth International Congress on X-Ray Optics and Microanalysis, G. Möllenstedt and K. H. Gaukler, Eds. (Springer-Verlag, New York, 1969), p. 146.
  9. H. Bichsel, Rept. USC-136-150 (1969), Univ. Southern California, Los Angeles.
  10. D. B. Brown and J. V. Gilfrich, Fourth National Conference on Electron Microprobe Analysis, Pasadena, 1969.



11. M. Green and V. E. Cosslett, Brit. J. Appl. Phys. 1, 425 (1968).
12. J. Durup and R. L. Platzman, Discussions of the Faraday Society, No. 31, 156 (1961).
13. M. Inokuti and R. L. Platzman, private communication from R. L. P.

## AN AUTOMATED ELECTRON MICROPROBE ANALYZER

by

E. Eichen and F. Kunz  
Ford Motor Company, Dearborn, Michigan

G. Matthews  
Canberra Data Industries, Meriden, Connecticut

Within the modern analytical laboratory, automated instrumentation is becoming commonplace and the electron microprobe is no exception to this trend. Since initial interest to automate an electron microprobe was shown, it was evident that general principles and guidelines to accomplish this end were lacking. Immediately two questions arise: why is it necessary or desirable to automate, and specifically how is automation defined when applied to electron microprobe analysis? In this respect, justification and general principles are now being formulated. First, there is a fundamental dichotomy within microprobe analysis in that instrument manipulation is relatively straightforward, while obtaining meaningful and reliable results is very complex. Automation should then be directed toward these two extremes. Defining an automated electron microprobe is also not without difficulty since the degree of automation must be determined. In general, it cannot be simply stated that an automated microprobe consists of the microprobe itself, the interfacing hardware, a computer, and software. The overall manner in which all of these facets interact is important in defining the system; for example, (1) is the computer dedicated or non-dedicated to the microprobe and (2) which functions are achieved by a hardwire system and which are achieved by software.

Once a decision has been made on the type of system desired, electron microprobe automation should then be concerned with instrument monitoring and control, data accumulation, data reduction and reporting. Monitoring consists of watching such operating functions as vacuum, water pressure, temperature and indicating when these parameters are unsatisfactory for operation of the microprobe. The control function consists of moving, starting, stopping or presetting electrical or mechanical parameters such as spectrometers, scalars, high voltage, beam current, pulse height analyzer, baseline and window, linear amplifier gain, and detector voltage. Data accumulation consists of the transfer of data from the hardware into the computer with speed and accuracy. The data reduction phase consists of applying the necessary corrections for absorption, fluorescence and atomic number effects. Data reporting consists of producing a finished report, listing as a matter of record all parameters used during the analysis and the final results.

The practicality of designing a fully automated system is not clear at this time. If, in fact, all possible parameters could be controlled is not known. For this reason the initial attempt

---

1. Pederson, E., "A Modular Approach to Laboratory Instrument Automation, American Laboratory, Feb. 1970, p. 69.

producing an automated system is being restricted to the control of the spectrometers and sample stage and to the area of data accumulation, reduction and reporting.

Figure 1 is a block diagram of the present automated hardware, which centers around a 8,000 word dedicated computer. As depicted, the computer treats the electron microprobe interface similar to other devices such as the high speed reader/punch, teletype or DECtape units but with lower priority. The interface has at its disposal a series of hardwired "command" lines for TURN ON, FLAG, READ, SET and TURN OFF. Through the use of these commands appropriate operation codes and addresses may be transmitted from the computer to the addressed device. The operation codes include such functions as START, STOP, RESET, RESET/START, SET BCD, CLEAR, SET ASCII and HALT. It is obvious that through such commands full control of the scalars, timer and spectrometer axis positioners is available. As an example, the spectrometers may be controlled by presetting an individual spectrometer axis positioner with 1 of 8 different speeds, 1 of 2 directions (increment or absolute for either), the desired wavelength and the step size. All such operation codes and addresses are transmitted by machine language code to and from the computer and for that matter, all programming to date has been in machine language.

A tentative outline of the software necessary to produce the desired automation is shown in Figure 2. The complete system will be "supervised" by an executive program which operates on the interrupt mode. This means that the control parameters such as starting, stopping, reading and resetting the scalars will be invoked by a FOREGROUND program, while the corrections for absorption and other effects will be handled by a program which will run when the foreground program is not being used, i.e. a BACKGROUND program. As shown in Figure 2, the programs will be modular in that 8,000 words of core memory is available at any one time.

Application of the automated system to quantitative analysis is shown by a series of copper-zinc analysis which also brings to light the advantages and disadvantages of X-ray peak counting versus X-ray peak integration. With the automated system, peak integration is relatively simple since both the spectrometers and scalars can be given the same start command, i.e. the scalars can be started at the same time as the spectrometers. The integrated area of the peak can easily be controlled by presetting the starting and stopping point for each spectrometer.

# AUTOMATED ELECTRON MICROSCOPE

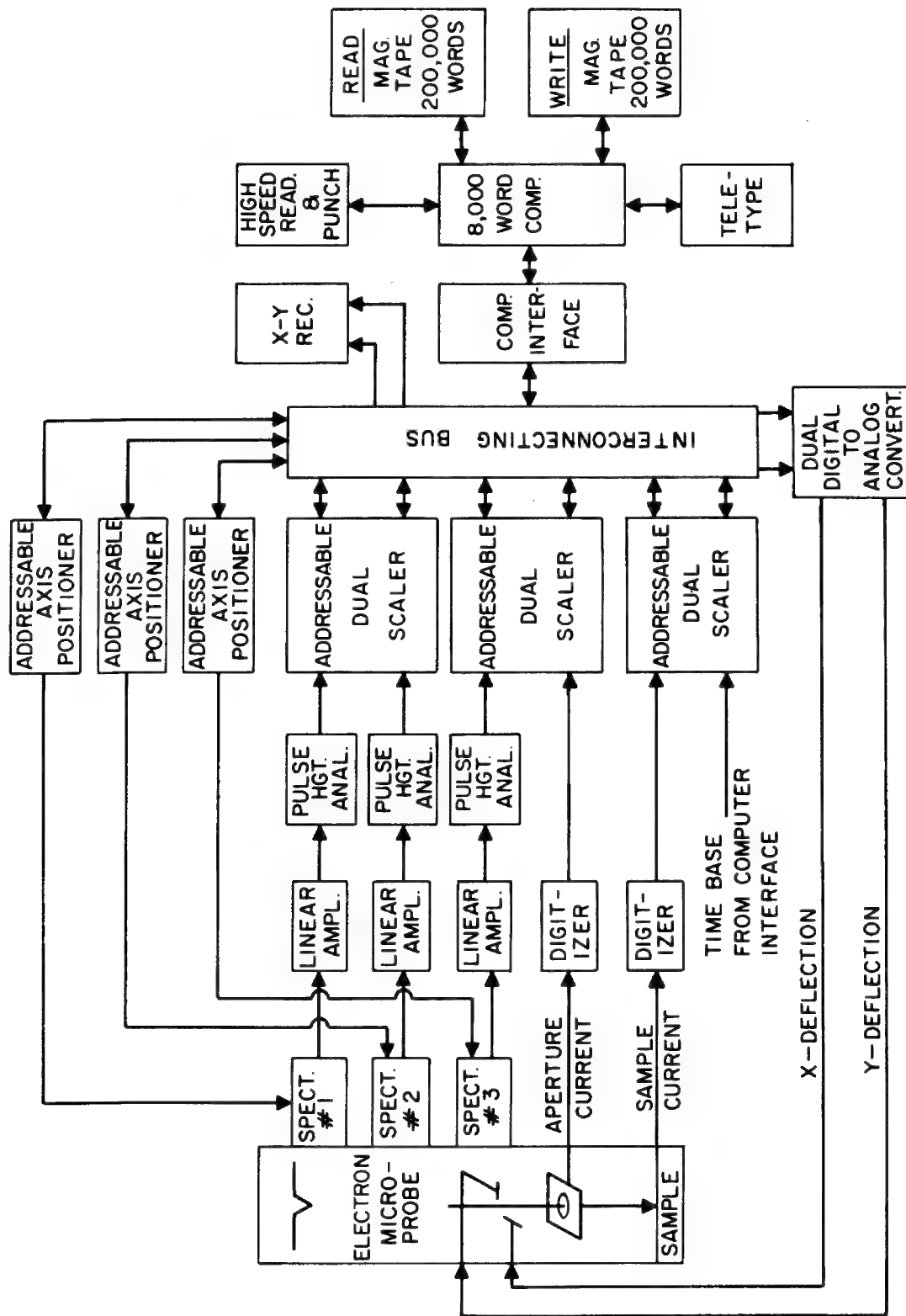
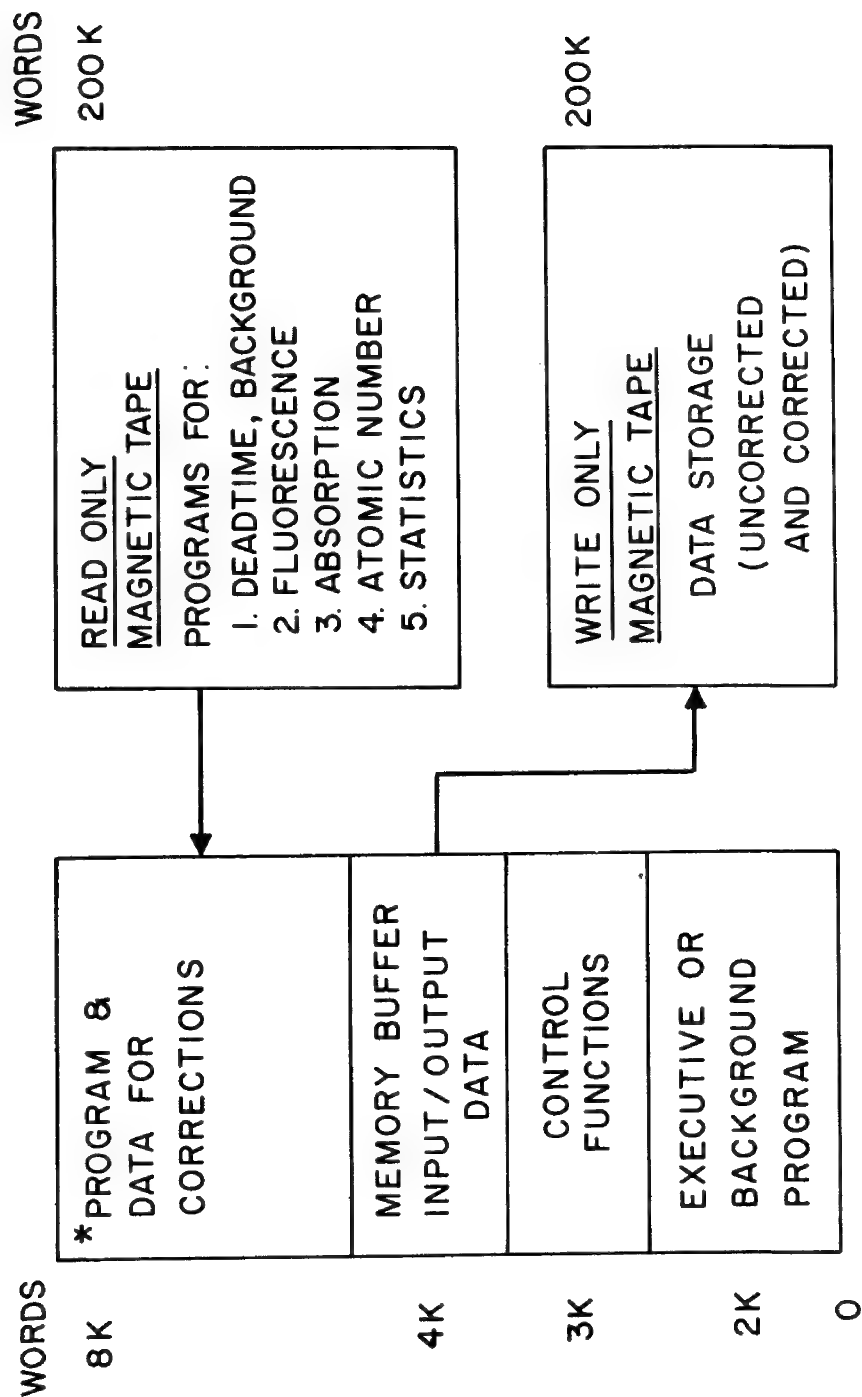


Figure 1

# COMPUTER MEMORY ALLOCATIONS



\* PROGRAMS ARE MODULAR

Figure 2

## COMPUTERIZED ELECTRON MICROPROBE

by

Richard Wolf and Arthur J. Saffir  
Materials Analysis Company  
1060 E. Meadow Circle  
Palo Alto, California

Automation of instrument control, data acquisition, and data handling is an integral part of modern microprobe analysis. We wish to describe a computerized microprobe system with the unique advantage of low cost combined with a conventional computer language.

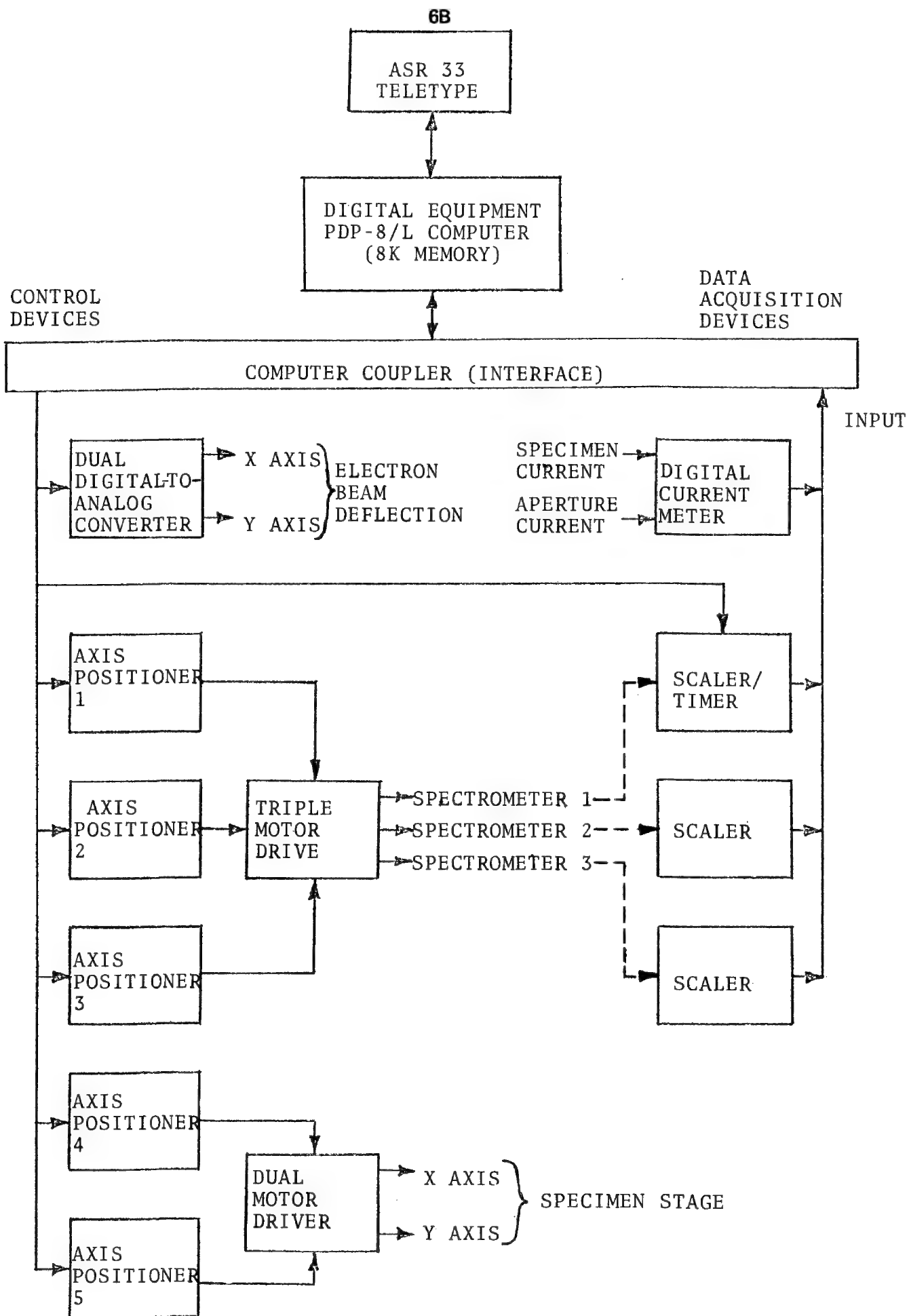
A PDP8/L computer with 8K memory is party-line linked to the control and data acquisition devices of a MAC-5 electron microprobe by means of a computer coupler. All data acquisition and control devices connected to the coupler can be individually addressed by the computer program in the PDP8/L. Axis positioners which control DC stepping motors set the 2 $\theta$  positions of the three spectrometers and also position the specimen. X-ray counting may be controlled by the computer through a scaler/timer and data from scalers read directly into the computer for storage, printout, or graphic display. The aperture current and specimen current are read into the computer from a digital current meter. X-Y beam deflection is provided by a dual digital to analog converter. Up to 64 separate devices for control or data acquisition can be addressed through the computer coupler.

The high-level conversational language, FOCAL\*, gives the operator extensive capability to acquire data and perform control functions. Because preset conditions are readily adjustable with FOCAL\*, collected data can be used to vary programming during execution. We have modified FOCAL\* by the addition of specific assembly language subroutines which link the interpreter to the control and data acquisition devices of the electron microprobe system. Thus, a previously inexperienced computer operator can learn to program the system efficiently in a few hours.

The use of this high-level language provides the following features:

- 1) extensive control command library,
- 2) mathematical operators and extended arithmetic functions,
- 3) direct and indirect programming modes,
- 4) error diagnostics
- 5) flexible editing for debugging,
- 6) specific subroutines,
- 7) control of a large number of peripheral systems such as disk memory or magnetic tape.

This instrumentation is ideally suited for diffusion gradient analysis, trace element analysis, particulate analysis (size, shape, and number determination), random sampling, phase distribution analysis, spectral analysis, and direct quantitative analysis. The system is both inexpensive and simple to use despite its extensive capabilities.



## A COMPUTER ASSISTED MICROPROBE LABORATORY \*

W. F. Chambers

Sandia Laboratories, Albuquerque, New Mexico

The 1962 vintage ARL-EMX microprobe at Sandia has been updated to include an all solid-state detection system and an on-line computer. The purpose in installing an on-line computer was four-fold: first, to provide a multichannel analysis system for a Li-drifted Si detector; second, to provide a mechanical means of performing such routine procedures as setting and peaking a spectrometer to a particular element or making repeated positionings of the spectrometers and the sample for a quantitative analysis; third, to have the capability of performing on-line quantitative analyses; and fourth, to provide a facility capable of unattended operation when desired.

To implement the above goals, a PDP 8/I with 8K 12-bit words of core and a 256K-word random access disk was chosen as the basic building block. An 8096 channel analog-to-digital converter with direct memory access to the computer provides the non-dispersive data collection and display facility. Once in core, the data can be massaged to the extent necessary. Through another interface, the computer can drive stepping motors attached to the scanners and the x, y, and z sample positioning controls; reset, start, and stop the counters; adjust the baseline of the single-channel analyzers; and matrix-position the electron beam.

The microprobe can be operated in any one of the three modes--manual, computer control, and interactive. In the interactive mode, the microprobe is operated through the computer by a set of switches located at the console. In this mode, up to 10 sets of x-ray coordinates of areas to be examined later under computer control may be stored either by giving store instructions to the computer each time an area of interest is observed or by entering the coordinates at the teletype. These areas may correspond either to standards or to unknowns and the computer can be instructed to return the sample to the referenced points in any order. Up to five element-line combinations may be associated with each point and the machine can re-focus both the spectrometers and the sample at each point. Backlash is accounted for by the software.

The 256K-word disk, which permits 16 millisecond access to any of our programs on file, has enabled us to circumvent the problems of storing large files normally associated with small computers. The fairly long interactive programs have been written in a chained manner where one program automatically calls another from the disk whenever it is needed. On-line quantitative analyses have been implemented through a chained version of "MAGIC" which has been rewritten in the Focal language with disk-stored and referenced files. This version of MAGIC is capable of accepting data directly from the microprobe or from the teletype.

---

\*This work supported by the United States Atomic Energy Commission



The availability of the large-capacity disk has also allowed the utilization of the computer for non-microprobe applications. For example, a Debye-Scherrer film reader has been interfaced to the computer to permit rapid collection of data and reduction to d-spacing for input to an ASTM file search. A card reader permits inputting data from a Metals Research Quantimet for statistical analyses. Focal and Fortran operating systems are available through a simple calling sequence from the teletype. The result has been that the computer has even less idle time than the microprobe. It has frequently been used during non-working hours and upon occasion has run over the weekend on random-walk diffusion problems.

## COMPUTER PROCESSING OF SOLID STATE X-RAY DETECTOR DATA

Eric Lifshin  
Metallurgy and Ceramics Laboratory  
General Electric Company  
Research and Development Center

The addition of solid state x-ray detectors to electron microprobes and scanning electron microscopes has recently become a popular method for rapid qualitative and semi-quantitative chemical analysis. The energy spectra of a given sample is typically displayed on a cathode ray oscilloscope, x-y recorder or printed out on a teletype. If the system is correctly calibrated to convert channel number to electron volts then the energy of a given peak can be easily determined and the source element identified with the aid of appropriate tables.

It is not uncommon, however, that the spectra encountered in practical problems may be sufficiently complex to lead to some ambiguity in the determination of peak positions or that small peaks may be totally obscured by larger ones. Although these difficulties can be partially overcome by multichannel analyzers equipped with spectrum stripping capabilities, the use of a computer can more accurately and completely characterize a given spectrum. To accomplish this, a data acquisition and processing system has been developed which uses a high speed transmission link between a Northern 630 multichannel analyzer and a time-shared GE 4020 process computer coupled to a GE 600 computer. At this point the data is placed in a file accessible for normal time sharing. A spectrum analysis program written in FORTRAN is used to obtain a sliding least squares fit to first smooth the data and subsequently to search for peaks which meet certain requirements based on detector resolution and statistical considerations. The locations of peaks are stored in a table and a least squares peak fitting routine is used to fit the spectrum to a summation of Gaussian curves each representing a spectral line. In this manner refined peak positions, peak heights, integrated areas, and detector resolution can be determined. Table I shows the peaks detected by the program for a series of steel samples using a 315 ev detector on a CEC/Cameca microprobe.

# SOLID STATE DETECTOR SENSITIVITY FOR STEEL STANDARDS

## ELEMENT

STANDARD	Si	Mn	Ni	Cr	Mo	V	Cu
1	0.013	0.16	[5.15]	0.044	[0.18]	0.034	0.090
2	[0.24]	0.016	[4.10]	[0.20]	0.007	[0.46]	0.11
3	[0.18]	0.35	[2.92]	[0.35]	[0.94]	0.220	[0.49]
4	[0.295]	0.525	[2.08]	[0.53]	[1.29]	[0.52]	0.11
5	[0.62]	[1.11]	[0.56]	[0.96]	[1.41]	[0.26]	0.24
6	[0.130]	[1.21]	0.18	[2.34]	[0.53]	0.36	0.23
7	[0.37]	[1.42]	[0.84]	[1.72]	[0.32]	0.11	0.30
8	[0.81]	0.79	0.048	[3.07]	0.42	[0.64]	0.18

8B

OPERATING CONDITIONS: 20 KV, 5na. BEAM CURRENT, 600 SECONDS:

[ ] DETECTED WITHOUT SPECTRUM STRIPPING

[ ] DETECTED WITH SPECTRUM STRIPPING

RAPID QUANTITATIVE BULK ANALYSIS OF BRASSES  
USING THE ENERGY DISPERSION XRAY ANALYZER

J. C. Russ  
JEOLCO (USA), INC., 477 Riverside Ave., Medford, Mass.

Interest in the Energy Dispersion (ED) Xray Analyzer for both qualitative and quantitative analysis on microprobes and scanning electron microscopes has increased rapidly with the improvements in these devices in recent years. ED Spectrometers offer simultaneous analysis of all elements above atomic number 11; they are insensitive to geometric alignment so that sample flatness and positioning requirements are relaxed, and their high efficiency and large solid angle of coverage yield high count rates. The limitations of the ED Analyzer are its inability to detect light elements and its relatively poor resolution in comparison to wavelength dispersion (WD) spectrometers. This makes the peak-to-background ratios of characteristic xray lines poorer by about an order of magnitude and sometimes necessitates deconvolution of interfering peaks.

Considering the possible advantages, which outweigh these limitations, we have used the ED spectrometer for the rapid quantitative bulk analysis of brass samples. In addition to the two major elements Cu and Zn, minor elements Sn, Al, Fe and Pb are present. The samples were examined in a Jeolco JSM-U3 scanning electron microscope using 40 kV accelerating voltage. The ED detector (Nuclear Diodes XS-25-JSM-U3) was mounted with a  $43^\circ$  takeoff angle and subtended a solid angle of .00444 steradian. With a counting time of 100 seconds and a beam current of 600 pA (measured with a Faraday cage) about 700,000 counts were obtained on copper.

Data was collected in a multichannel analyzer and the spectrum then transferred to a 4000 word general purpose computer. Because the ED system was calibrated to 20 ev. per channel it was possible to absolutely assign certain channels to each of the various elements of interest. The integrated peak intensity of each line was obtained by adding the counts in channels bracketing the peak to approximately the one-tenth maximum point. Since the detector used had a full-width-at-half-maximum (FWHM) resolution of 220 ev, essentially unchanged over the energy range of the xray lines of interest, and since the full-width-at-tenth-maximum (FWTM) resolution is about twice the FWHM resolution, the energy brackets used for each element were  $\pm 220$  ev (22 channels wide). These are listed in Table 1. The background count for each peak was determined from a nearby portion of the spectrum and subtracted.

The only interference present was that of the Cu  $K_{\beta}$  and Zn  $K_{\alpha}$  lines. Deconvolution with a gaussian peak subroutine proved satisfactory but slow, so we chose instead to sum the Zn  $K_{\alpha}$  count over a larger bracket to include all of the Cu  $K_{\beta}$  and then subtract 14.4% of the Cu  $K_{\alpha}$  intensity. This  $K_{\beta}/K_{\alpha}$  ratio was measured on pure Cu and its use is appropriate since the average atomic number and absorption factors are similar for the brass samples.

Our correction procedure used the classic Ziebold (1) linear equations

$$\frac{C}{K} = a + C(1-a) \quad ; \quad a_{\text{keff.}} = \sum_i^n a_{ki} \frac{C_i}{(1-C_k)}$$

which assume that whatever absorption and fluorescence effects occur due to each element, they are linearly proportional to the concentration of that element, and that the effects of several elements can be linearly superimposed. The "a" values were chosen to give the best fit in the concentration range of interest. This range, along with the "a" matrix and the pure element count rates are listed in Table 1. The standards used to determine the matrix were prepared using one and two elements at a time in a Cu matrix, by mixing  $1/2 \sim 1 \mu\text{m.}$  powders of the pure elements. (2) These were pressed and sintered to less than 1/2% porosity. Areas  $100 \mu\text{m.}$  square were analyzed for both the standards and unknowns.

Table 2 shows two representative results. In comparison to chemical analysis on 32 samples, the corrected xray results gave Cu and Zn concentrations with 72% less than  $\pm 1.5\%$  relative error. The Fe and Sn results were 69% and 62% respectively, less than  $\pm .004$  absolute error, and the Al and Pb results were 59% and 62% respectively, less than  $\pm .007$  absolute error. The relatively poor Al results were due to the large absorption effects, which made the  $\frac{C}{K}$  vs. C curve very non-linear, while the Pb results were thrown off by the non-uniform distribution of Pb in small highly-concentrated inclusions in the real brass samples.

In conclusion we found that in a system with two major elements and several minor ones, the ED xray system offers acceptable accuracy and great speed. The 100 second analyzing time could be reduced somewhat by using electronics with faster response times to permit using higher beam currents. The data transfer and calculating time was less than 30 seconds. The advantage of simultaneous analysis of all major and minor elements makes this system very attractive.

- (1) T. O. Ziebold, R. E. Ogilvie "An Empirical Method for Electron Microanalysis" Analytical Chemistry 36 p. 322 (Feb. 1964)
- (2) S. Moll "Practical Methods for Experimentally Calibrated Concentration Determination in the Electron Beam Microanalyzer" Proc. 1st Int'l Conference on Electron and Ion Beam Tech. Wiley, 1965, p. 825

Table 1

Element	Line	energy range integrated (KeV.)	pure element count rate C/S/pA.	valid concen- tration range	"a" matrix					
					Cu	Zn	Fe	Sn	Al	Pb
Cu	K $\alpha$	7.82								
		-8.26	11.644	.40-1.0	0	1.217	1.059	1.812	1.03	1.99
Zn	K $\alpha$	8.40*								
		-9.16	10.408	0-.40	1.164	0	1.050	1.805	1.03	2.00
Fe	K $\alpha$	6.18								
		-6.62	13.879	0-.05	0.605	0.628	0	0.97	1.02	1.65
Sn	L	3.22**								
		-3.88	10.573	0-.10	1.223	1.238	1.07	0	1.04	2.09
Al	K	1.26								
		-1.70	7.963	0-.10	4.05	4.07	3.75	5.36	0	8.3
Pb	M	2.12								
		-2.56	4.281	0-.05	0.97	0.98	0.95	0.92	1.15	0

\*Includes Cu K $\beta$  - see text.    \*\*Includes L $\alpha_1$ , L $\alpha_2$  and L $\beta_1$

Table 2

		Cu	Zn	Fe	Sn	Al	Pb
Spec. A	chem.	.654	.213	.023	.034	.042	.037
	xray	.651	.215	.023	.031	.049	.043
Spec. B	chem	.741	.105	.014	.009	.083	.050
	xray	.736	.104	.017	.005	.090	.055

COMPUTER EVALUATION OF MULTIPLE X-RAY AND ELECTRON IMAGES  
FROM THE SEM

H. Görz, E. W. White, R. E. McMillan and J. Lebieczik  
Materials Research Laboratory  
The Pennsylvania State University  
University Park, Pennsylvania

---

Basic techniques for the computer processing of SEM images to yield quantitative size and shape analysis of dispersed particles have been developed over the past three years in this laboratory and results have been reported elsewhere<sup>1,2,3,4</sup>. A limitation of this early work is that no provision was made for distinguishing, chemically, among the different kinds of particles in a sample. This paper describes several extensions of the basic techniques including, primarily, the simultaneous multi-element x-ray analysis of particle chemistry and the procedures for extracting the size and shape characteristics for each of the phases in complex particulate samples. In addition to the chemical analysis of particles, the basic procedures are readily extended to problems of modal analysis and quantitative metallography.

A model JSM scanning electron microscope has been equipped with a variety of x-ray detectors including: nondiffractive flow proportional and scintillation detectors, and a curved graphite spectrometer. A multi-channel x-ray recording system has been specially designed and built for rapid recording of up to six channels of information at one time onto digital magnetic tape.

The fundamental characteristic of the CESEMI (Computer Evaluation of SEM Images) approach is that the entire image is recorded on digital magnetic tape and all data reduction is left to the computer. This approach differs quite markedly from some of the alternative techniques such as point by point analysis (equivalent to point counting) or the proposed computer-controlled methods.

The signal preprocessor package includes: 1) specially designed high gain amplifiers for the electron signals (absorbed, secondary, and back-scattered electrons); 2) high gain, low time constant, amplifier-ratemeter circuits for up to five x-ray signals in parallel; 3) an improved sweep circuit which replaces the original system supplied with the SEM so that the sweep may actually consist of a continuous line sweep or point scan on a closely spaced grid.

One of the first applications of the x-ray analysis capability has been to extend the basic particulate characterization procedures to include information on the chemistry of individual particles. A test sample consisted of mixed titania and alumina powders dispersed on a polished beryllium substrate. The secondary electron image was used for calculation of the size and shape of each particle. The TiK $\alpha$  x-ray image identified each titania grain. The computer program then calculated the size and shape distributions for the two phases.

For modal analysis by this technique, samples from the lower Devonian sandstone in the Harz Mountain (in Germany) were chosen which previously had been determined with

regard to their chemical and mineralogical compositions. For the earlier quantitative mineralogical determination, three thin sections, cut perpendicular to each other, were examined by the point counting method (1000 points per section)<sup>5</sup>. A comparison of those values with this new technique yields quantitative chemical values in good agreement for the major minerals (quartz, mica, plagioclase and prochlorite). The SiK $\alpha$  x-ray image was used for quartz, NaK $\alpha$  for plagioclase, FeK $\alpha$  for prochlorite and the K K $\alpha$  x-ray image for mica.

This work is supported by the Office of Naval Research, Metallurgy Program, under Contract No. N00014-67-A-0385-0007.

- 
1. E.W. White, G.G. Johnson, Jr. and H.A. McKinstry, Proc. Symposium on Scanning Electron Microscopy/1968, IIT Research Institute, Chicago, 95-103 (1968).
  2. R.E. McMillan, G.G. Johnson, Jr. and E.W. White, Proc. Symposium on Scanning Electron Microscopy/1969, IIT Research Institute, Chicago, 441-444 (1969).
  3. E.W. White, H. Götz, G. G. Johnson, Jr. and R.E. McMillan, Proc. Symposium on Scanning Electron Microscopy/1970, IIT Research Institute, Chicago, to be published.
  4. W.L. Matson, H.A. McKinstry, G.G. Johnson, Jr., E.W. White and R.E. McMillan, 1970 Symposium on Computational Photogrammetry, Washington, DC, January 1970.
  5. Herta Götz, Beiträge Min. Pet. 8, 232-266 (1962).



## COMMENTS ON THE CONTINUUM FLUORESCENCE CORRECTION

R. L. Myklebust, H. Yakowitz and K. F. J. Heinrich  
 National Bureau of Standards  
 Washington, D. C. 20234

## Abstract

Two models for the continuum fluorescence correction are currently used. These are Henoc's formulation [1,2] and Springer's modification of Henoc's approach [3]. We investigated the significance of the continuum fluorescence correction in practical quantitative electron probe microanalysis with the aid of Henoc's model. This model has been programmed for digital computer by Henoc, Heinrich and Myklebust as a subsection of an overall correction scheme program [4]. The modular nature of this subsection made it relatively simple to vary conditions affecting the magnitude of the continuum fluorescence correction.

The continuum fluorescence subsection occupies about one-third of the computer core memory that the entire program requires. The computation of the continuum fluorescence correction data requires at least half the time required for the total computation in the case of binary specimens. This time factor increases rapidly as the number of components to be analyzed increases. Therefore, we investigated the continuum fluorescence correction in order to pinpoint cases where this correction can be safely ignored in order to simplify and reduce the time and cost of the computation.

The concentration of a set of binary alloys was assumed known for purposes of calculation. The entire programmed correction procedure including corrections for absorption, atomic number and characteristic fluorescence as well as continuum fluorescence was carried out. The result gives the computed intensity ratio,  $k$ , for a particular system. Then the continuum fluorescence correction factor was made unity and a new  $k$ , called  $k_0$ , was determined. We define

$$H \equiv (k - k_0) / k_0 \quad (1)$$

Thus,  $H$  is the relative change in intensity ratio produced by using Henoc's correction for continuum fluorescence. Table I shows all of the systems chosen for study as well as the results for  $H$  using an operating voltage of 25 kV.

We found that the continuum fluorescence correction is less than 1% relative and can be ignored when  $f(\chi)$  of the material containing the analyte is about 0.9 or less. In addition, for any analyte in any matrix, the correction can be neglected when the concentration of the analyte exceeds 0.5. The correction cannot be ignored whenever  $f(\chi)$  of the material exceeds 0.9 and the analyte concentration is less than 0.5. Therefore, analysis using

very hard analytical lines in matrices of low atomic number always requires a continuum fluorescence correction. These findings are essentially independent of the operating voltage in the 15 to 35 kV range.

Our results suggest that if there is a choice of using an analytical line from the K or the L shell, then the L shell line should be chosen in order to reduce the magnitude of the continuum fluorescence correction. Operating parameters should be adjusted so that  $f(\chi)$  is 0.8 or more and absorption correction uncertainties are reduced [5].

The effect of changing input parameters such as absorption jump ratios and fluorescent yield factors had no significant effect on the continuum fluorescence correction. A reduction of one degree in the x-ray take-off angle, from  $52.5^\circ$  to  $51.5^\circ$ , also did not have an appreciable effect on H. Lowering the take-off angle to  $18^\circ$  reduced H by a small amount in all cases. Actual values for the 10% Zr-B case at 25kV gave  $H = 0.32$  and  $H = 0.26$  at  $52.5^\circ$  and  $18^\circ$  respectively.

We have drawn the following conclusions from this study:

- (1) The magnitude of the continuum fluorescence correction cannot be neglected in cases where  $f(\chi)$  of the material is 0.9 or greater. This corresponds to analysis using hard x-ray lines in a light matrix, e.g. analysis of the "heavy" component in an oxide.
- (2) Voltage variation and errors in the take-off angle, fluorescence yield factor and jump ratio have no significant effect on the continuum fluorescence correction.
- (3) The continuum fluorescence correction may be ignored when  $f(\chi)$  is 0.9 or less or when the concentration of the analyte is greater than 0.5.
- (4) All of the results do not contradict the operating parameters suggested for quantitative analysis: Low overvoltage and high take-off angle [5].

#### References

- [1] J. Henoc, Thesis, University of Paris 1962, (Translation available from H. Yakowitz, NBS).
- [2] J. Henoc, NBS Special Publ. 298 (K.F.J. Heinrich, ed.) 1968, pp.197-214.
- [3] G. Springer, N. Jahrbuch f. Mineralogie 106, 241 (1967).
- [4] J. Henoc, K.F.J. Heinrich and R. L. Myklebust, COR, A Program for Computer Calculation for Quantitative Electron Probe Microanalysis, to be published.
- [5] H. Yakowitz and K.F.J. Heinrich, Mikrochim Acta 1968, p.182.

TABLE I

Factor H at 25 kV for Analyte Concentration of 0.1

Analytical Line*											
	Matrix, Z	Na K $\alpha$	Ca K $\alpha$	Zn K $\alpha$	Zr K $\alpha$	Zr L $\alpha$	Cs L $\alpha$	Yb L $\alpha$	Hg L $\alpha$	Cu K $\alpha$	Mo K $\alpha$
Beryllium, 4		ND	ND	ND	ND	ND	ND	ND	ND	0.076 <sup>+</sup>	0.307 <sup>+</sup>
Boron, 5		0.001	0.015	0.105 <sup>+</sup>	0.321	0.012 <sup>+</sup>	0.016	0.028	0.034	ND	ND
Phosphorus, 15		0.002	>0.001	0.040	0.280	0.003	0.004	0.016	0.027	ND	ND
Zinc, 30		>0.001	0.003	--	0.022	0.001	0.009	0.028	0.001	ND	ND
Rhodium, 45		>0.001	>0.001	0.010	0.136	0.002	0.001	0.005	0.013	ND	ND
Neodymium, 60		>0.001	>0.001	>0.001	0.043	0.001	0.002	0.001	>0.001	ND	ND
Rhenium, 75		--	>0.001	>0.001	0.004	>0.001 <sup>+</sup>	0.001	0.001	>0.001	ND	ND

\* ND - not determined

- not calculated by program

+ Systems also analyzed for analyte concentrations of 0.5 and 0.9

&gt; H less than amount shown

## INDIRECT DETERMINATION OF MASS ABSORPTION COEFFICIENTS FOR SOFT X-RAYS

D. F. Kyser

IBM Research Laboratory  
San Jose, California

One of the most important corrections required for quantitative electron probe microanalysis, especially for "soft" X-rays, is that for absorption of the generated X-rays by the target. Because a lack of direct measurements of mass absorption coefficients  $\mu/\rho$  exists for many "soft" X-rays, there is a need for alternate techniques to determine the coefficients. Andersen<sup>1</sup> showed that an empirical relation existed between the accelerating voltage  $E_0$  which produced the maximum observed X-ray intensity, and the best-known values for  $\mu/\rho$  in various targets. In this paper, a quantitative basis is established for such empirical observations.

The observed X-ray intensity as a function of  $E_0$  is assumed to be proportional to the product of the relative generation rate,  $(E_0 - E_c)^n$ , and the fraction  $f(\chi)$  of X-rays generated which escape the target at a particular angle  $\psi$ , where  $\chi = (\mu/\rho) \csc \psi$ . In practice,  $E_0 \gg E_c$  where  $E_c$  is the critical excitation potential for the X-ray under study. Hence one can determine  $E_p$ , that value of  $E_0$  which produces a maximum intensity, by setting

$$\frac{d}{dE_0} [E_0^n f(\chi)] = 0 \quad (1)$$

and solving for  $E_p$  as a function of  $\chi$ . This formulation neglects effects due to backscattered electrons and secondary fluorescence.

A particular expression for  $f(\chi)$  which includes voltage-dependence has been derived, based on assumptions originally proposed by Wittry.<sup>2</sup> A Gaussian distribution of X-ray generation with distance is used, namely

$$\Phi(\rho Z) = A \exp \left[ - \left( \frac{\rho Z - \rho Z_0}{\rho \Delta Z} \right)^2 \right] \quad (2)$$

The associated  $f(\chi)$  is then

$$f(\chi) = \frac{\exp[-(Z_0/\Delta Z)^2] \exp(u^2) [1 - \operatorname{erf} u]}{1 + \operatorname{erf}(Z_0/\Delta Z)} \quad (3)$$

where 
$$u = \left[ \frac{\chi \rho \Delta Z}{2} - \frac{Z_0}{\Delta Z} \right] \quad \text{and} \quad \text{erf } u = \frac{2}{\sqrt{\pi}} \int_0^u e^{-t^2} dt$$

The appropriate constants  $Z_0$  and  $\Delta Z$  were determined by matching the Gaussian  $\Phi(\rho Z)$  to a calculation for energy loss  $dE/dZ$  with distance  $Z$  via a transport equation model,<sup>3</sup> and are assumed to be valid for  $\Phi(\rho Z)$  when  $E_C \leq 2$  keV. The constants were determined for  $E_0 = 30$  keV in a Cu target, and are the same as those used by Wittry and Kyser to describe the voltage-dependence of cathodoluminescence.<sup>4</sup> The constants are then scaled with voltage  $E_0$  in the same manner as the electron range  $R$ . Thus

$$\rho Z_0 = 0.125R, \quad \rho \Delta Z = 0.350R \quad (4)$$

where

$$R = 2.56 \times 10^{-3} \left( \frac{E_0}{30} \right)^m \text{ gm/cm}^2 \quad (E_0 \text{ in keV}).$$

The value for the exponent  $n$  to be used in Eq. (1) appears to be different than 1.63 as proposed by Green.<sup>5</sup> Based on measurements reported by Duncumb and Melford<sup>6</sup> for  $C_{K\alpha}$  in diamond and corrected for absorption with  $f(\chi)$  given by Andersen and Wittry,<sup>7</sup> and on measurements by the author for  $Fe_{L\alpha}$  in Fe corrected for absorption, it appears that  $n \approx 1.2$  for these soft X-rays. This is consistent with Green's data for  $C_{K\alpha}$ ,  $Al_{K\alpha}$ , and  $Au_{M\alpha}$  where  $n < 1.63$  for  $E_0 \gg E_C$ .

The justification for using the Gaussian distribution for  $\Phi(\rho Z)$  and its associated  $f(\chi)$  lies in the fact that it gives good agreement with the values for  $f(\chi)$  obtained by Andersen and Wittry,<sup>7</sup> who used a formulation based on the "effective" mean depth of ionization  $(\bar{\rho Z})^*$ . For mid-atomic-number targets, the voltage-dependence of the Gaussian  $f(\chi)$  and the Andersen-Wittry  $f(\chi)$  is nearly identical, especially when a modification to the Gaussian  $\Phi(\rho Z)$  is made to account for the fact that it predicts excessive X-ray generation for  $Z < Z_0$ . The agreement is not surprising when one considers that the Gaussian  $\Phi(\rho Z)$  gives a mean depth of generation  $(\bar{\rho Z})_G = 2\rho Z_0 = 0.25R$ , and for  $\chi(Fe, Fe_{L\alpha}) = 3720$ ,

$$\frac{1.44 \times 10^{-5} (\bar{\rho Z})^*}{(\bar{\rho Z})_G} \approx 1 \quad (5)$$

The constant  $1.44 \times 10^{-5}$  arises from the calculations of Archard and Mulvey.<sup>8</sup> This suggests that atomic-number dependence could be included in the Gaussian  $\Phi(\rho Z)$  and  $f(\chi)$  by scaling  $\rho Z_0$  and  $\rho \Delta Z$  as  $A/Z^{4/3}$ , the same way that  $(\bar{\rho Z})^*$  is scaled. However the voltage-dependence of  $(\bar{\rho Z})_G$  and  $(\bar{\rho Z})^*$  is not identical. The latter appears to scale as  $E_0^{1.60}$ , whereas the former scales with the range  $R$ .

For  $m = 1.68$ ,  $n = 1.20$ , and the constants given in Eq. (4) for a mid-atomic number matrix, the theoretical result obtained from Eqs. (1) and (3) is

$$\chi(\text{cm}^2/\text{gm}) = \left(\frac{2660}{E_p}\right)^{1.68} (E_p \text{ in keV}) . \quad (6)$$

This is close to a previous estimate given by Andersen and Hasler,<sup>9</sup>

$$\chi = \left(\frac{1060}{E_p}\right)^2 \quad (7)$$

Note that for the Gaussian formulation,

$$\frac{d\chi}{\chi} = -1.68 \frac{dE_p}{E_p} \quad (8)$$

so that a 10% relative error in determining  $E_p$  results in a 16.8% relative error in  $\chi$ .

In practice, one measures the X-ray intensity with increasing voltage  $E_0$  at constant specimen current using the specimen target of interest. The value of  $E_p$  then determines the value of  $\chi$  in that matrix, using Eq. (6). Table 1 shows experimental results obtained on various elemental and compound targets for  $\psi = 52.5^\circ$ . The results for Fe and Cu agree well with values for  $\chi$  proposed by others. For As  $L\alpha$  in GaAs, the discrepancy is large. For AlAs,  $\chi(\text{AlAs}, \text{Al}K\alpha) = 3,840$  produces good agreement in the expected intensity ratio  $K$  using an Al standard.<sup>11</sup>

The values of  $\chi(\text{Fe}, \text{Fe}L\alpha)$  and  $\chi(\text{Fe}, \text{Fe}L\beta)$  in Table 1 have been shown<sup>7</sup> to account for most of the voltage-dependence observed in the intensity ratio  $L\beta_1/L\alpha$ . With the present technique,  $\chi$ -values can be determined for various transition-metal oxides, and then the effect of chemical valence state on intensity ratio<sup>12,13</sup> can be quantitatively studied.

The absolute value of the constant in Eq. (6) is sensitive to the value of  $n$ , increasing with increasing  $n$ . However the exponent remains the same as that found in the range relation, namely  $m$ . The data plotted by Andersen<sup>1</sup> scatter, but appear to be described best with an exponent of 1.5-1.6 in Eq. (6). However the values for  $\chi$  used there may be in error, and there is also a range in atomic number. The usefulness of Eq. (6) will ultimately be determined by the accuracy of quantitative microanalysis with soft X-rays in a wide variety of targets for which  $\chi$ -values are presently inaccurate or unknown.

- 
1. C. A. Andersen, Brit. J. Appl. Phys. 18, 1033 (1967).
  2. D. B. Wittry, J. Appl. Phys. 29, 1543 (1958).
  3. D. B. Brown, private communication.
  4. D. B. Wittry and D. F. Kyser, J. Appl. Phys. 38, 375 (1967).

5. M. Green, Proc. 3rd Intl. Symp. on X-Ray Optics and X-Ray Microanalysis (Stanford, 1962), p. 185.
6. P. Duncumb and D. A. Melford, Proc. 4th Intl. Symp. on X-Ray Optics and X-Ray Microanalysis (Orsay, 1965), p. 240.
7. C. A. Andersen and D. B. Wittry, Brit. J. Appl. Phys. (J. Phys. D.), Ser. 2, 1, 529 (1968).
8. G. D. Archard and T. Mulvey, Proc. 3rd Intl. Symp. on X-Ray Optics and X-Ray Microanalysis (Stanford, 1962), p. 393.
9. C. A. Andersen and M. F. Hasler, Proc. 4th Intl. Symp. on X-Ray Optics and X-Ray Microanalysis (Orsay, 1965), p. 310.
10. K. F. J. Heinrich, The Electron Microprobe, (Wiley and Sons, New York, 1966), p. 296.
11. W. Reuter, private communication.
12. D. W. Fischer, J. Appl. Phys. 36, 2048 (1965).
13. A. L. Albee and A. A. Chodos, Proc. 4th Natl. Conf. on Electron Microprobe Analysis (Pasadena, 1969), paper #32.

Table 1

Line	$E_c$ (keV)	Target	$E_p$ (keV)	$\chi^+$	$\chi^{++}$
Fe $L\alpha$	0.708	Fe	19.5	3,900	3,720 <sup>a</sup>
Fe $L\beta_1$	0.721	Fe	9.0	14,000	15,500 <sup>b</sup>
Cu $L\alpha$	0.933	Cu	26.0	2,400	2,360 <sup>a</sup>
As $L\alpha$	1.325	GaAs	18.0	4,400	6,160 <sup>c</sup>
Al $K\alpha$	1.559	AlAs	18.0	4,400	6,400 <sup>c</sup>

<sup>†</sup>Calculated from Eq. (6).

<sup>††</sup>Calculated from  $\chi = \sum_i (\mu/\rho)_i C_i \csc \psi$  with  $\psi = 52.5^\circ$ .

Sources of  $(\mu/\rho)$ : (a) ref. 1  
 (b) ref. 7  
 (c) ref. 10

## THE X-RAY CONTINUUM FROM THICK TARGETS\*

T. S. Rao-Sahib and D. B. Wittry

Departments of Materials Science and Electrical Engineering  
University of Southern California, Los Angeles, California 90007

On the basis of Kramers' equation,<sup>1, 2</sup> the intensity of the X-ray continuum produced by electron bombardment of thick targets has been further investigated.<sup>3</sup> Results obtained indicate that (i) the continuum may require an absorption correction which can differ greatly from that required for characteristic radiation; (ii) Green's results<sup>4</sup> regarding the efficiency of production of the continuum as a function of  $Z$  are not confirmed; (iii) if the observed deviations from Kramers' equation can be satisfactorily explained, then this technique may be used to estimate  $\mu$  for an element at any wavelength provided the element does not have any characteristic lines nearby.

According to Kramers<sup>1</sup>, the energy between frequencies  $\nu$ ,  $\nu + d\nu$  radiated per electron impact is given by

$$I_{\nu} d\nu \sim Z(\nu_0 - \nu) d\nu \quad (1)$$

In equation (1),  $Z$  is the atomic number,  $\nu_0 = V_0 e/h$  where  $V_0$  is the accelerating potential,  $e$  is the electronic charge, and  $h$  is Planck's constant.

Twenty-two elements, ranging in atomic number from 12 to 92, were examined using an EMX-SM with a take-off angle of  $52.5^\circ$ . Beam voltage was kept constant at 30 kV. X-ray continuum intensities were measured in the range  $1 \text{ \AA} - 8 \text{ \AA}$ , at intervals of approximately  $1 \text{ \AA}$ . Pulse height discrimination was used in each case. Beam current, measured with a Faraday cage, was kept constant.

Absorption and atomic number corrections were made under the following assumptions:

- 1) The spatial distribution of excitation for the X-ray continuum is the same as for the characteristic X-rays.

\* Research supported by the Air Force Office of Scientific Research, Office of Aerospace Research, United States Air Force, under Grant # AF-AFOSR-68-1414.



- 2) The mass absorption coefficients are known. (Heinrich's values<sup>5</sup> for  $\mu$  were used).
- 3) For 1 Å and 2 Å, where  $f(\chi) > 0.6$  for all elements, Macres'  $f(\chi)$ <sup>6</sup> was used. For these values of  $f(\chi)$ , the difference is less than 2% between Macres'  $f(\chi)$  and the Philibert  $f(\chi)$  using Duncumb and Shields' voltage dependence with Heinrich's coefficient for voltage. From 3 Å - 8 Å, where in general  $f(\chi) < 0.5$ , the Andersen and Wittry<sup>7</sup>  $f(\chi)$  was used.
- 4) The cross-section  $Q$  for production of the continuum is independent of the energy of the electrons.
- 5) The atomic number correction is calculated from equation (10) of Duncumb and Reed<sup>8</sup> using  $E_k = 12.4/\lambda$  ( $E_k$  in kV,  $\lambda$  in Å), together with assumption (4) above and Bishop's data for backscatter coefficient  $\eta$ .

To facilitate comparison of the results at different wavelengths,  $\log$  (intensity) vs.  $\log Z$  was plotted. If equation (1) is correct, the  $\log$  (intensity) vs.  $\log Z$  curve should be a straight line of slope unity, and independent of wavelength. The dashed curve in Figure 1 shows the results for 1.128 Å (Ge  $K\beta_1$ ). The predicted behavior is obtained only for elements for which  $Z > 50$ . For  $Z < 50$ , the slope is greater than unity, and the relation  $I \sim Z^{4/3}$  seems to hold. This result needs to be explained. Green's measurements<sup>4</sup> on the efficiency of production of the X-ray continuum as a function of  $Z$  show variations up to  $\pm 40\%$  from the constant value given by Compton and Allison.<sup>2</sup> Green's results are not supported by the present work, since such large variations in efficiency would have been easily detected.

In the range 3 Å - 8 Å, the corrected intensities no longer vary smoothly with  $Z$ . The curve for 7.981 Å (Al  $K\beta$ ) shown in Figure 1 is typical. If it is assumed that the  $\mu$  values are reliable, and that Kramers' equation is valid, then such a curve would seem to indicate over-correction by the absorption correction function. To eliminate the possibility that radiation from the visual optical components due to backscattered electrons might be contributing to the observed intensities, the experiment was repeated with a Mylar shield placed in the bore of the objective lens just above the specimen. This resulted in a reduction by a factor of 8 of the backscattered electron current monitored by the optical instrumentation. However, this did not produce any change in the "over-corrected" appearance of the final results.

This raises the possibility that a separate correction function is required for the continuum. Preliminary calculations, based upon the assumption that the corrected intensities for all wavelengths should follow the smooth curve obtained at 1.128 Å, have yielded a fairly consistent  $f(\chi)$  curve for

the continuum which, for values of  $f(\chi) < 0.5$ , diverges considerably from the  $f(\chi)$  curve of Andersen and Wittry.

---

#### REFERENCES

- 1) H. A. Kramers, Phil. Mag., 46, 836 (1923).
- 2) A. H. Compton and S. K. Allison, "X-Rays in Theory and Experiment", Van Nostrand Co., New York (1935), p. 105.
- 3) T. S. Rao-Sahib and D. B. Wittry, Proc. 4th National Conf. on Microprobe Analysis, Pasadena, California.
- 4) M. Green, Brit. J. Appl. Phys., Ser. 2, 1, 425 (1968).
- 5) K. F. J. Heinrich in "The Electron Microprobe", John Wiley & Sons, New York (1966), pp. 351 - 377.
- 6) V. G. Macres, Proc. 4th National Conf. on Microprobe Analysis, Pasadena, California.
- 7) C. A. Andersen and D. B. Wittry, Brit. J. Appl. Phys., Ser. 2, 1, 529 (1968).
- 8) P. Duncumb and S. J. B. Reed, "Quantitative Electron Probe Microanalysis", NBS Spec. Publ. 298.
- 9) H. E. Bishop in "Optique des Rayons X et Microanalyse ", Hermann, Paris (1967), p. 158.

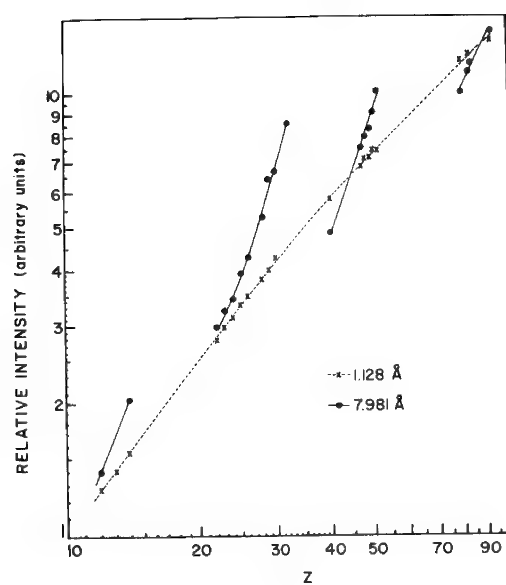


Figure 1. X-ray continuum intensities at 1.128 Å and 7.981 Å, corrected for absorption and atomic number effects. (Intensities from the two wavelength curves should not be compared).

# TIME SHARING COMPUTER PROGRAMS FOR DATA PROCESSING AND CORRECTIONS IN MICROPROBE ANALYSIS

F. Borile

Consiglio Nazionale delle Ricerche, Laboratorio Metalli  
non Tradizionali, Cinisello Balsamo, Italy.

The time-sharing computer system offers the possibility to access a large computer from remote locations with a teletype machine located in the individual laboratory<sup>1</sup>. It basically consists of sharing a large computer among many input, output stations. Perhaps the most important advantages of this system are: a) fast access to a large computer with a convenient easy to learn interface; b) on time users can monitor the program while is running, they are prompted to produce forgotten informations and are immediately informed of their programming or data input errors; c) but, most important, an analyst, with very little computer experience, can program his own calculations in a very short amount of time.

The following modular programs have been written using the BASIC language which is particular easy to learn and to use for the non expert programmer: PROBERATIO, FLOUR, ABAN, TAUPLOT. These programs have been written keeping in mind four basic aims: a) flexibility; b) use of an appropriate correction procedures; c) elimination of data sorting and manual calculations; d) give to the user the possibility to check the out-put of each correction segment before feeding it into the next one. In order to use the programs informations and instructions are supplied to the users as the programs are called from the library or are sequentially asked by the program to the operator as the program is running. The output of each program is punched on a paper tape and it is ready to be used as input to the next program.

PROBERATIO: it process x-ray intensities data, previously punched on a paper tape, as they are simultaneously recorded on the teletype. The out-put is a probe ratio corrected for dead-time, background and drifting. The program requires a limited amount of informations, the operator, however, must use the following sequence while collecting the data.

- a) Intensities pure element A, B, C ..... etc.
- b) Intensities unknown element A, B, C ..... etc.
- c) Background high side pure element A, B, C ..... etc.
- d) Background low side pure element A, B, C ..... etc.
- e) Background unknown intensities.

For the background correction in the unknown and pure elements inten-

sities, the program can also perform as follows: when performing distribution or diffusion studies, where it would be desirable to take background measurements after each serial point, and assuming the availability of a reproducible programmed scanner, the program can take background intensities on the high and low side of the analytical line of interest, after having established that the line is free of interference<sup>2</sup>. If however this is not the case then the program can calculate background of composite targets from measurements on the pure specimen at the wavelength of interest<sup>3,4,5</sup>. No limitations are imposed by the program as far as the number of intensity measurements are concerned on the pure elements or on the unknowns. A character code is typed by the operator at the end of each set of counting. Drifting is corrected either by an integrated beam current type of x-ray counting termination or by monitoring the integrated beam current variations during the analysis. Dead-time of the detectors and associated electronics is readily determined using the current method<sup>6</sup> with the program TAUPLOT.

FLOUR: the program corrects for KK, KL, LK, LL, fluorescence using the model of J.B. Reed<sup>7</sup> with the approximation formula. It is assumed to use K lines for analysis if  $z < 35$  and L lines if  $z \geq 35$ . A decision array for the fluorescing elements is made by the operator using the table I provided by Reed's paper and following the instructions supplied while running the program. The input data consists of number of elements, atomic number of elements, working voltage, take-off angle, and the mass absorption coefficients. Using the file system the program keeps in memory the atomic numbers, the  $z^*$  (Reed's imaginary atomic number for KL and LK fluorescence correction) the  $J(A)$ , the  $D$  values, and the "Lenard coefficient"  $\sigma$ .

ABAN: the program corrects for absorption and atomic number using the model of Ducumb and Shield<sup>8</sup> for the absorption correction and Ducumb and Reed<sup>9</sup> for the atomic number correction. It is assumed to use the  $K\alpha$  lines for analysis from  $z_A = 5$  to  $z_A = 35$  and the  $L\alpha$  lines for  $z_A > 35$ , since these are the analytical lines most commonly used in a vast majority of analytical problems. The input data consists of number of elements, atomic number of elements, working voltage, take-off angle, and mass absorption coefficients. The permanent input data consists of atomic numbers, atomic weights, critical excitation potentials, "J" and "R" values from Ducumb and Reed tabulation. Concentrations are normalized in the following manner: during the first iteration the concentration of element A is assumed to be its experimental probe ratio, i.e.,  $C_A = K_A$ . The concentration of element B is given by:

$$C_B = \frac{K_B}{K_B + K_C + \dots K_n} (1 - C_A) \quad (1)$$

In the second and following iterations the concentration of element A is given by:

$$C_A = \frac{(C_{calc.})_{n+1} + (C)_{n-1}}{2} \quad (2)$$

where  $n$  is the number of iteration. Concentration of element B is still calculated from eq. (1). Since we are on a time sharing system the convergence or divergence of the calculated concentration during iteration can be monitored while the program is running. The number of iterations can be changed by a single line statement according to a preestablished value of  $C_n - C_{(n-1)}$  where  $n$  is the number of iterations.

TAUPLLOT: it is desirable to determine the values of dead-time at different photon energies for the various detectors and counting electronics, and to be able to control very quickly if any change occurs in time to the values found. The program will simultaneously process the data, punched on a paper tape, and calculate the values of " $\tau$ " for up to four counting channels using the current method<sup>6</sup>. The ratios  $N/i_s$ , where  $N$  is the observed count rate and  $i_s$  is the digitized sample current will be simultaneously plotted as a function of  $N$ . A least square fit is applied to the curves obtained, the values of  $K$  ( $K$  is the extrapolated value of  $N/i_s$  for  $N=0$ ) is determined and the dead-time for the various counting channels is calculated.

Although many correction computer programs are available to the microprobe users<sup>10</sup>, the complexity of most of them and the impossibility to access a large computer may discourage to use them. The purpose of the present work is to offer a series of simple programs that, although by no means will offer the highest accuracy for all analytical conditions and range of elements<sup>11</sup>, will however help the every day analyst in correcting electron probe intensities in most of the practical problems.

- 
1. B.J. Mitchell, Advances in x-ray analysis Vol.II Plenum Press, New York 1968 p.132.
  2. J. Philibert, Metaux Corrosion Ind. 40: 325 1964.
  3. T.O. Ziebold, Lecture Notes, Massachusetts Institute of Technology, Summer Session, 1965, S-5.
  4. G. Moreau and D. Calais, J. Phys. Radium 25: 83 A, 1964.
  5. D.B. Wittry, Advances in x-ray Analysis Vol.7 Plenum Press, New York 1963 p.404.
  6. K.F.J. Heinrich, D. Vieth and H. Yakowitz, Advances in x-ray analysis, Vol.9, Plenum Press, New York, 1965, p.208.
  7. S.J.B. Reed, British J. Appl. Phys. 16, 913 (1965).
  8. P. Ducumb and P.K. Shields, T.D. McKinley, K.F.J. Heinrich and D. B. Wittry eds.) "The Electron Microprobe", John Wiley and Sons Inc, New York 1966 p.284.
  9. P. Ducumb and S.J.B. Reed, Tube Investment Research Laboratory Technical Report N.221 (1967).
  10. D.R. Beaman and J.A. Isasi, from Proceeding Fourth National Conference on Electron Microprobe Analysis, Pasadena, California, 1969.
  11. D.R. Beaman, Analytical Chemistry 39, 419 (1967).

## ELECTRON PROBE ANALYSIS OF THIN FILMS

W. Reuter

IBM Thomas J. Watson Research Center, Yorktown Heights, New York 10598

In spite of various approximations made in the theory, quantitative microprobe spectroscopy has become a reality, provided the sample is homogeneous and larger in dimension than the probing beam. When the sample is thin in comparison to the range of the electrons in the target, a special case arises in the quantitative treatment of the data. Colby<sup>1</sup> suggests a solution to this problem, if the total mass deposition  $\rho x$  is known. Philibert and Tixier<sup>2</sup> propose a model, permitting the determination of the composition of a film, provided energy losses in the film are negligible, restricting the applicability of this model to very thin films. G. Hutchins<sup>3</sup> discussed a method for the determination of film thicknesses, requiring the experimental determination of a normalization factor.

In this paper we propose a method for thin film analysis permitting the determination of the mass deposition  $\rho x$  over a wide range. In the absence of secondary excitation and disregarding the discontinuity in the backscatter properties at the interface we have:

$$K = \frac{f(\lambda)_{\text{Film}} \int_{E_I}^{E_0} \frac{Q}{S} \cdot dE}{f(\lambda)_{\text{STD}} \int_{E_C}^{E_0} \frac{Q}{S} \cdot dE} \quad (1)$$

where  $k$  is the measured intensity ratio and  $E_I$  the energy at the interface.  $f(\lambda)_{\text{Film}}$  is calculated<sup>1</sup> by substitution of  $E_C$  by  $E_I$ . For thin films  $f(\lambda)_{\text{Film}}$  can also be approximated by  $\exp(-\mu \cos \theta \rho x / 2)$ . The value of  $E_I$  is determined by successive numerical integration of Eq. (1) until the observed value of  $k$  is reached within 0.1%. This value of  $E_I$  is then used to determine  $\rho x$  via an appropriate range equation. When we used high overvoltages Colby's<sup>1</sup> range equation gave values for  $\rho x$  which are in good agreement with separate measurements (e.g., interferometry, tallysurf, chemical analysis) of  $\rho x$ . For overvoltages less than two Bethe's equation gave the best agreement. The mass deposition of a large variety of films was determined by this technique and agrees within 10% with the data obtained by other methods. Composite films can also be analyzed, provided the mass deposition  $\rho x_{\text{Film}}$  is small in comparison to the total range. Most films analyzed were deposited on low atomic number substrates. Work is presently in progress, testing the reliability of this approach when high atomic number substrates are used. Particularly for thin films a further refinement of the calculation may be required by substituting<sup>3</sup>

$$\int_{E_I}^{E_0} \frac{Q}{S} dE \quad \text{by} \quad (1 + A\eta) \int_{E_I}^{E_0} \frac{Q}{S} dE$$

to account for enhancement due to backscattering.

1. J. W. Colby, Advances in X-Ray Analysis (Plenum Press, N. Y., 1968), vol. 11, p. 287.
2. J. Philibert and R. Tixier, Brit. J. Appl. Phys., Ser. 2, Vol. 1, 685 (1968).
3. G. A. Hutchins, The Electron Microprobe (John Wiley & Sons, Inc., N. Y., 1966), p. 390.



# SOME PROBLEMS IN THE DETERMINATION OF VALENCE STATE OF IRON USING Fe L X-RAY EMISSION SPECTRA

D.G.W. Smith and R.K. O'Nions  
University of Alberta, Edmonton, Canada

Details of Fe L<sub>II</sub>, L<sub>III</sub> X-ray emission spectra from metal and several oxides have been investigated using operating voltages between 1.5 & 30 KV. Simple measurement of the L<sub>II</sub> & L<sub>III</sub> peak heights gives erroneous values for the Fe L<sub>II</sub>/L<sub>III</sub> intensity ratio, but more accurate values are obtainable by integrating techniques in which total energy under the L<sub>II</sub> & L<sub>III</sub> peaks is determined (Fig. 1). Differential self-absorption effects on the relative intensities of the L<sub>II</sub> & L<sub>III</sub> bands are extreme, requiring a correction factor greater than 900% at 30 KV for Fe metal. Of several formulae applied to make the absorption corrections, those of Theisen (1966) and Heinrich (1967) appear to give the most consistent results, although none stand up completely to this extreme test. Uncertainties in the mass absorption coefficients of Fe, O, and Ti etc. for the wavelengths of the L<sub>II</sub> and L<sub>III</sub> bands contribute significantly to the errors involved in making the corrections; those coefficients derived from the formulae of Kelly (1966) appear most satisfactory. However, for Fe metal, the true value of the Fe L<sub>II</sub>:L<sub>III</sub> ratio appears to be near 0.5 at all operating voltages (Fig. 1). This value corresponds to that expected theoretically (e.g. Compton & Allison, 1935), but differs from values hitherto reported (e.g. Andersen & Wittry, 1968).

Uncorrected and absorption corrected integrated intensity ratios for a number of Fe & Fe-Ti oxides are shown in figs. 2, 3. Corrections were made using Heinrich's (1967) formula and Kelly's (1966) mass absorption coefficients. Corrected ratios show a general increase with operating voltage, tending to level off at high KV. Other correction formulae (e.g. Theisen, 1966) give qualitatively similar results. Notwithstanding uncertainties in the correction formula and mass absorption coefficients, increases in the ratios with operating voltage are undoubtedly real.

In oxides the Fe 3d electrons are involved in bond formation with the oxygen ligand. Thus it is more realistic to consider features of their Fe L spectra in terms of molecular orbital theory (Ballhausen and Gray, 1964). For octahedral complexes, the  $\pi^b$  t<sub>2g</sub> and  $\sigma^b$  e<sub>g</sub> molecular orbitals (symmetry consistent with dipole selection rules) are largely filled with oxygen 2p electrons, whereas the more localized antibonding  $\sigma^*$  e<sub>g</sub> and  $\pi^*$  or non-bonding t<sub>2g</sub> orbitals will be occupied only by Fe 3d electrons. Some features of the L<sub>II</sub>:L<sub>III</sub> spectra may be easily explained if the L<sub>II</sub> band results from transitions from antibonding molecular orbitals (MO) and the L<sub>III</sub> band results, in part, from transitions from bonding MO's. Some change in the L<sub>II</sub>:L<sub>III</sub> ratio with operating voltage is to be expected since the O K spectrum could arise from bonding orbitals with the same wave function. The probability of the MO → O K transition should be greater than the MO → Fe L<sub>III</sub> transition (see Reed, 1965) and the intensity of the Fe L<sub>II</sub> band might increase at a slower rate than that of the L<sub>III</sub> band with increasing KV. Atomic number effects would tend to enhance this divergence, due to differences in stopping power for Fe and O.

These results are particularly significant in attempts to determine  $\text{Fe}^{2+}:\text{Fe}^{3+}$  ratios in minerals. In simple series (such as ilmenite-hematite) it will not be important to take absorption and bonding effects into consideration, since variation in the uncorrected value of the Fe LII:LIII intensity ratio can be used as an indication of the position of a particular specimen in a solid solution series (Albee & Chodos, 1969). However, little will be gained from such a procedure since the specimen composition can be deduced, probably more accurately, by straightforward microprobe analysis and assumption of stoichiometry. Since, at the present time, corrections cannot be made for effects dependent upon the presence of O-ligands, it is highly unlikely that the Fe-oxidation state for more complex solid solutions can be deduced from measurements of L X-ray emission spectra obtained at a single KV.

1. ALBEE, A.L., & CHODOS, A.A., 1969, Proc. IVth Nat. Conf. Electron Microprobe Analysis, pp. 32.
2. ANDERSEN, C.A., & WITTRY, D.B., 1968, Brit. J. Appl. Phys (J. Phys. D). Ser. 2, 1, pp. 529-540.
3. BALLHAUSEN, C.J., & GRAY, H.B., 1964, Molecular orbital theory (New York: Benjamin).
4. COMPTON, A.H., & ALLISON, G.K., 1935, X-rays in theory and experiment. (New York: Van Norstrand), 838 pp.
5. HEINRICH, K.F.J., 1967, Trans. 2nd Nat. Conf. Electron microprobe Analysis, Boston 1967. (Boston: Mass. Inst. Tech).
6. KELLY, T.K., 1966, Inst. Min. and Metal., 75. B59-B71.
7. REED, S.J.B., 1965, Brit. J. Appl. Phys., 16, pp. 913-926.
8. THEISEN, R., 1966, X-ray optics and microanalysis (Castaing, Deschamps & Philibert, Eds), (Paris: Hermann), pp. 224-229.

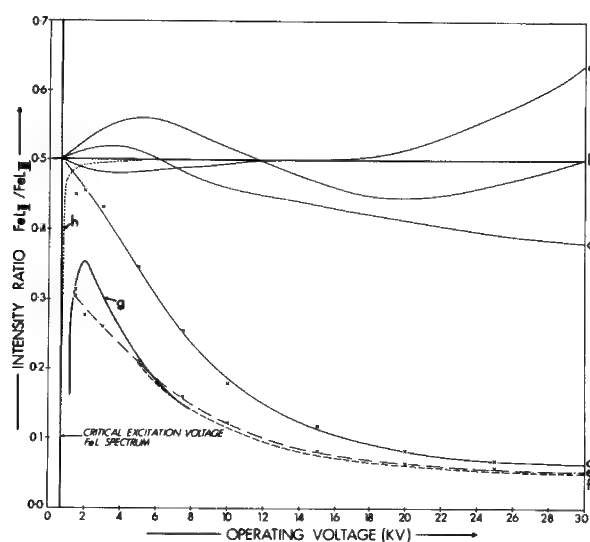


Fig. 1. Fe LII:LIII intensity ratios for Fe metal corrected and uncorrected for absorption. Corrected integrated intensity ratios: a = Theisen formula & fitted  $\mu/\rho$ , b = Heinrich formula & Kelly  $\mu/\rho$ , c = Andersen & Wittry formula and  $\mu/\rho$ . Uncorrected ratios: d = integrated intensity ratios and e = peak height ratios (this study); peak height ratios: f = Andersen & Wittry (1968) and g = Fischer (1965). h = theoretical attenuation of 0.5 ratio due to different  $E_{LII}$ ,  $E_{LIII}$ .

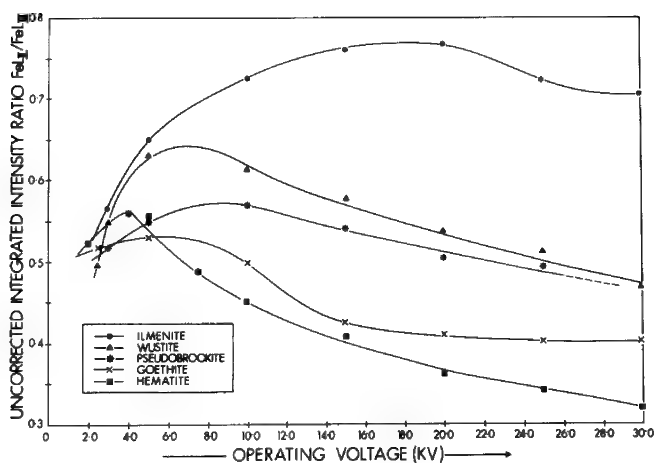


Fig. 2. Integrated Fe  $L_{II}:L_{III}$  intensity ratios from 2.0 - 30.0 KV for hematite, wustite, goethite, ilmenite and pseudobrookite.

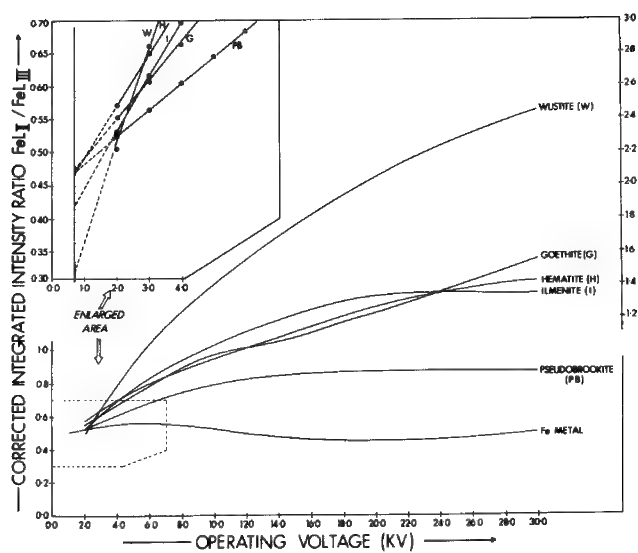


Fig. 3. Absorption corrected Fe  $L_{II}:L_{III}$  integrated intensity ratios for hematite, wustite, goethite, ilmenite and pseudobrookite using heinrich formula and Kelly  $\mu/\rho$ . Extrapolation of corrected ratios to critical excitation voltage inset (N. B. data points are values read from corrected curves).

# THE SIMULTANEOUS DETERMINATION OF CALCULATED CONCENTRATIONS IN QUANTITATIVE ELECTRON MICROPROBE ANALYSIS

D. R. Beaman and R. Klimpel  
The Dow Chemical Company, Midland, Michigan

In quantitative electron microprobe analysis the chemical composition,  $C_A$ , is usually calculated from the measured x-ray intensity ratio,  $k_A$ , using the ZAF expression

$$C_A = k_A \left( \frac{F(O)^0}{F(O)'} \right) \left( \frac{f(\chi)^0}{f(\chi)'} \right) \left( \frac{1}{(1+\rho)} \right) \quad (1)$$

where the three terms in brackets represent the atomic number, absorption and characteristic fluorescence correction factors respectively. The superscripts, prime and zero, refer to the unknown and standard material respectively. For each species in the system there is a corresponding Eq. 1. Forty computer programs are now available for converting  $k$  to  $C$  because the analytical expressions involved are lengthy and some of the parameters are functions of concentration. In this report, three computational methods used to solve for  $C_A \dots C_n$  are compared with a new method.

Many programmers assume a set of concentrations (usually based on the experimental  $k$  values), evaluate the functions that are concentration dependent ( $F(O)'$ ,  $f(\chi)'$  and  $\rho$ ), and obtain  $C_A$  from Eq. 1. A method of successive iteration is employed (e.g. Wegstein) to promote convergence until the assumed and calculated values of  $C_A$  differ by a negligible amount. The same procedure is used to determine  $C_B \dots C_n$  but the previously calculated values of composition are not utilized in subsequent steps, i.e., the series of  $n$  equations ( $n$ =number of components) are solved independent of each other. There are three objections to this approach: 1) the concentrations of the unanalyzed elements are not properly partitioned; 2) there is no guarantee of system convergence; 3) the equations are not solved simultaneously. When the calculated values of concentrations (the best available at the moment) are used in later calculations and the entire sequence repeated until convergence is attained, (1) these objections are partially overcome.

Some authors have attempted to circumvent these difficulties by assuming that the concentration variables were separable. Zeller et al. (2) use a series of  $n$  equations of the form

$$\ln k_i - \ln C_i - \sum_{j=1}^n C_j \ln G_{ij} = 0 \quad (2)$$

where  $G_{ij}$  is not a function of concentration but is determined from ZAF expressions evaluated for an infinitely dilute  $ij$  alloy ( $C_i \rightarrow 0$ ,  $C_j \rightarrow 1$ ). The  $n$  equations are solved simultaneously using a Newton gradient technique. Mathematically this approach is rigorous, but physical assumptions are necessary in the development of Eq. 2. This type of approach is utilized because of the difficulty involved in calculating the derivatives of the functions represented by the parameters in Eq. 1. The solution of a series of simultaneous equations using the Newton technique requires first partial derivatives of the function. Powell(3) has described a method for finding the function minimum without the use of derivatives and Klimpel(4) has incorporated this into a program which will solve a set of  $n$  simultaneous nonlinear equations without resorting to first partial derivatives. The physical significance of Eq. 1 is retained and a truly simultaneous solution is obtained. The calculated values are unique and convergence is guaranteed. The program is efficient, e. g., six seconds computation time on a Burroughs 5500 system, is required for a six component system.

The data in the table illustrates the usefulness of the technique. Compositions were assumed in two alloy systems and the probe x-ray intensity ratio,  $k$ , was calculated in a single step calibration process ( $k$  from  $C$ ) using Eq. 1. The calculated  $k$  values in column 3 were then used in the classical correction scheme described above ( $C_A \dots C_n$  from Eq. 1 in individual steps) to obtain the calculated concentrations in column 4. The same  $k$  values were used in the newly suggested program to calculate the concentration values in column 7. The optimized  $C$  values are in excellent agreement with the originally assumed concentrations, while some of the classical  $C(\text{calc})$  values are considerably different. The correction scheme used consisted of the Duncumb and Reed atomic number correction, the Duncumb and Shields absorption correction and the Reed characteristic fluorescence correction. The take-off angle was  $18^\circ$ , the acceleration potential was 15kV and Heinrich's mass absorption coefficients were utilized.

- 
1. J. Bomback, private communication (1969), U. S. Steel Research Center, Monroeville, Pennsylvania.
  2. C. Zeller, J. Babkine, J. C. Reither, J. Bolfa and F. Zeller, Bull Acad. et Soc. Lorraines des Sciences 8, 122 (1969).
  3. M. Powell, The Computer Journal 7, 155 (1964).
  4. R. Klimpel, Computation Research Laboratory Report, The Dow Chemical Company, Midland, Michigan (1970).

## COMPARISON OF RESULTS OBTAINED WITH CLASSICAL AND OPTIMIZATION PROGRAMS

<u>System</u>	<u>CLASSICAL</u>				<u>OPTIMIZATION</u>		
	<u>C</u>	<u>k(calc)</u>	<u>C(calc)</u>	<u>Iterations</u>	1st assumed C value	<u>C(calc)</u>	<u>Iterations</u>
Mg	41.0	11.0	41.0	4	33.3	41.0	
Gd	55.0	42.7	54.4	4	33.3	55.0	5
Sn	4.0	2.8	3.7	4	33.3	3.8	
Fe	48.0	40.2	49.0	5	20.0	48.1	
Cr	22.0	21.6	21.4	6	20.0	22.2	
Ni	18.0	12.8	18.2	3	20.0	18.0	6
Mo	9.0	5.3	8.7	3	20.0	9.0	
Si	3.0	0.7	2.9	3	20.0	2.9	

# AN INVESTIGATION OF ELECTRON PROBE MICROANALYSIS CORRECTIONS IN Ni-Co BINARY ALLOYS

G. L. Fisher, International Nickel Co., Inc.  
Sterling Forest, N. Y.

Archard and Mulvey(1) were the first to suggest that an appreciable atomic number effect should sometimes be observed when analyzing binary alloys of elements adjacent in the periodic table. In order to observe the atomic number effect there must be significant differences in the  $Z/A$  ratios between the two elements. Ranzetta and Scott(2) were able to verify the atomic number effect for copper in nickel-copper alloys (atomic numbers 29 and 28) although the scatter in their data made an evaluation of the correction procedures impossible. Another correction that must be considered when analyzing elements adjacent in the periodic table is due to secondary fluorescence of  $K_{\alpha}$  radiation by  $K_{\beta}$  radiation.

The present investigation measured the magnitude of the atomic number and  $K_{\beta} - K_{\alpha}$  secondary fluorescence corrections when analyzing elements adjacent in the periodic table. The nickel-cobalt binary alloy system was chosen because of the significant difference in the  $Z/A$  ratios of nickel and cobalt and because the alloys show little tendency to segregate(3). In addition, this combination of elements is found in many alloys of commercial importance. Eight nickel-cobalt binary alloys (five nickel-rich and three cobalt-rich) were vacuum induction melted from 99.9% pure materials. Each ten-pound ingot was hot rolled to one-half inch bar and the middle three feet retained for wet chemical analysis and electron probe microanalysis. After additional hot and cold working each alloy was given a homogenizing anneal at 1800°F for 1000 hours. At least two separate wet chemical analyses were performed on the alloys with the results shown in Table I.

The alloys were analyzed in an ARL EMX-SM microanalyzer operating at accelerating voltages of from 10 to 30 KV. Intensities were limited to less than 10,000 cps to minimize effects of detector dead-time. Pulse height analysis was used and counting was terminated on a fixed value of beam current which limited drift to 1.0% or less. K-ratios were calculated after correcting the raw intensities for dead-time and background. Each reported K-ratio is the average of five separate determinations taken at random on the specimen. The homogeneity of the alloys was excellent. The standard deviation of the five determinations was less than 1% in all cases.

The results of the microanalysis of the high cobalt alloys is shown in Figure 1 where the percent relative error of each analysis is plotted versus accelerating voltage. The percent relative error is given by:

$$\frac{\text{measured composition} - \text{true composition}}{\text{true composition}} \times 100$$

The measured composition is the experimentally determined K-ratio. K-ratios were also calculated from the true compositions using the Modified Philibert absorption correction(4) and the Philibert and Tixier atomic number correction(5). The percent relative error calculated from these K-ratios is shown by the solid line in Figure 1. Notice that nickel, because of its greater stopping power, has a positive relative error. The measured percent relative error for nickel is greater than the calculated value at the lower nickel levels. Therefore the above correction schemes do not entirely correct for the error in the cobalt-rich alloys.

The results of the microanalysis of the high nickel alloys are shown in Figure 2. The cobalt analyses should show a negative relative error because of the lower stopping power of cobalt. However secondary fluorescence of the  $\text{CoK}\alpha$  line by  $\text{NiK}\beta$  radiation causes the relative error to become positive. The calculated percent error derived from the above corrections and the Reed secondary fluorescence correction(6) is also shown in Figure 2. Note that these corrections do not entirely correct for the error. Reasons for this discrepancy will be discussed.

#### REFERENCES

1. G. D. Archard and R. Mulvey, Brit. J. Appl. Phys., 14, 626-34, 1963.
2. G. V. T. Ranzetta and V. D. Scott, Brit. J. Appl. Phys., 18, 1403-1406.
3. M. Hansen, Constitution of Binary Alloys, (McGraw-Hill Book Co., New York, New York) 485-487, 1958.
4. P. Duncumb and P. K. Shields, The Electron Microprobe, ed. T. D. McKinley, K. F. J. Heinrich and D. B. Wittry, (J. Wiley and Sons, Inc., New York, New York) 284-95, 1966.
5. J. Philibert and R. Tixier, Brit. J. Appl. Phys., 1, No. 2, 685-94, 1968.
6. S. J. B. Reed, Brit. J. Appl. Phys., 16, 913-26, 1965.



TABLE I  
CHEMICAL ANALYSES OF THE Ni-Co BINARY ALLOYS

<u>Average Chemical Analysis</u>	<u>Results of Individual Chemical Analysis</u>
	Wt. % Nickel
2.86% Ni, bal Co	2.83, 2.89
5.81% Ni, bal Co	5.79, 5.82
9.52% Ni, bal Co	9.50, 9.54
12.44% Ni, bal Co	12.46, 12.41
14.21% Ni, bal Co	14.22, 14.19
	Wt. % Cobalt
4.93% Co, bal Ni	4.89, 5.00, 4.95
11.05% Co, bal Ni	10.93, 11.12, 11.10
17.63% Co, bal Ni	17.52, 17.64, 17.74

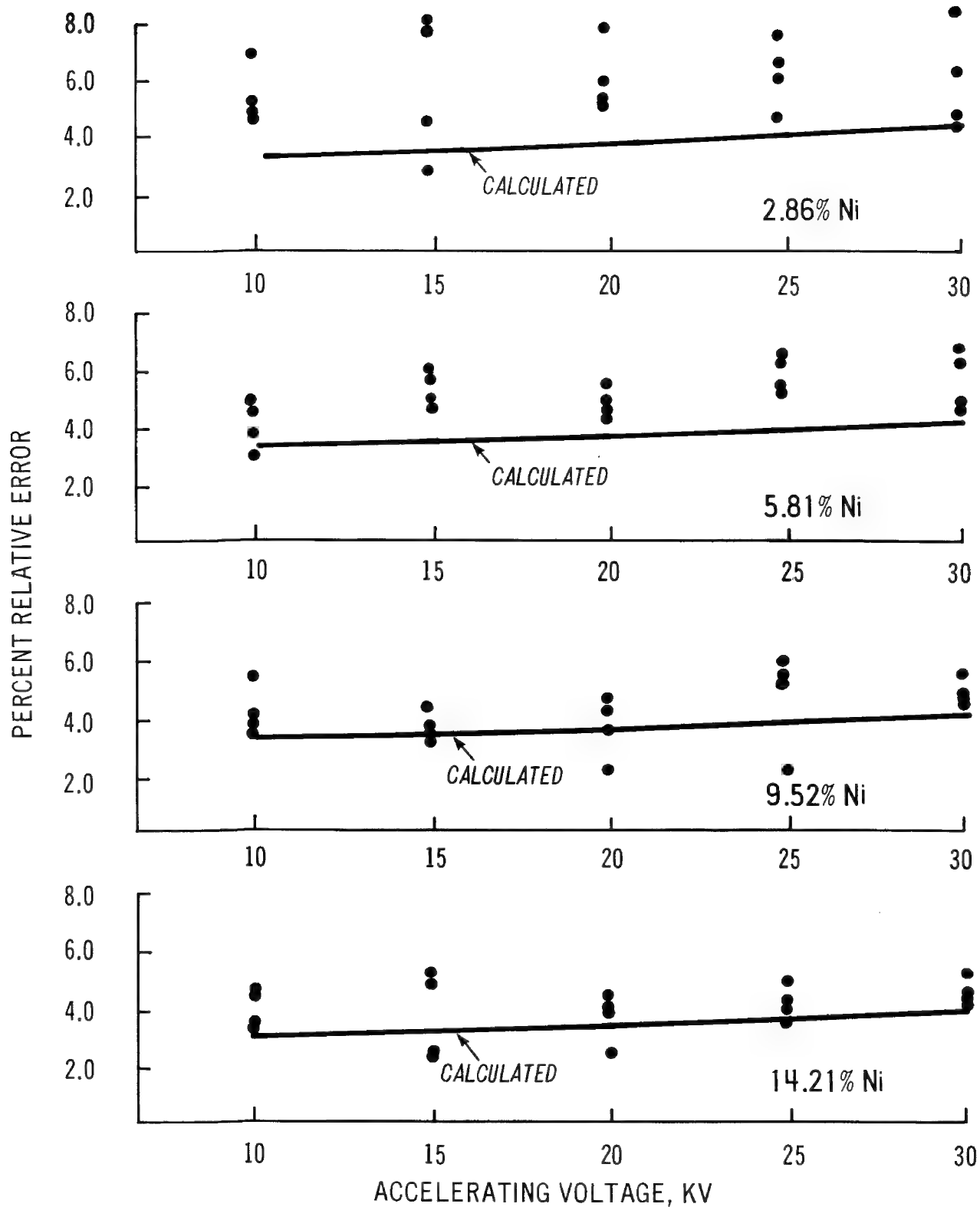


FIGURE 1 - PERCENT RELATIVE ERROR VS. KV FOR THE HIGH Co ALLOYS.

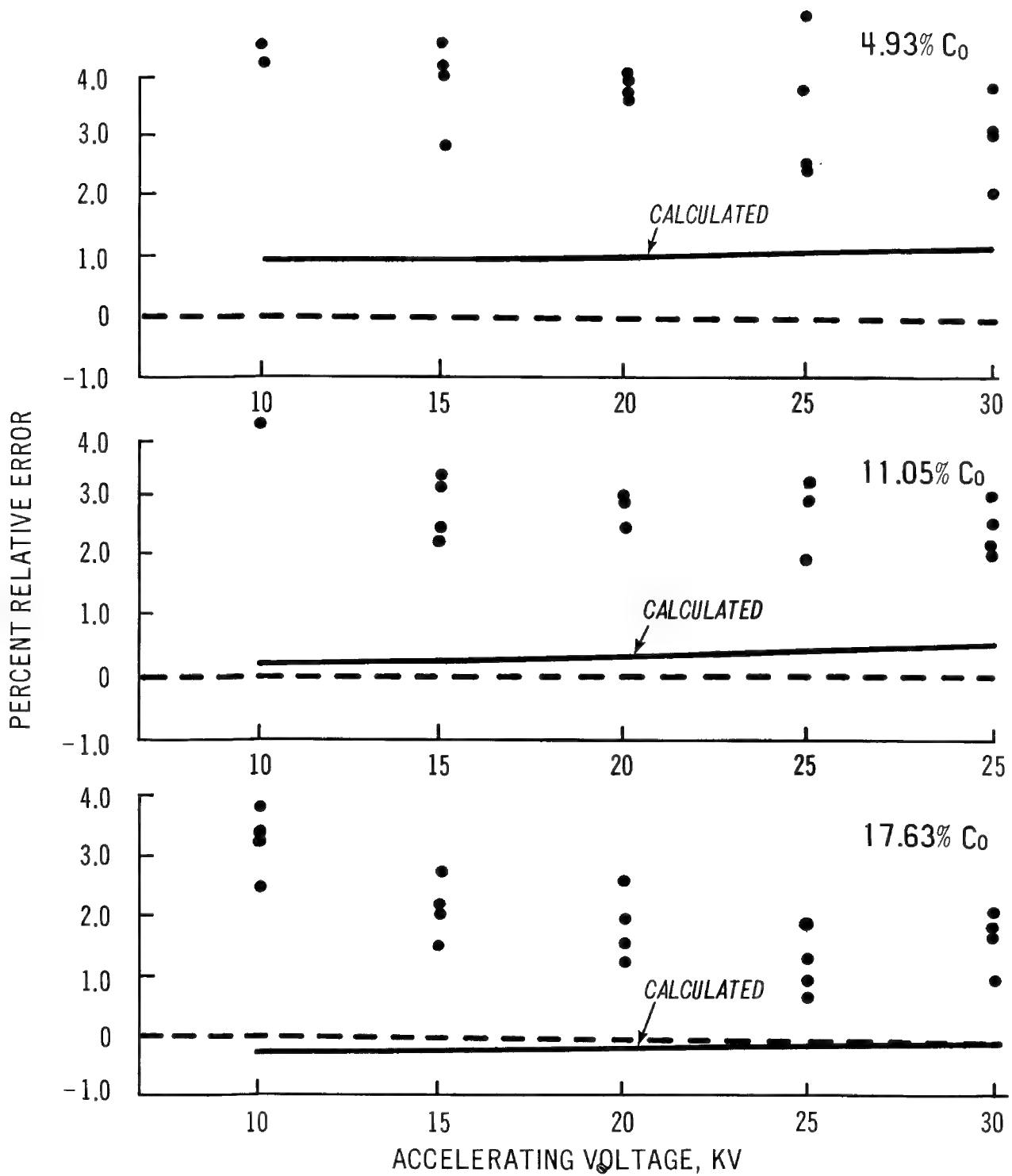


FIGURE 2 - PERCENT RELATIVE ERROR VS. KV FOR THE HIGH Ni ALLOYS.

AN EVALUATION OF THE PHILIBERT-TIXIER ATOMIC  
NUMBER CORRECTION FOR AU-CU BINARY ALLOYS

P. J. Walitsky  
Westinghouse Electric Corp.  
Bloomfield, New Jersey

J. W. Colby  
Bell Telephone Laboratories  
Allentown, Pennsylvania

Three copper-gold binary alloys were analyzed by the Metropolitan Section of the Electron Probe Analysis Society of America, to evaluate the effectiveness of the Philibert-Tixier<sup>1</sup> atomic number correction as included by Colby in version 3 of his 'MAGIC' computer program.

The alloys, Au-20Cu, Au-50Cu, and Au-80Cu, were prepared at Engelhard Industries, Newark, New Jersey. Each of the alloys was melted and drawn to wire having a diameter of .020 inches. Each material was chemically analyzed and certificates of assay were supplied. Members of the Section received two samples of each material, separated by a distance of about three feet along the wire. This provided a check on the long range homogeneity of the material. The subsequent microprobe analyses indicated that both the long and short range homogeneity were satisfactory.

The specimens were analyzed by 9 laboratories using microprobes from five different manufacturers, and having x-ray take-off angles ranging from 15.5 degrees to 52.5 degrees. The majority of the analyses were made at 20.0 keV, although one laboratory made analyses at 22.5 keV, and one laboratory made the analyses at 25.0 keV. Copper  $K\alpha$ , and gold  $L\alpha$  were the lines used for the analyses, and one laboratory also used the gold  $M\alpha$  line. The absorption correction employed, was that of Philibert<sup>2</sup>, as modified by Duncumb and Shields<sup>3</sup>, and further modified by Heinrich<sup>4</sup>. The fluorescence correction employed, was that of Reed<sup>5</sup>. These corrections were used in conjunction with both the atomic number corrections of Duncumb and Reed<sup>6</sup>, and Philibert and Tixier<sup>1</sup>, as contained in versions 2 and 3 of 'MAGIC'.

The data are summarized in Table I, and show that a significant improvement in the copper results occurred through the use of the Philibert-Tixier atomic number correction. In all three alloys, the microprobe results were in agreement with the chemical assay to within 2.5% relative to the amount present. However the results obtained through the use of the Duncumb-Reed correction deviated by as much as 8% from the chemical assay. It is apparent that the use of the Philibert and Tixier atomic number correction in version 3 of 'MAGIC' is justified, and results in a significant improvement in accuracy when the elements analyzed differ widely in atomic number.

TABLE I

## COMPARISON OF RESULTS FOR COPPER - GOLD BINARY ALLOYS

	Chemical Assay	Average Duncumb-Reed	Average Philibert-Tixier	Differences	
				D-R	P-T
Cu	19.97	18.4	19.6	-1.6	-0.4
Au	<u>80.02</u>	<u>79.5</u>	<u>80.5</u>	-0.5	+0.5
Total	99.99	97.9	100.1		
Cu	49.88	45.8	48.7	-4.1	-1.2
Au	<u>50.10</u>	<u>49.8</u>	<u>50.5</u>	-0.3	+0.4
Total	99.98	95.6	99.2		
Cu	79.92	77.2	80.0	-2.7	+0.1
Au	<u>20.06</u>	<u>20.4</u>	<u>20.0</u>	+0.3	-0.1
Total	99.98	97.6	100.0		

- 
1. J. Philibert and R. Tixier, B. Jour. App. Phys., 1, (1968), p. 685.
  2. J. Philibert, X-Ray Optics and X-Ray Microanalysis, Academic Press, (1963), p. 379.
  3. P. Duncumb and P. K. Shields, The Electron Microprobe, John Wiley & Sons, (1966), p. 284.
  4. K. F. J. Heinrich, Proceedings of the 2nd National Conference on Electron Microprobe Analysis, (1967) paper number 7.
  5. S. J. B. Reed, B. Jour. App. Phys., 16, (1965), p. 913.
  6. P. Duncumb and S. J. B. Reed, Quantitative Electron Probe Analysis, NBS Special Publication 298, (1968), p. 133.

## APPLICATIONS OF SCANNING ELECTRON MICROPROBES TO SOLID STATE ELECTRONICS

D. B. Wittry

Departments of Materials Science and Electrical Engineering  
University of Southern California, Los Angeles, Calif. 90007

---

In recent years, there has been a merging of the fields of electron probe microanalysis and scanning electron microscopy. The electron probe microanalyzer originally developed by Castaing and Guinier as an instrument for point-to-point quantitative analysis was transformed into a scanning x-ray microscope by the addition of scanning techniques by Duncumb and Cosslett. More recent developments have provided improved resolution and capabilities for using other signals such as secondary electron emission, cathodoluminescence, electron beam induced currents, etc.

In a parallel fashion, early scanning electron microscopes emphasized only one type of signal information, in this case, secondary electron emission. However, modifications over the past several years have added capabilities for detection of additional signals and there has been increased emphasis on obtaining quantitative information. Thus, in principle, these two instruments are capable of providing the same type of information.

In this review paper we will give examples of investigations on materials and devices for solid state electronics using electron probe microanalysis or scanning electron microscopy. These applications will cover a variety of materials including metals, semiconductors, and insulators and also materials with interesting ferroelectric, piezoelectric and ferromagnetic properties. The applications will be discussed in terms of the kind of information derived from the measurement, i.e. composition, topography, crystal structure, crystal orientation, crystal defects, properties of excess carriers, electronic band structure and local variations in electric or magnetic fields.

The problems of quantitative analysis of materials for solid state electronics are similar to those encountered in applications to metallurgy, geology and glass technology, i.e. effects due to atomic number, chemical bonding, damage or changes produced by the beam, specimen charging, and difficulties imposed by the limits of detectability of electron probe x-ray microanalysis. Additional problems may also be present because of special geometries, for example thin film structures.

Because the problems of quantitative analysis are common to many fields of application, this paper will emphasize applications in which signals other than characteristic x-ray lines are used. These signals include electron beam induced currents, secondary electrons, Auger electrons, cathodoluminescence and optical reflectance. Applications reported during the past two years will receive major attention.

## REVIEW OF METALLURGICAL APPLICATIONS OF THE

## ELECTRON MICROANALYZER

by

Robert E. Ogilvie

The electron microanalyzer has been applied to a wide variety of metallurgical studies since its development by Castaing<sup>1</sup>. The ability to measure the chemical composition of any predetermined area 1  $\mu$  in diameter has enabled the metallurgist to analyze problems that here-to-fore were essentially impossible to deal with. This unique method of analyzing minute quantities of material immediately suggested many new applications in other fields. This cross fertilization with the geologist, biologist, and other fields has been extremely fruitful.

The metallurgist has applied the electron microanalyzer to the study of diffusion, phase diagrams, segregation, precipitation and of course the study of meteorites. Many other applications could be discussed but these mentioned make up a large portion of the papers published in metallurgical journals.

In most of these studies the metallurgist is interested in quantitative analysis and this is where we meet with a variety of approaches with which we may use to analyze the data. In all of the instruments it is easy to obtain intensity data from the unknown specimen and variety of standards, correct these for backgrounds, and feed this information into a computer. Here is where the metallurgist has nightmares. He must not only keep up with the literature but he must assess these techniques for converting the X-ray data into chemistry. The factors that limit the accuracy of this extremely precise instrument lie not only in the correction procedures but the "uncertainty" in the factors that must be used in the expressions used in the correction procedures.

In spite of the shortcomings in the correction procedures, the metallurgist has been able to solve many problems. However, we must admit that with the advent of the scanning X-ray images we were able to produce qualitative information which was more than adequate to solve many problems.

It is interesting to note that in the late 50's and early 60's we were developing energy dispersion techniques with the gas flow proportional X-ray detector, now we are using the solid state lithium-compensated silicon detector. It is my opinion that this new technique has many advantages and will be used almost exclusively in the next few years. The principle advantage of this new technique is the simultaneous analysis of the entire spectrum of radiation emitted by the sample. The analysis time is cut to a few minutes. There are disadvantages of course and all factors

---

1. R. Castaing, Ph.D. Thesis, University of Paris (1957).



must be considered. However, because of the time, simplicity and ease in which the data can be sent to the computer, the metallurgist will be able to handle new problems that up until now he found too time consuming.

## QUANTITATIVE MEASUREMENT OF TRANSFERRED SURFACE MATERIAL

J. Aronstein, International Business Machines Corp.

G. Judd, Rensselaer Polytechnic Institute

W. E. Campbell, Rensselaer Polytechnic Institute

With the electron microprobe measurement is made of the quantity of material transferred from a spherical lead specimen contacted to a gold flat specimen. These material transfer measurements are important to an investigation of the effects of lubrication on friction, wear and electrical behavior of low-energy microcontacts.

Using a scanning beam and constant specimen current while accumulating lead  $M_{\alpha_1}$  X-ray counts, all portions of the area under study are uniformly exposed to the incident electrons. With a fine raster line spacing relative to the size of the beam at the specimen surface, uniformity of exposure is essentially independent of the actual beam size and electron density distribution within the beam.

Figure 1 shows lead transferred to a gold flat specimen as a result of contact with a 0.025 cm diameter lead spherical specimen at 10 grams normal force and with 0.0025 cm relative tangential motion. The contact spot, about 0.0075 cm in diameter, is completely contained within the scanned area at 1000x magnification with the particular instrument used. On this instrument it has been determined experimentally for the conditions of this investigation that no loss of X-ray detection sensitivity results from off-center beam positioning to the extremes of the scanned area for magnifications above 700x and that there is no difference in counting rate on a thin-film lead-on-gold specimen between scanning-beam operation at 700x or above and fixed-beam operation anywhere within the scanned region.

Given uniform exposure to the incident electrons over the area of interest and uniform detection sensitivity for X-rays emitted from any point within that area, the lead  $M_{\alpha_1}$  counts accumulated above the background counts should be directly related to the amount of transferred lead on the flat-specimen surface provided that the thickness of the lead particles or film is small compared to the penetration of the incident electrons and provided that self-absorption of emitted X-radiation is negligible. To determine the particle or film thickness for which these conditions hold a set of gold specimen was prepared with evaporated lead films of different thickness. Figure 2 shows the counting rate, above background, for lead  $M_{\alpha_1}$  versus film thickness. The intensity is proportional to the amount<sup>1</sup> of lead on the surface to

within 10% for films up to 0.3 microns and to within 20% for films up to 0.5 microns with the 25kv beam accelerating potential. The 25kv accelerating potential was selected to optimize uniformity of incident electron exposure throughout the volume of transferred material.

Counts are accumulated for the area of interest, an adjacent unused area of the flat specimen, and for one of the thin-film standards. The quantity of lead in the transfer spot is determined as:

$$w = \frac{C_X - B}{C_O - B} t_O \rho A$$

where  $w$  = wt of lead in the area of interest  
 $t_O$  = thickness of lead on the calibration standard  
 $\rho$  = density of lead  
 $C_X$  = counts accumulated in time  $T$  on the area of interest  
 $C_O$  = counts accumulated in time  $T$  on the thin-film standard  
 $B$  = counts accumulated in time  $T$  on a substrate area known to be free of transferred lead.  
 $A$  = scanned area

The counts  $C_X$ ,  $C_O$ , and  $B$  are taken in fairly rapid sequence to minimize any effect of instrument drift. No effect of change in scanning rate is seen provided that either the counting time is an integral multiple of the raster scanning time or the number of raster scans during the counting time is large.

By this method, the amount of lead transferred in the contact spot shown in Figure 1 was determined to be about  $200 \times 10^{-12}$  gram. Measurements on the same spot on various days yielded values of 184, 228, and  $214 \times 10^{-12}$  gram.

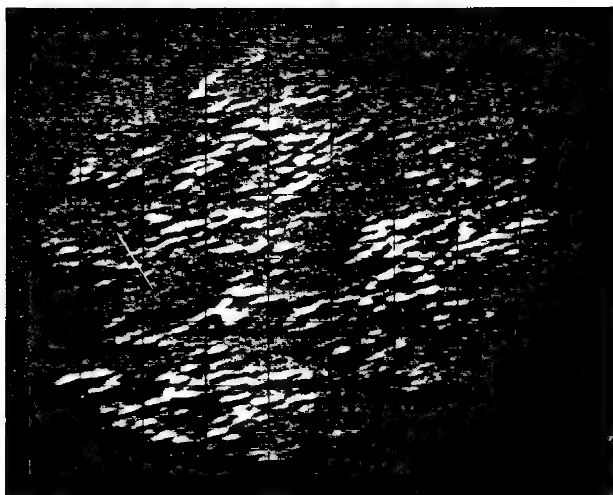


FIGURE 1 - TYPICAL CONTACT SPOT

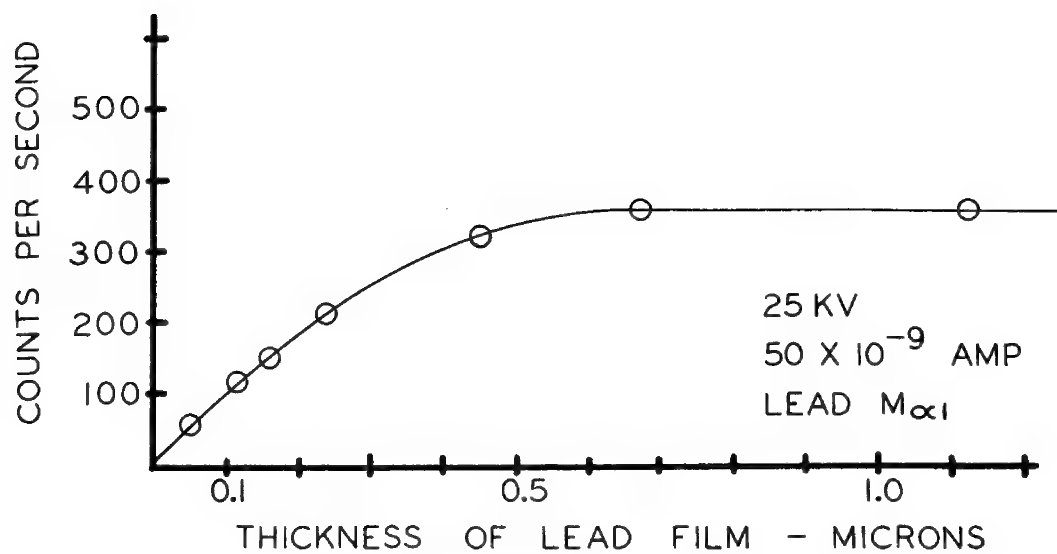


FIGURE 2 - FILM THICKNESS VS.  
COUNTING RATE

AN INVESTIGATION OF THE SOLUTE DISTRIBUTION IN  
THE GRAIN BOUNDARY REGION IN AN Al-Zn-Mg ALLOY

C. R. Shastry, Rensselaer Polytechnic Institute  
G. Judd, Rensselaer Polytechnic Institute

The published work on the Al-Zn-Mg alloy system relating to precipitation has been mainly concerned with the correlation of precipitate distribution with the stress corrosion behavior. Formation, during ageing, of anodic paths by solute impoverishment around grain boundaries was one of the earliest explanations for stress corrosion susceptibility of these alloys. The purpose of the present investigation is to determine the nature of solute distribution around the grain boundaries in an Al-Zn-Mg alloy as a function of heat treatment.

An Al-Zn-Mg alloy sheet, 50 mil thick, and of average composition 6.8% Zn, 2.3% Mg, balance Al was used. Specimens of suitable size for microanalysis were cut from the sheet and solutionized at 478 ( $\pm 2$ )°C for 3 hrs. after which they were quenched into brine (10% NaCl solution), water and air at room temperature. The brine quenched specimen was aged at room temperature for 54 days whereas the water quenched and air cooled specimens were aged at 200 ( $\pm 3$ )°C for 4 hrs. Specimens for microanalysis were prepared by the usual metallographic techniques. For easy identification, the grain boundaries were marked using a microindentation hardness tester. All the specimens were examined in the flat, polished condition. Spectrographically pure aluminum, zinc and magnesium were used as standards.

Materials Analysis Company microanalyser model 400S was used for analysis. Point counts were taken across the grain boundary region, scanning two or three boundaries for each specimen. In order to extend the narrow region around the grain boundary, each scan was made along a straight line inclined at an acute angle to the boundary. This method is similar to that used by Clark<sup>1</sup>. A computer program was used to correct the raw microprobe x-ray intensity data for dead time losses, background, absorption, characteristic fluorescence and atomic number effects. The distribution of Zn and Mg for the three different heat treatments is shown in Figs 1, 2, and 3. The specimen aged at room temperature (Fig. 1) shows a significant segregation of Zn and Mg to the grain boundary. The solute profile of the air cooled specimen (Fig. 2) shows a narrow solute impoverished region adjacent to the grain

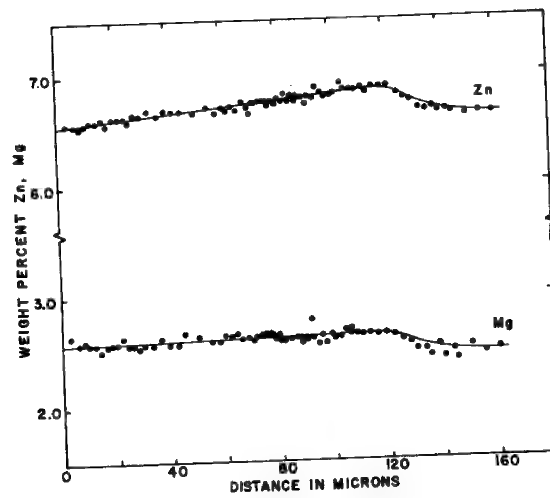


Fig. 1 Solute profile at 15° angle across grain boundary.  
Al-Zn-Mg alloy, brine quenched and aged at 27°C for 54 days.

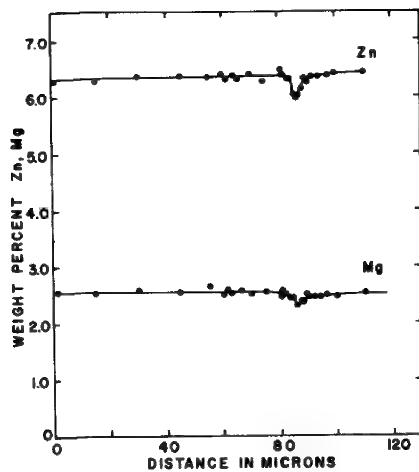


Fig. 2 Solute profile at 43° angle. Air cooled and aged at 200°C for 4 hrs.

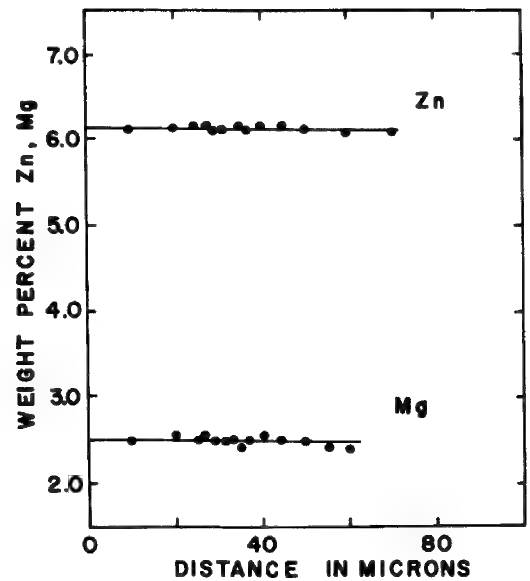


Fig. 3 Solute profile at 27° angle water quenched and aged at 200°C for for hrs.

boundary. No depletion or segregation of solute is seen in the specimen which was water quenched and aged at 200C (Fig. 3).

Reference:

1. Clark, J. B., Acta met. vol. 12, 1197. (1964)

## DIFFUSION ENHANCEMENT EFFECTS IN EXPLOSION WELDED METALS

Lucien F. Trueb

Denver Research Institute, Metallurgy and Materials Science Division,  
University of Denver, Denver, Colorado 80210

Continuous and practically diffusionless welding of an almost unlimited variety of metals can be achieved by explosively impacting plates under such conditions that the material forming the colliding surfaces is ejected forward in the form of a jet. High-velocity impact thus brings uncontaminated surfaces within interatomic distances, which results in solid-state metallurgical bonding. During this process, the metals are subjected to forces exceeding their dynamic elastic limit and behave like viscous fluids; this explains the characteristic wavy profile of explosively welded interfaces which is reminiscent of an eddy lane (1), (2). Localized melting and alloy formation can occur in discrete spots along the weld and particularly in the center of the vortices found beyond the crest of the waves; this latter effect is attributed to adiabatic heating of trapped air pockets. However, most of the bond is normally free of diffusion effects, despite the high temperatures that are generated in the collision front. This is due to the extreme rapidity of the bonding process and the fact that deformation is limited to a zone less than 100  $\mu\text{m}$  wide. It has been shown that explosively welded interfaces are characterized by an abrupt transition from one metal to the other, the boundary itself being a continuous surface which has many of the characteristics of a grain boundary (3). The very large shear stresses induced along the plate-collision front causes strong grain elongation and the formation of a symmetrical pattern of subgrains in the bonding direction (3).

Annealing of explosively welded metals results in thermally induced diffusion and the formation of alloy zones and intermetallic compounds. These processes appear to be significantly enhanced by the very high density and anisotropic distribution of dislocations, pressure-induced twins and other types of lattice defects which are present in the immediate vicinity of the interface. In order to gain an understanding of these processes, a microprobe study of explosion welds before and after a series of heat treatments was undertaken in the instance of the systems nickel to copper, copper to steel and tantalum to steel. These couples cover the cases of unlimited mutual solubility (Ni-Cu), very limited mutual solubility (Cu-Fe) and the formation of an intermetallic compound (Ta-Fe).

In the nickel-copper system, the diffusion penetration resulting from heat treatments between 500 and 950°C was measured by means of microprobe traverses and compared to the diffusion penetration produced in copper electroplated to nickel that had been subjected to the same heat treatments. Table 1A shows that a distinct diffusion enhancement occurs in the explosively welded specimens; this effect is particularly strong at the nickel wave tops. The diffusion penetration was also determined for both the explosion welded and electroplated couple within the 7.5 to 11.8 at.% nickel concentration range for which Jost (4) has published the diffusion coefficients. Figure 1 shows that the D-values obtained from these data plotted vs.  $1/T$  are significantly higher for



the explosion-welded metals than for the similar electroplated system. The two plots appear to merge at the melting point of copper.

Heat treatment of ETP copper explosion welded to A212B steel mainly resulted in intergranular diffusion and segregation of nearly pure iron and copper crystallites in the copper and steel respectively. This process was investigated by electron microscopy in its early stages; after heat treatment at 1000°C the phase segregation could also be readily observed in electron probe area scans such as Figure 2. Large iron particles in the copper were always found at the top of the steel waves, while only small crystallites were found in the valleys. This is indicative of cyclical variations of the nature and density of lattice defects along the weld interface which significantly affect the diffusion kinetics.

Because of the high melting point of tantalum, the effects caused by heat treatment of tantalum explosion welded to A201B steel are very slight even at relatively high temperatures. No diffusion effects were observed at 500°C; at 840°C a 0.1 to 0.2  $\mu\text{m}$  wide band of a high-tantalum alloy was observed by electron microscopy. At 1100°C the concentration profile across the bond zone indicated the presence of the intermetallic phase  $\text{TaFe}_2$ . In this instance too, the diffusion zone was significantly thicker near the top of the steel waves than at other locations along the weld interface. The average values are given in Table 1B.

The present investigation shows that diffusion is enhanced in a cyclically variable manner by the high density of defects characterizing the bond interface of explosively welded metals. The specific microstructural effects resulting from diffusion depend on the type of phase diagram to which the individual metal pairs belong.

#### References

1. COWAN G.R. and HOLTZMAN A.H. J.Appl.Phys. 34, 1928 (1963)
2. LUCAS W., WILLIAMS J.D. and CROSSLAND B. Proceedings, Second International Conference of the Center for High Energy Forming, Estes Park, Colorado, 2, 8.1.1 (1969)
3. TRUEB L.F. Trans. Met.Soc.AIME 262, 1057 (1968)
4. JOST W. Diffusion in solids, Liquids, Gases. Academic Press 218 (1952)

TABLE 1A

Width of diffusion zone for nickel explosively welded and electroplated to copper after various heat treatments

Temp. (°C)	Time (hr)	Diffusion Zone Width (μm)		
		Explosively Welded		Electroplated
		Ni Wave Trough	Ni Wave Top	
500	1	10.8	11.3	10.8
	4	16.1	16.3	14.7
	16	20.8	21.6	19.5
750	1	23.1	24.9	19.9
	4	31.1	35.4	25.0
	16	55.8	57.9	48.7
950	1	72.0	78.3	61.2
	4	97.4	98.8	77.7
	16	146.5	161.6	120.8

TABLE 1B

Width of diffusion zone for tantalum explosively welded to steel after various heat treatments

Temp. (°C)	Time (hr)	Average Diffusion Zone Width (μm)
500	1	< 1
	4	< 1
	16	1.2
840	1	2.0
	4	5.0
	16	8.3
1100	1	8.0
	4	14.6
	16	33.8

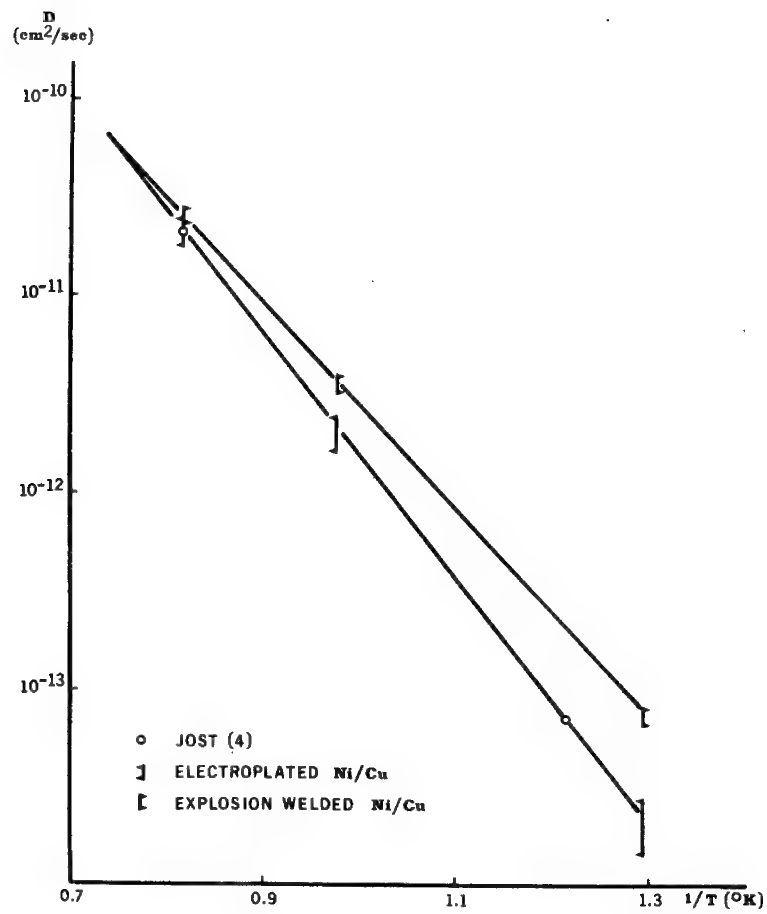


Fig.1. Diffusion coefficient vs.  $1/T$  for nickel electroplated and explosion welded to copper for the 11.8 to 7.5 at.% Ni concentration range.

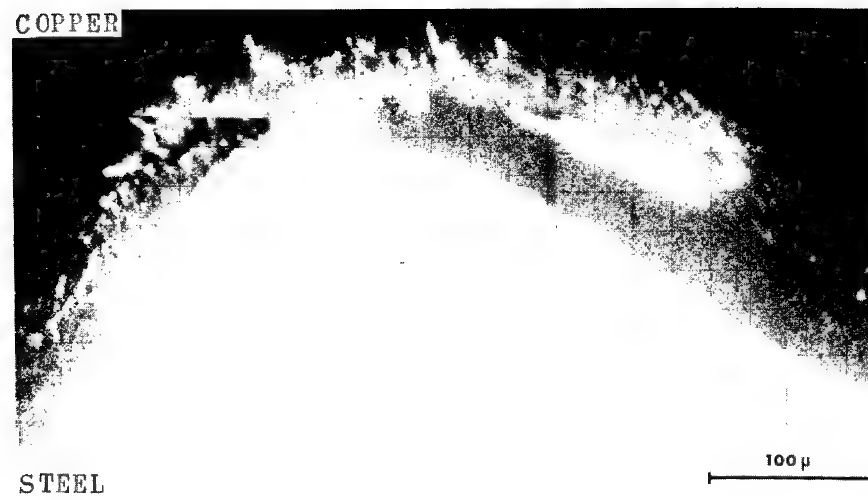


Fig.2. Fe K $\alpha$  area scan mosaic showing copper to steel explosion bond area after 16 hr at 1000°C.

TECHNIQUES FOR THE DETERMINATION OF INTERACTION  
PRODUCTS OF PLUTONIA-URANIA NUCLEAR FUEL WITH SODIUM\*

T. E. Lannin and H. S. Rosenbaum

General Electric Company, Vallecitos Nuclear Center  
Pleasanton, California

G. F. Melde

General Electric Company, Breeder Reactor Development  
Operation, Sunnyvale, California

This report presents preliminary results of techniques used in the analysis of sodium-fuel interaction products. Additional work is in progress. The techniques used in sample preparation with a non-aqueous media will be discussed along with the steps taken to minimize the sample's exposure to the atmosphere.

A section from an experimental pin was examined using a shielded microprobe for sodium-fuel interaction products, plutonium, and uranium gradients. In this pin the cladding had failed during operation so that sodium entered the pin and was in contact with the fuel. The encapsulated fuel pin contained (0.2 Pu, 0.8 U) $O_{2.03}$  fuel and attained  $\sim 6$  at.% burnup in the Experimental Breeder Reactor II with a maximum linear power rating of 16 KW/ft. (Figure 1). The uranium portion of this fuel pin was fully enriched (93% U-235). This section was received in excellent condition as a result of the extra efforts and techniques used in sample preparation. The assymetry of the central void apparently occurred as a result of the ingress of the sodium coolant. Figure 2 indicates plutonium, uranium, and Pu/(Pu + U) gradients along the radii examined. The non-symmetric plutonium and uranium distribution (Figure 2) could, in part, be accounted for if a significant central void existed prior to failure and the failure caused a mass transfer of uranium and plutonium. The relative intensity of the Pu-M $\beta$  line was determined and calibrated against a pure PuO $_2$  standard. The relative intensity of the U-M $\alpha$  line was determined and calibrated against a pure UO $_2$  standard. In addition, (U $_{0.8}$ , Pu $_2$ )O $_2$  standard was used to check the mixed oxide system. The Pu/(Pu + U) ratio was determined as follows:

$$\frac{\frac{I_{\text{Pu Sample}}}{I_{\text{Pu Standard}}}}{\frac{I_{\text{Pu Sample}}}{I_{\text{Pu Standard}}} + \frac{I_{\text{U Sample}}}{I_{\text{U Standard}}}} \times 100$$

where: I = intensity

The ratio Pu/(Pu + U) can be in error because it does not account for the uranium and plutonium atoms which have fissioned.

---

\* Work performed under the auspices of the United States Atomic Energy Commission on Contract AT(04-3)-189, PA-10.

In analyzing for Na in a matrix of very heavy atoms, the following difficulties are encountered:

1. The mass absorption of the Na-K $\alpha$  x-ray is very high, and the absorption coefficient in heavy elements is not known with certainty.\*
2. High current densities have to be used to achieve a statistically significant x-ray intensity.
3. Surface contamination effects are severe.
4. Well characterized standards are difficult to obtain.

In item 3 the surface contamination is aggravated by high beam current; this causes local heating and possible vaporization as well as deposition of hydrocarbons at a high rate. The absorption of Na-K $\alpha$  by carbon cannot be ignored.

Despite these difficulties, the early results clearly showed that the sodium-fuel interaction product(s) in the microstructures shown in Figure 1 is of variable Na content. However, at this time it is not yet certain whether the observed interaction product(s) are compounds or are simply an admixture of oxidized Na in varying proportions in the fuel. Experiments to characterize these phases in the fuel by x-ray diffraction are in progress.

The Pu/(Pu + U) ratio in the reaction product was found to remain relatively constant, although both species were found in lesser quantity in the interaction product than the matrix material. It is significant that no partitioning of the uranium and plutonium occurred. Very little information is available on sodium-plutonium and sodium-mixed oxide systems.

Two of the three techniques used to indicate the variation of sodium content of the mixed oxide fuel are illustrated in Figure 3. The lighter areas of the negative specimen current image indicates a localization of lighter elements (Na and O). The intensity trace indicates the relative distribution of sodium (Figure 3). The third technique used was the x-ray image which indicated the relative distribution of uranium and sodium.

### References

1. Birks, L. S., "Electron Probe Microanalysis", Inter-Science Publishers, 1963, p. 201.
2. Heinrich, K.F.J., "X-Ray Absorption Uncertainty", Published in "The Electron Microprobe", John Wiley & Sons, 1960, edited by McKinley, T. D., Heinrich, K.F.J., Wittry, D. B.
3. Lauritzen, T., "Compatibility of Urania-Plutonia Fuels with Stainless Steel and Sodium", GEAP-5633, June, 1968.

---

\*For example, the mass absorption coefficient of Na-K $\alpha$  x-rays passing through uranium is shown by Birks<sup>(1)</sup> to be 7000(?). Other references (e.g. Heinrich<sup>(2)</sup>) do not even quote a coefficient for absorption of Na-K $\alpha$  by U or Pu.

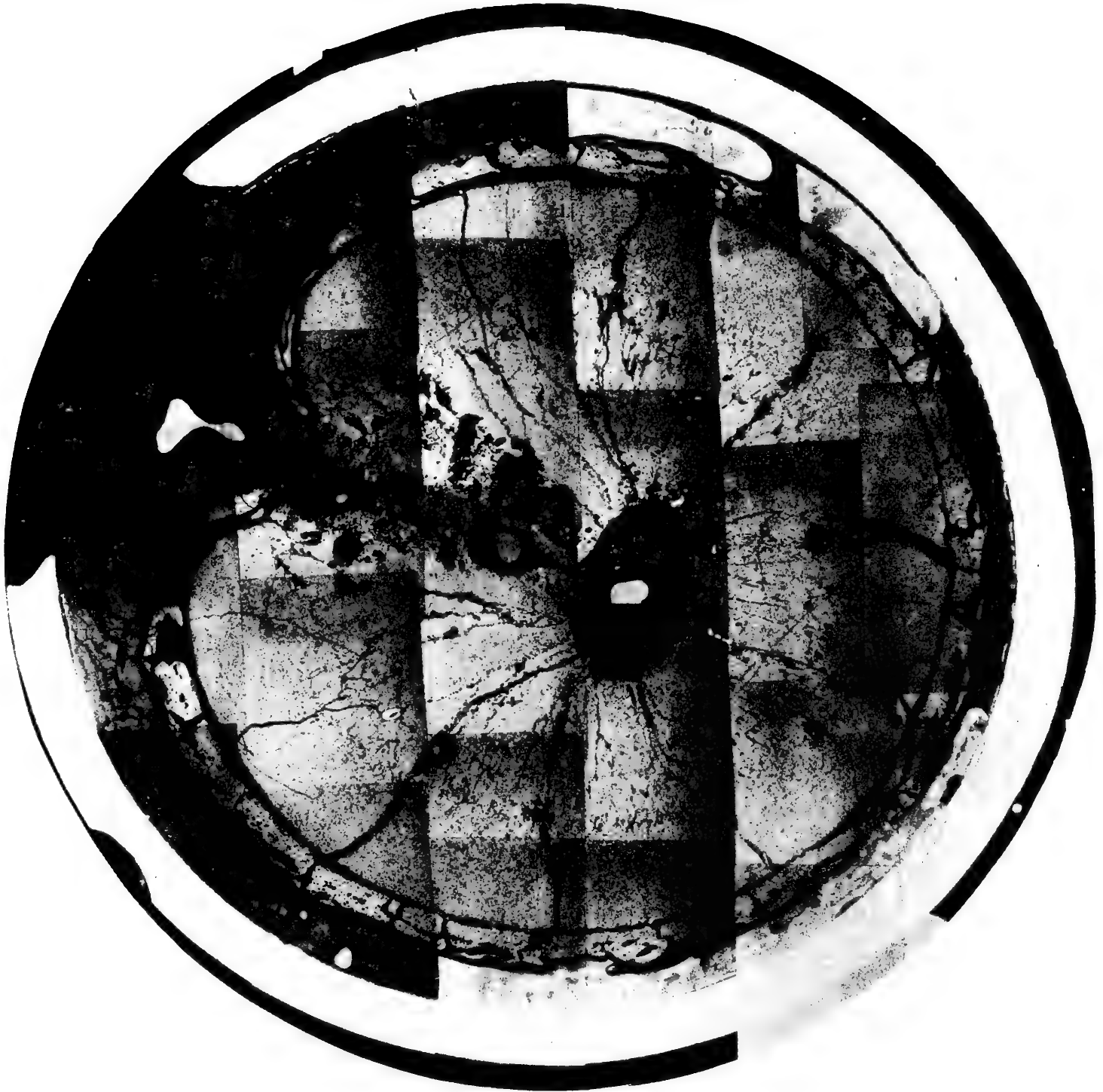


FIGURE 1. CROSS-SECTION OF IRRADIATED FUEL EXAMINED

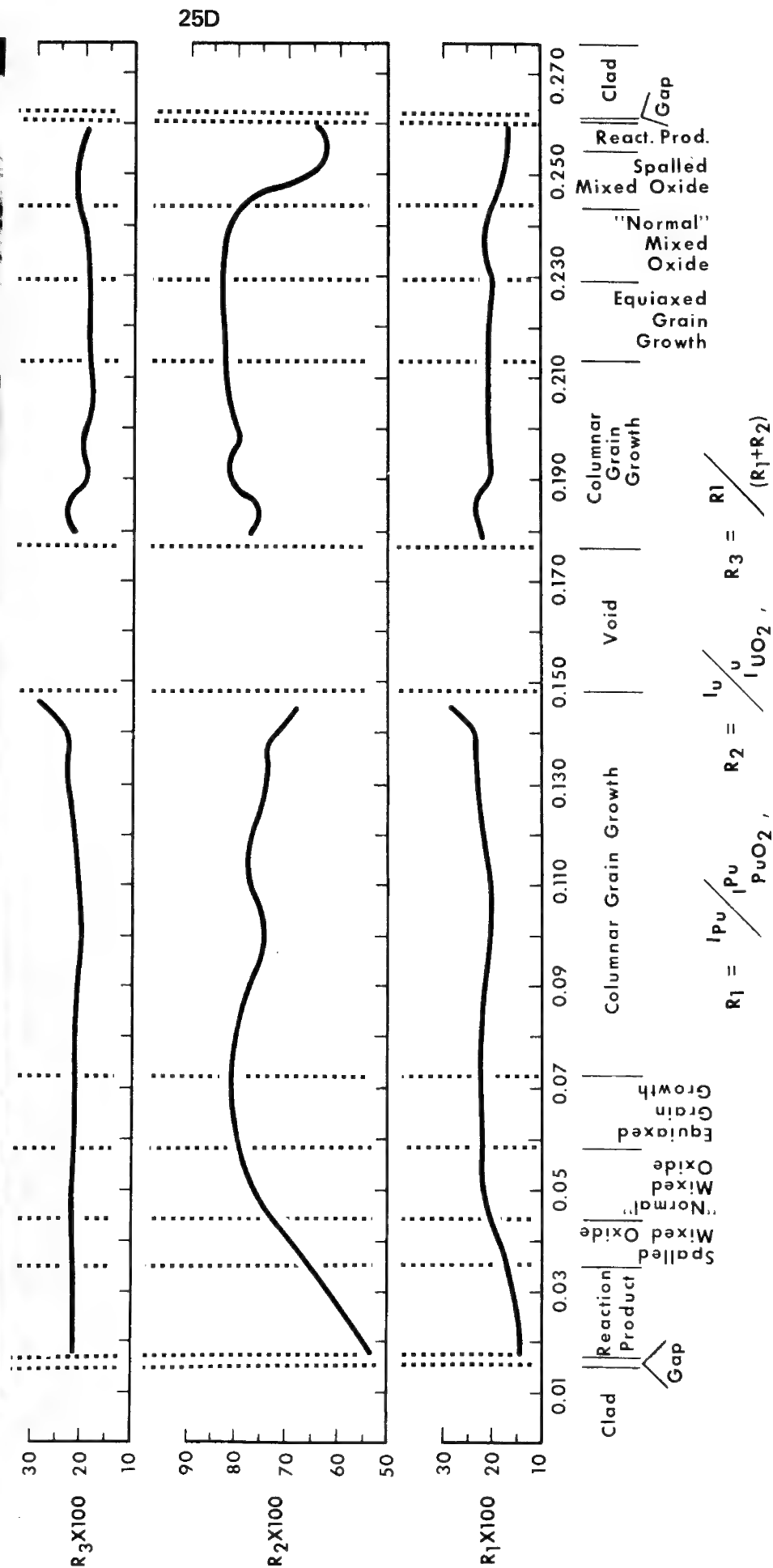


FIGURE 2. VARIATION OF THE INTENSITY RATIOS FOR U, Pu AND Pu/U+Pu AS A FUNCTION OF THE RADIAL POSITION FOR SAMPLE 1a



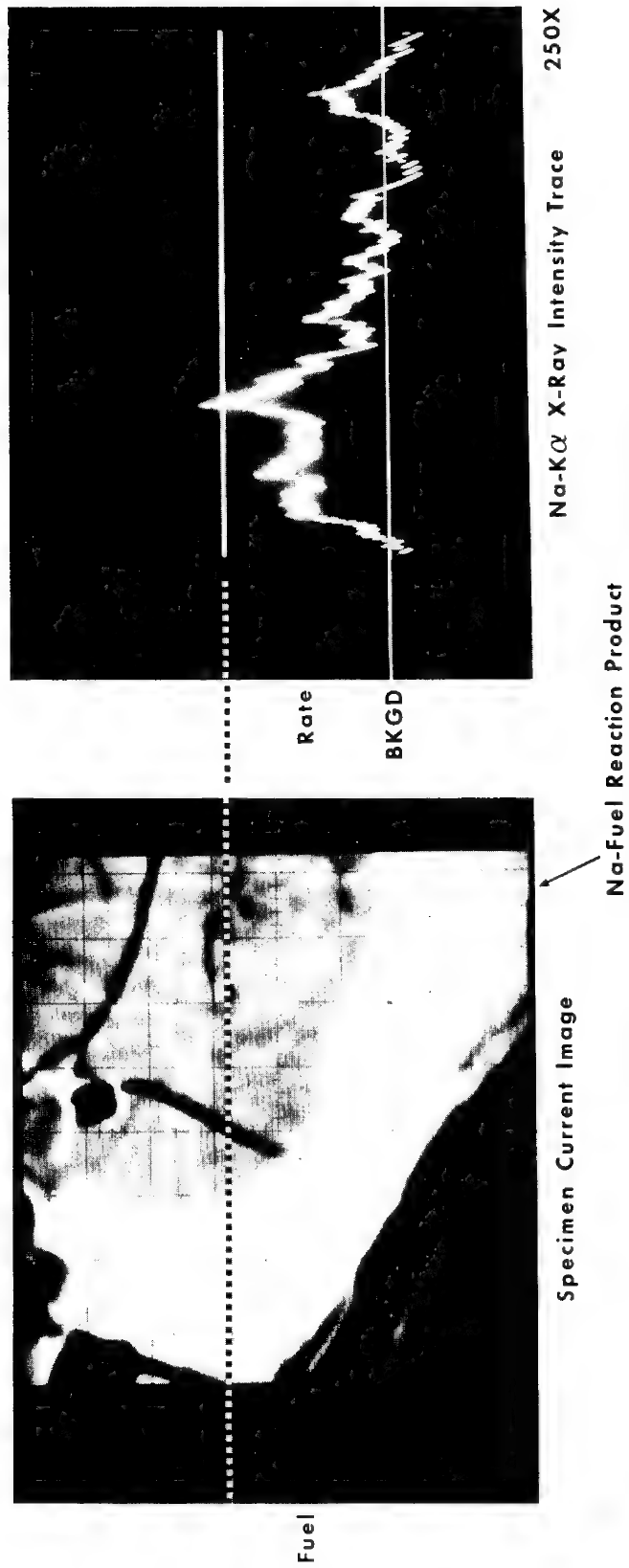


FIGURE 3. COMPARISON OF THE SPECIMEN CURRENT IMAGE TO THE Na-K $\alpha$  X-RAY INTENSITY OF A PARTICLE OF FUEL AT THE CLAD OPENING

## LOCAL COMPOSITIONS IN DENDRITIC STRUCTURES

H. M. Pielet, Graduate Student, Department of Metallurgy and Materials Science, Massachusetts Institute of Technology.

A. J. Saffir, Director of Biological Instrumentation Research, Materials Analysis Company.

J. F. Elliott, Professor, Department of Metallurgy and Materials Science, Massachusetts Institute of Technology.

In a study of the effect of convection in the remaining liquid on the dendritic structure of an alloy, an experimental method has been developed (1) which allows detailed examination of the liquid and solid regions as they coexist during solidification. A thin ingot of liquid Al-4.5% Cu alloy is frozen slowly causing dendrites to grow parallel to the broad faces of the mold. A rapid quench on these faces converts the liquid around the dendrites into a solid consisting of very fine dendrites.

The prepared surface of a section through the quenched ingot is examined by the electron microprobe to determine both local and average compositions in various areas and the curve of concentration vs. fraction solid. Data are obtained using interval counting with continuous motion of the sample. The method for taking the data and the use of a computer for interpreting them constitutes a new method of applying the probe.

Figure 1 is a photomicrograph of a section of one of the ingots showing the location of the probe trace. The liquid regions just at the time of quench are clearly indicated because of their very fine structure. The determining characteristics of the specimen are the variation of copper concentration from approximately 1 per cent at the center of the dendrite arms to 33 per cent in the interdendritic eutectic, and the variation in the dendrite arm spacings, i.e., from 70 $\mu$ m in the large dendrites to 15 $\mu$ m in the quenched liquid.

Because of the size of the beam spot and the much larger dimensions of the dendrite arms, it is necessary to average the results across the dendrite arms and the adjacent eutectic. The sample, therefore, is moved at a constant velocity,  $V$ . The counts are accumulated

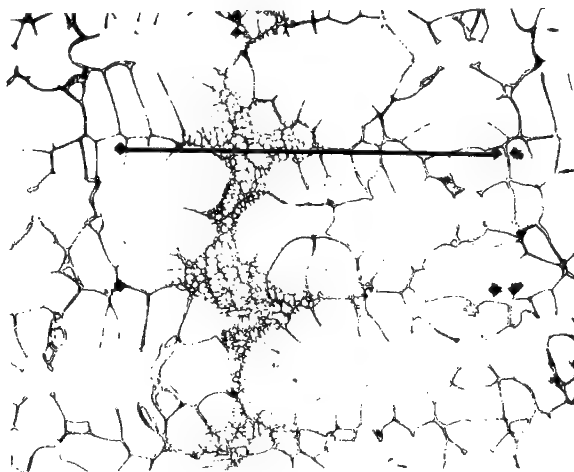


Fig. 1 Section of ingot partially solidified and then quenched showing fine dendritic structure obtained in liquid regions. Magnification 50 times.

for a time interval,  $t_c$ , during which the sample is displaced a distance  $V \cdot t_c$ . The results are printed in the time interval,  $t_p$ , and counting is resumed. The fraction of the sample counted along the trace is  $f_c = t_c / (t_c + t_p)$ . The sample moves about 9.5 microns in each interval.

The data are keypunched for processing by the computer. Each value is converted to relative copper intensity and a plot is made, Fig. 2 (top), giving a chart of composition vs. distance with only slight loss of the structural details. The spacings of the maxima on this curve reflect the nature of the structure, and their locations correspond to visual observations of the interdendritic eutectic (the dark lines in Fig. 1).

The first use of the data is to separate the values for each region and, with a density correction, to compute the average relative intensity of copper in the liquid and solid regions. The results show rejection of copper into the liquid region.

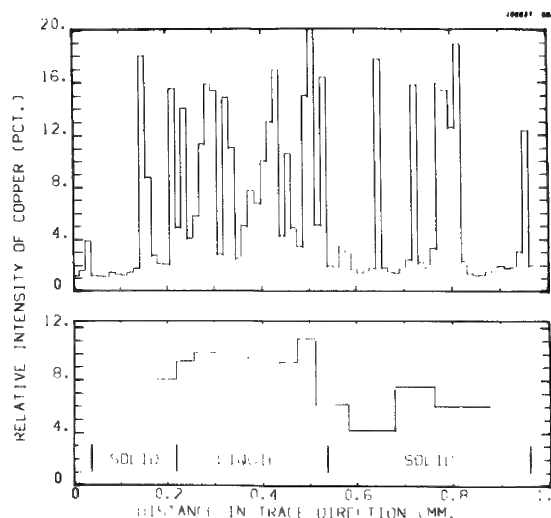


FIG. 2. COMPARISON OF ORIGINAL DATA WITH DATA AVERAGED BETWEEN TWO DENDRITE ARMS. TOP DATA AS OBTAINED. BOTTOM MOVING AVERAGE OF DATA VALUES BETWEEN TWO MAXIMA.

The second treatment is to obtain the local composition by computing the average of all of the data within two adjacent dendrite arms. By developing an algorithm for determining maxima in the original curve, which mark the separation between dendrite arms, it is possible to calculate on the computer a moving average over two dendrite arms at a time, as shown in Fig. 2 (bottom). There is a marked change in local average composition at the solid-liquid interface.

A third use of the same data is to obtain a curve of relative intensity vs. weight fraction solid. This is done simply by reordering the data from lowest to highest relative intensity and plotting them as a function of the fraction solid (2). The entire curve is higher in the liquid region, indicating that the copper concentration was greater in the liquid throughout freezing.

In sum, a simple method has been developed for obtaining by computer several different types of information from a single continuous probe trace across a highly segregated dendritic region. In particular, the use of computational algorithm to define structural regions of varying size and to search for solute gradients by averaging highly segregated dendritic regions is unique to this study.

1. H. M. Piolet, Ph.D. Thesis, Massachusetts Institute of Technology, 1970.
2. P. J. Ahearn, Ph.D. Thesis, Massachusetts Institute of Technology, 1966.

# ELECTRON MICROPROBE STUDY OF THE ROLE OF DIFFUSION IN THE ADHESION OF COPPER TO NICKEL

Gilbert H. Walker and Beverley W. Lewis  
National Aeronautics and Space Administration, Hampton, Virginia

Metal surfaces exposed to the environment of outer space may lose their oxide and adsorbed gas coatings. If two such unprotected surfaces come into contact, they may cold weld or adhere. Previous studies of adhesion of metals have consisted mainly of measuring the strength of the couple. (See for example References 1, 2.) The purpose of the present investigation is to study the role of diffusion in the adhesion of copper to nickel in an effort to understand the mechanism of adhesion.

Copper and nickel samples were machined from 99.999% pure metals such that the test surface of the copper sample was 1/4 inch diameter and the test surface of the nickel sample was 1/8 inch in diameter. These samples were polished, cleaned with solvents, and installed in a vacuum chamber at  $10^{-9}$  torr. The samples were then cleaned of their surface contaminants at  $10^{-6}$  torr by use of an ion bombardment and heating technique. The relative work function of the metal surfaces was measured after each cleaning cycle by a retarding field diode technique (Reference 3). The surfaces were assumed to be clean when the relative work function was no longer changing with increased number of cleaning cycles. The clean samples were then contacted at a known force and heated rapidly (in less than one minute) by electron bombardment to the desired test temperature. After one hour at this temperature the samples were separated and the separation force measured. The ratio of the separation force to the contact force yields the adhesion coefficient. This procedure was repeated at 25°C intervals between 200°C and 300°C at the same contact force. The results for these cleaned samples are shown as a plot of adhesion coefficient vs. temperature in Figure 1.

The data for the uncleaned samples shown in Figure 1 were obtained by the same procedure as for the cleaned samples except that ion bombardment and heating treatments were omitted. The adhesion coefficients for the uncleaned samples vary from 0.00 at 200°C to 0.96 at 300°C while those for the cleaned samples vary from 0.18 at 200°C to 1.76 at 300°C. The cleaned samples have a higher adhesion coefficient at each temperature than do the uncleaned samples.

To determine if this difference in the adhesion coefficient was due to differences in bulk diffusion, the samples were cross-sectioned and subjected to electron microprobe analysis. With the electron beam in the form of a line approximately 10 microns long by 0.5 microns wide and parallel to the interface of the sample, the maximum distance from the interface that copper was detectable in the nickel sample was recorded. This result is shown in Figure 2 as a plot of this penetration distance vs. temperature of formation of the couple. Figure 3 shows the penetration distance vs. temperature obtained by a similar procedure for nickel in the copper part of the couple.

For the cleaned samples the penetration of copper into nickel is below the detection limits of the microprobe even at a distance of 1.0 microns while for the uncleaned samples copper penetrates into the nickel sample as far as 7.0 microns at 300°C. The same trend is seen for the penetration of nickel into copper. The penetration distance is 0.0 for the cleaned samples at all temperatures tested while for the uncleaned samples the penetration distance increases from 0.0 at 250°C to 12 microns at 300°C.

In summary this study shows that the adhesion strength of cleaned copper-nickel surfaces in the temperature range of 200°C to 300°C is not related to bulk diffusion; whereas the adhesion strength of uncleaned surfaces may be related to bulk diffusion. One possible explanation for bulk diffusion not occurring in the cleaned samples would be that surface diffusion on clean surfaces requires much less energy than does diffusion into the bulk; hence, surface diffusion occurs preferentially to bulk diffusion.

1. M. J. Hordon, "Adhesion of Metals in High Vacuum," p. 109, ASTM Special Technical Publication No. 431 - American Society For Testing and Materials, Philadelphia, Pa., 1967.
2. P. M. Winslow, and D. V. McIntyre, "Adhesion of Metals in the Space Environment," American Institute of Aeronautics and Astronautics Proceedings of Seventh Structures and Materials Conference, Cocoa Beach, Florida, 1966.
3. J. M. Bradford, "A Study of the Adhesion of Nickel," Ph.D. Thesis, North Carolina State University, Raleigh, 1968.

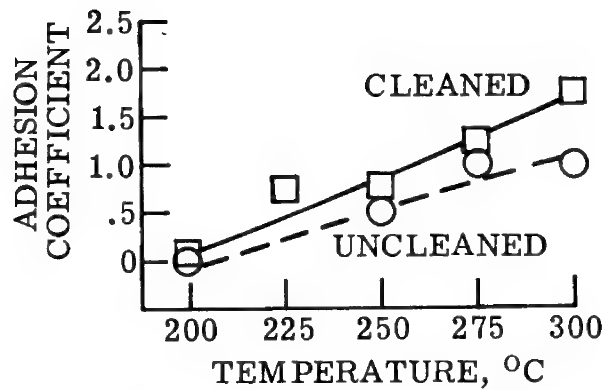


Figure 1. - Plot of adhesion coefficient vs temperature of formation for cleaned and uncleaned copper-nickel couples.

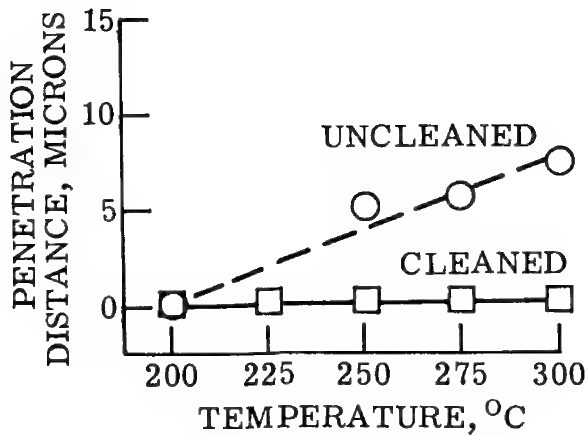


Figure 2. - Plot of penetration distance of copper into nickel vs temperature of formation for cleaned and uncleaned samples.

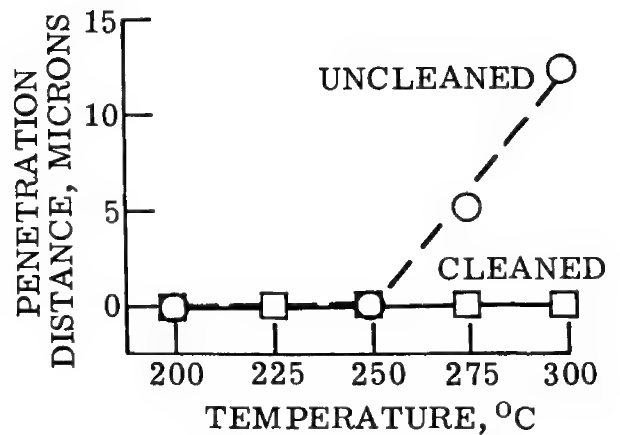


Figure 3. - Plot of penetration distance of nickel into copper vs temperature of formation for cleaned and uncleaned samples.

## CONCENTRATION PROFILES ACROSS BRAZED HASTELLOY X JOINTS USING ELECTRON MICROPROBE ANALYSIS

W. Barry Lisagor and Harry L. Bloxom  
NASA Langley Research Center, Hampton, Virginia

---

Elemental concentration profiles across brazed superalloy joints have been determined by electron microprobe analysis. Quantitative determinations of the complex alloy system were accomplished using a computer program<sup>1</sup> incorporating the correction factors necessary for accurate analysis. The effect of the various correction factors was examined independently to determine the magnitude of each correction.

The electron microprobe analysis was accomplished employing a computer program<sup>1</sup> which was modified to take into account L-K, and K-L fluorescence<sup>2</sup> and to allow for analysis of up to ten different elements. Concentration profiles were determined for virgin braze material of both nominal alloy compositions as well as across brazed joints to ascertain how effectively the computer program could provide accurate quantitative data regarding elemental concentration. Computer runs were made on the same data with various corrections omitted to determine the magnitude of the correction factors employed. The microprobe analyses were accomplished using an 18 kV accelerating potential and 0.05 microamps beam current. Point counts were determined for each element in five micron steps.

Multicycle brazing techniques are being utilized to fabricate complex regeneratively cooled panels in the Hypersonic Research Engine currently under development at the Langley Research Center of NASA<sup>3</sup>. The gold-palladium-nickel braze alloy system is being employed for brazing operations in the 2050° - 2200° F temperature range. Because of the high temperatures employed in the braze cycle and the subsequent high temperature exposure expected in application, a study was undertaken to determine elemental concentration profiles across simple overlap brazed joints and actual panel sections. Concentration profiles were determined for the simple specimens both after brazing and after various thermal cycles simulating engine operation. Profiles were determined on panel cross sections from specimens cut from panels after thermal cycling only. Two nominal braze alloy compositions were utilized in the study: a 50 percent gold, 25 percent nickel, 25 percent palladium braze alloy by weight with braze temperature of 2070° F; and a 30 percent gold, 36 percent nickel, 34 percent palladium alloy with a braze temperature of 2170° F. The simple overlap specimens were cycled between 500° and 1600° F for 200 cycles. A typical cycle consisted of a temperature rise from 500° to 1600° F in 30 seconds, a hold at 1600° F for 20 seconds, and a decrease to 500° F for 30 seconds. The same two braze alloys were utilized for panel fabrication, and similar thermal cycling histories were employed as described for the overlap specimens.

Results of the microprobe analysis indicate that the atomic number correction had the most significant effect upon the apparent elemental concentrations of the virgin braze material. Table I lists the nominal compositions of the braze alloys investigated along with the indicated concentrations determined by microprobe analysis

with and without incorporation of the atomic number correction. Concentration profiles of constituent elements of the alloy and the braze material (30 percent Au, 36 percent Ni, 34 percent Pd) after brazing a simple overlap joint are shown in Fig. 1(a). The results indicate a slight tendency toward nickel segregation at each end of the braze zone. Considerable dilution of the various superalloy constituents can also be observed in the braze zone. The palladium concentration appears to maintain a relatively constant level of concentration through the joint while other elements have more gradual change. Concentration profiles of a similar joint are shown in Fig. 1(b) after 200 cycles from 500° to 1600° F. No significant differences were observed indicating little change in joint composition because of diffusion. The results indicate that the computer program is relatively effective for quantitative analysis of complex alloy systems.

- 
1. James D. Brown: Comprehensive Computer Program for Electron Probe Microanalysis. Analytical Chemistry, Vol. 38, June 1966, pp. 890-894.
  2. S. J. B. Reed: Characteristic Fluorescence Corrections in Electron-Probe Microanalysis. British Journal of Applied Physics, Vol. 16, 1965, pp. 913-926.
  3. Braze Alloy Investigation, NASA Contract No. NAS1-6666, Hypersonic Research Engine Project - Phase IIA. NASA CR-66845, May 27, 1969.

TABLE I

NOMINAL COMPOSITION OF BRAZE ALLOYS INVESTIGATED  
AND INDICATED CONCENTRATIONS BY MICROPROBE ANALYSIS

Element	50-25-25 Braze			30-36-34 Braze		
	Nominal braze comp.	Composition by probe analysis		Nominal braze comp.	Composition by probe analysis	
		without α correc.	with α correc.		without α correc.	with α correc.
Au	50	44.0	50.0	30	26.5	31.5
Ni	25	31.1	25.8	36	42.3	37.2
Pd	25	24.9	24.2	34	31.2	31.3



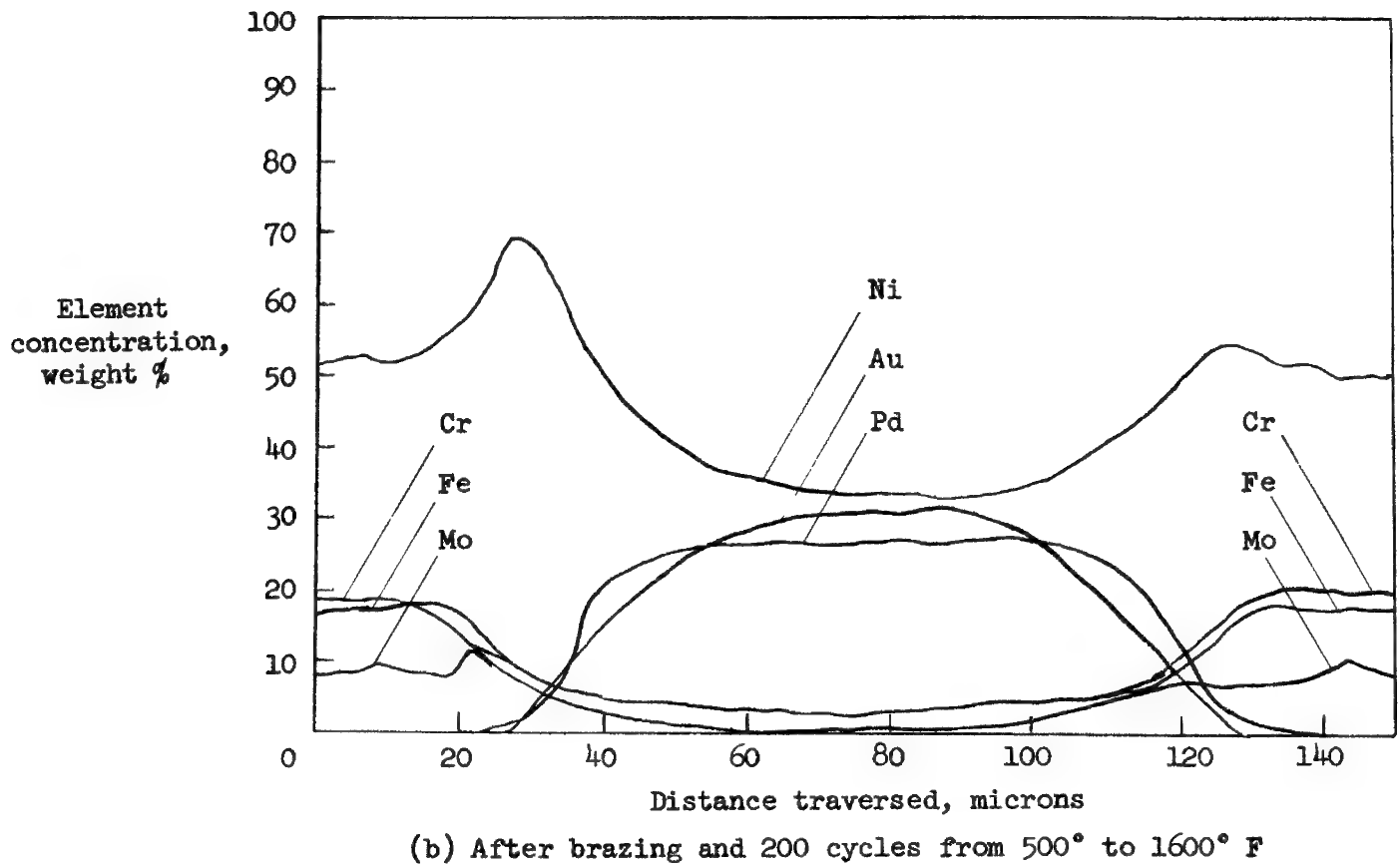
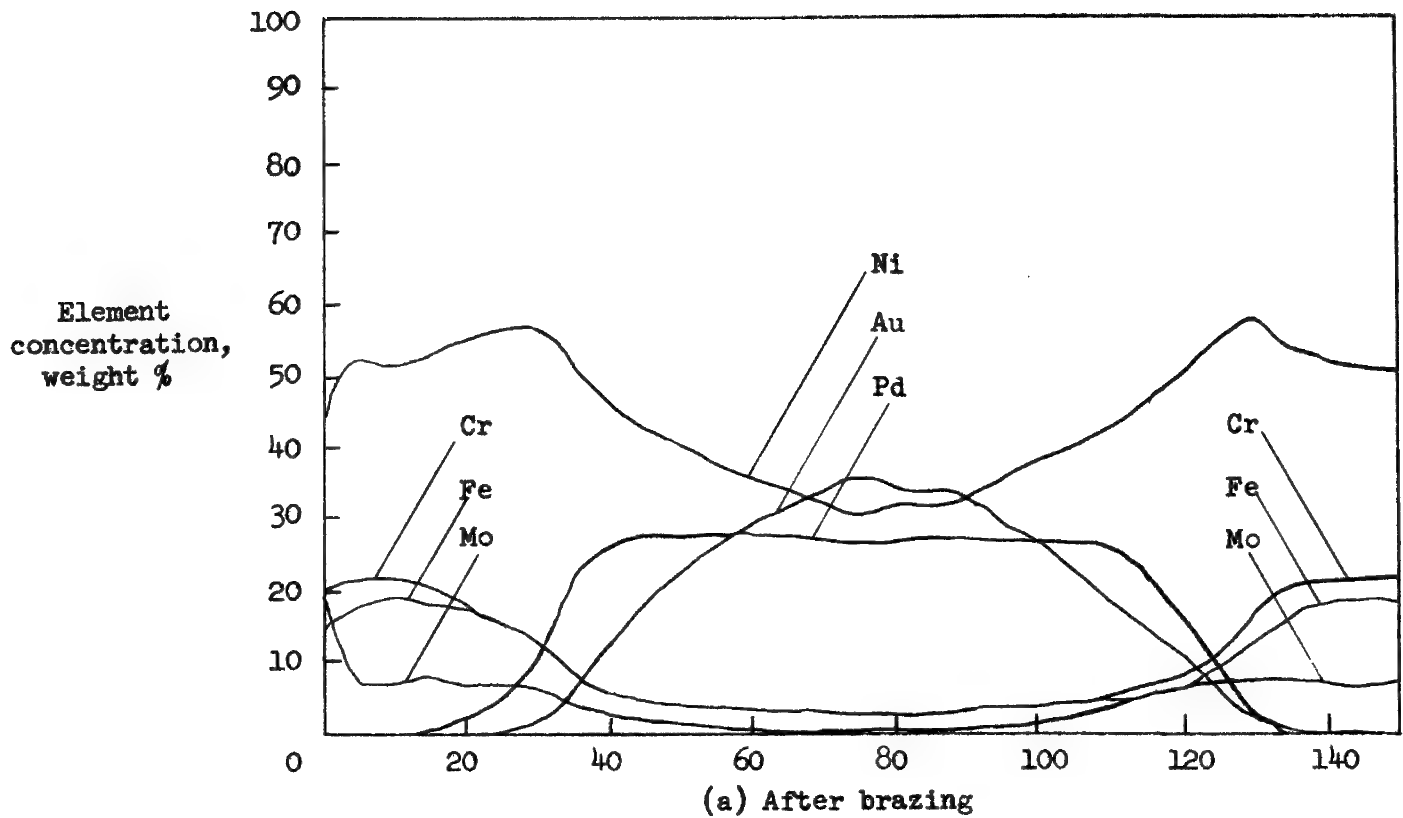


Figure 1.— Elemental concentration profiles of Hastelloy X joints after brazing with 30 Au - 36 Ni - 34 Pd braze alloy.

## ELECTRON MICROPROBE ANALYSIS OF PARTICLES IN TISSUE

C. Berkley, A. M. Langer, I. Rubin  
 Mount Sinai School of Medicine  
 New York, N. Y.

Humans are frequently exposed to aerosols of inorganic particles through occupational pursuits. Subsequently, these particles may be inhaled, ingested, and come to rest permanently in tissue where they cause pathologic biological responses. Quartz, a widely used mineral material, produces a fibrotic response in lung tissue called "silicosis". However, some materials may induce tumor responses in man. Asbestos, a generic term for five fibrous, hydrated, silicate minerals, produces malignant tumors in almost half the men who use the substance occupationally. Its importance has increased because asbestos is used in areas far removed from where it is mined and processed; it is commonly used in construction trades and has been implicated as a common air pollutant in urban centers. Asbestos fibers and bodies have been found in the lung tissue of almost half the people who come to autopsy in large urban cities around the world. These fibers may be observed in tissue as uncoated forms or as the more commonly observed "asbestos body", which is an iron-protein coated fiber.

Our laboratory has concentrated on the study of asbestos and tissue response to asbestos materials. The five asbestos types are made up of four amphibole minerals and one fibrous serpentine mineral. This latter mineral, chrysotile, accounts for over 95 per cent of the asbestos consumed in this country. Bulk chemistry of these minerals differs significantly and fiber types may be so differentiated.

Commonly, the fibrous minerals and asbestos bodies observed in lung tissue are small in size. Some of the larger particles are .2 microns in width and may attain a length of some 40 microns. Occasionally the "needles" display an iron protein coating. Analytical techniques previously used relied on transmission electron microscopy and electron diffraction for identification and characterization of the fiber core. The nature of chrysotile asbestos (its unique morphology and electron diffraction pattern) presents no problem in its identification. However, the nature of the amphibole asbestos types, which are basically the same structure, give more problems for unique identification and characterization. Because of the chemical and physical differences between the fiber types, the 9:1 ratio expected for chrysotile amphibole bodies does not hold and each body must be identified individually.

It was decided to utilize the electron microprobe to characterize the fiber nuclei of the asbestos bodies chemically. To do this, there were two major problems which had to be resolved: 1) The presentation of the fiber nucleus to the electron beam; and 2) The analysis of the raw data.

Because no fibers of the same dimension as the unknown were available with known chemistry on an individual basis, it was decided not to attempt absolute quantitative analysis. A system was devised which allowed the unique identification of various asbestiform minerals on a semi-quantitative basis.

Standard asbestos types were obtained from a number of localities, representing a range of chemical varieties.

After selection of a proper substrate and coating technique, emission values for Si, Mg, Na, Ca, Fe K-alpha were determined for each fiber type on a range of fiber sizes. Asbestos types may be differentiated chemically.

The presentation of the fiber within the asbestos body was the most difficult problem to solve. This involved finding a suitable substrate and exposure of the fiber from the Fe protein coating. The various attempts to achieve the proper combination of conditions will be discussed in detail. Thus the identification of micron and sub-micron particulates will be described.

Methods involving choice of substrates, coating techniques, instrumental methods of analysis, particle isolation, and data presentation will be described.

RISE AND DECAY TIME AND POLARIZED CATHODOLUMINESCENCE EMISSION  
BY SPECIAL MICROPROBE TECHNIQUES

R. J. R. S. B. Bhalla and E. W. White  
Materials Research Laboratory  
Pennsylvania State University  
University Park, Pennsylvania

---

### Introduction

The electron microprobe is often used to study cathodoluminescence of minerals for qualitative or semiquantitative determinations of the distribution of activator or impurities<sup>1,2</sup>. Wittry<sup>3</sup> has made extensive use of electron microprobe to study cathodoluminescence emission in the IR region from many samples of GaAs and has correlated intensity variations with distribution of Te impurity. However, despite these and many other similar studies, full potentialities of the electron microprobe as a tool for detailed measurements of the spectral characteristics and rise and decay times has not been fully explored. Using a microprobe, information can be obtained from comparatively very small single crystals (<50 microns). Single crystal characteristics of individual grains of a powder also can be accomplished.

### Approach

The aim of this work was to develop the electron microprobe instrumentation for studying single crystal cathodoluminescence characteristics of common phosphors.  $Mn^{2+}$  activated, as well as unactivated synthetic and natural willemite ( $Zn_2SiO_4$ ) were studied. Some measurements have also been made on  $CaWO_4$ .

Cathodoluminescence characteristics measured from oriented crystals included: (1) Spectra of luminescence, (2) Polarization of the observed emission and polarization directional dependence of the spectra and (3) Rise and decay time characteristics.

Samples were usually prepared as polished thin microscopic sections and crystals with desired orientations were identified by examination in a petrographic microscope. An ARL model EMX microprobe equipped with a simple light spectrometer and photomultiplier readout<sup>4</sup> was used to record spectra of luminescence. Whenever needed, a POLAROID analyzing cap was attached to the probe microscope, making it possible to record the emission spectrum in any polarization direction. For the measurements of the rise and decay time characteristics, a special pulsed voltage generator was built and used. The output of the pulse generator was coupled to one set of electrostatic deflection plates ordinarily used for sweeping the electron beam. The deflecting pulse could be fired either singly or in a sequence at rates continuously variable from  $5 \times 10^4$  pulses per second to a pulse every 5 seconds. The pulse length was variable from  $5\mu$  seconds to 5 seconds. The intensity of light output from the phosphor surface, measured by photomultiplier, was displayed on an oscilloscope screen and the rise and decay times measured directly from the scope. This method of pulsing the electron beam has an advantage in

that excessive sample heating could be avoided or reduced greatly by keeping the beam on the observed area only for a short time.

### Results

The luminescence emission from both  $Mn^{2+}$  activated and unactivated willemite is found to be polarized<sup>5</sup>. In case of  $Mn^{2+}$  activation, the electric vector is perpendicular to the c-axis while the luminescence of unactivated willemite has its electric vector parallel to the c-axis. The measurements were made on crystals oriented with the c-axis in the plane of the polished section. These measurements clearly show that the site symmetry of the activator,  $Mn^{2+}$ , is higher than the space group symmetry ( $C_1$ ) of  $Zn^{2+}$  ions in the crystal structure of  $Zn_2SiO_4$ . The intrinsic luminescence of  $CaWO_4$  oriented with the c-axis in the plane of the section, was also found to be strongly polarized. It has been suggested for a long time that the intrinsic emission of this type is due to basic tetrahedral  $(SiO_4)^{4-}$  or  $(WO_4)^{2-}$  groups.

In a recent study, Walter and Butler<sup>6</sup> have made LACO - Molecular Orbital calculations to determine the energy levels thought to be involved in the excitation and emission processes for tungstate and vanadate groups. They also concluded that the symmetries of  $(WO_4)^{2-}$  in  $CaWO_4$  is  $D_{2d}$  (tungstate tetrahedra contracted along z-axis) which makes some forbidden transitions allowed. Group theory arguments, based on the symmetry of levels as given by Walter and Butler<sup>6</sup>, show that the emission of these groups should be polarized for lower symmetry  $D_{2d}$ , in comparison to perfect  $Td$  symmetry. Thus, we clearly see that valuable supplementary crystallographic information can be obtained from the measurements of the polarized luminescence emission of both activated and unactivated crystals.

Rise and decay measurements were made on a few selected natural  $Mn^{2+}$  activated willemites. A value of decay time of 1-2 m secs (for decay to 1/10 of peak intensity) was found in comparison to the 10-15 m sec value usually reported for bulk powder phosphors. This value of decay time was obtained using a sample current of  $1 \times 10^{-8}$  amp at 20 KeV and spot diameter of 10  $\mu m$ . The value of decay and rise times are found to be dependent on the acceleration potential of the beam.

### Acknowledgment

This work is supported by ARPA under contract No. DA-49-083-OSA-3140.

- 
1. J.V. Smith and R.C. Stenstrom, Journal of Geology, 73, G27, 1965.
  2. J.V.P. Long and S.O. Agrell, Mineralogical Magazine, 34, 318, 1965.
  3. D.B. Wittry, Appl. Phys. Letters, 8, 142-144 (1966).
  4. R.T. Greer and E.W. White, Trans. Second Nat. Conf. on Electron Probe Analysis, paper 51 (1967).
  5. R.J.R.S.B. Bhalla and E.W. White, 137th Natl. Meeting, The Electrochem. Soc., Abs. 53 (1970).
  6. W. Walter and K.H. Butler, J. Electrochem. Soc., 116, 1245 (1969).

# ELECTRON MICROPROBE ANALYSIS OF LUNAR GLASSES AND PYROXENES FROM APOLLO 11

John C. Drake, Cornelis Klein, Jr., and Maurice Campot  
Department of Geological Science  
Harvard University  
Cambridge, Massachusetts, 02138

The major constituents in the lunar materials returned by Apollo 11 are glass and pyroxene (C. Frondel, et al., 1970, *Geochimica et Cosmochimica Acta*, in press). Both occur in the fines (< 1 mm) and the rocks. The most abundant type of glass in the lunar fines is a dark, scoriaceous variety, occurring as angular, crustiform, and spherical to subspherical particles, and which exhibits extensive compositional variation. It commonly contains unfused crystalline fragments of pyroxene, plagioclase and ilmenite. Frequently flow bands of different color, index of refraction, and chemical composition are visible. Other glasses, ranging in color from opaque, dark brown to colorless and transparent, through various shades of reddish brown, yellowish brown, green, yellowish green, also occur in both angular and rounded forms (spheres, teardrops, dumbbells ellipsoidal bodies, etc.) (Fig. 1), and there is a good correlation between color, index of refraction, density, and chemical composition. These glasses range in composition from essentially pure plagioclase glass ( $\text{An}_{61} - \text{An}_{94}$ ) to glasses rich in  $\text{FeO}$ ,  $\text{TiO}_2$ , and  $\text{MgO}$  (Fig. 2). This wide compositional range represents fused mixtures of varying proportions of pyroxene, ilmenite, and plagioclase in the lunar fines.

Pyroxene, the most common crystalline component in both the Apollo 11 rocks and fines, varies widely in composition (including augite, subcalcic augite, ferroaugite, titanaugite and pigeonite) (Fig. 3), and exhibits extensive compositional zonation and exsolution phenomena. Frequently an exsolution pattern of pigeonite in an augite host is superimposed on a relatively continuous zonation profile in a single grain (Fig. 4). Most commonly, the Fe content increases from the core of a zoned pyroxene towards its rim. The highest Fe contents are found in small interstitial, yellowish-brown pyroxenes and on the outer edges of large augite grains. In one pyroxene from a fine grained gabbro, the zonation from the core towards the rim (D-E, Fig. 3, Fig. 4) projects towards the composition of pyroxferroite, a new triclinic pyroxenoid with the composition  $(\text{Fe}_{.85}\text{Ca}_{.14}\text{Mg}_{.03}\text{Mn}_{.02})_{1.04}(\text{Si}_{.97}\text{Ti}_{.01}\text{Al}_{.01})_{.99}\text{O}_3$ , which has been found in several lunar rocks.

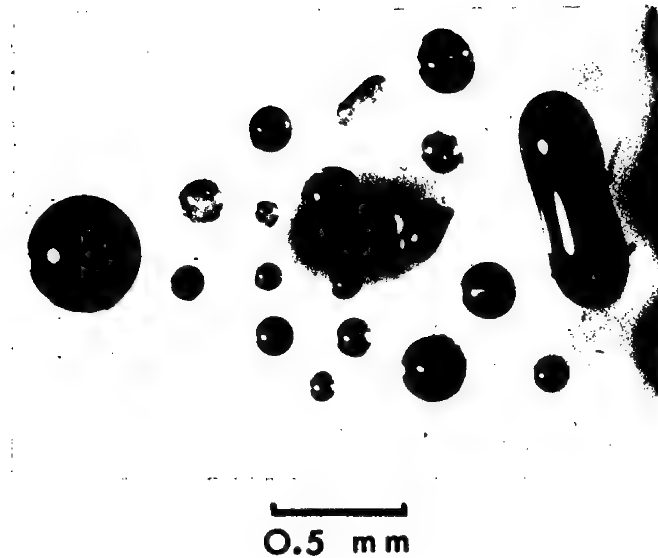


Figure 1: Examples of glass spherules and dumbbells of varying color and composition extracted from the lunar fines

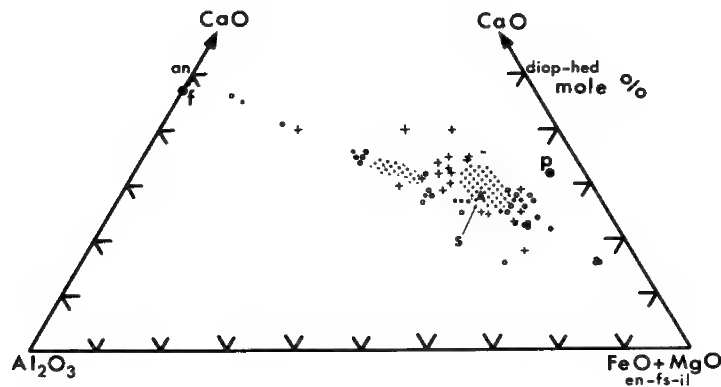


Figure 2: Electron microprobe analyses of glasses from the lunar fines in terms of molecular percentages of  $(\text{FeO} + \text{MgO})$ ,  $\text{CaO}$ , and  $\text{Al}_2\text{O}_3$ . Solid dots represent angular fragments, circles are spherules and crosses are scoriaceous glass. Large shaded area represents 43 scoriaceous, 13 angular and 23 sphere analyses. Small shaded area represents 14 scoriaceous, 6 angular and 2 sphere analyses.

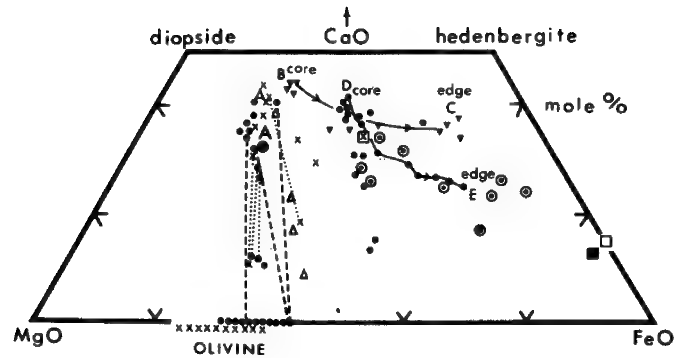


Figure 3: Pyroxene, olivine and pyroxferroite compositions in terms of molecular percentages of CaO, MgO, and FeO. Point A represents the bulk analyses of two clinopyroxenes. X represents the composition of pyroxenes from the lunar fines and ● ◉ ▼ and △ for pyroxenes from various rock types; ■ is lunar pyroxferroite, □ is synthetic pyroxferroite. D-E is the probe traverse shown in Fig. 4.

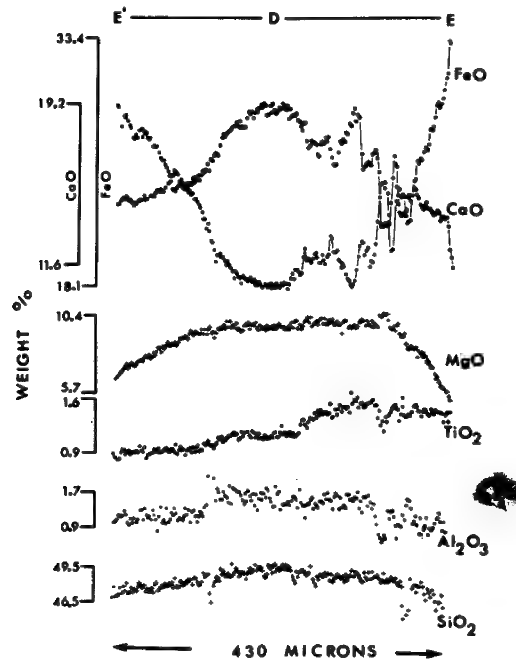


Figure 4: Compositional profiles across a single pyroxene grain in a microgabbro.



# THE USE OF THE ELECTRON MICROPROBE TO ANALYSE VERY MINUTE AMOUNTS OF LIQUID SAMPLES

C. LECHENE

Département de Physiologie. Université de Sherbrooke  
SHERBROOKE (Qué) Canada.

The electron microprobe may be developed into a powerful tool for the analysis of biological fluids. Minute amounts of liquid when available from intercellular spaces, as in micropuncture experiments, may be analysed quantitatively.

Preliminary reports on the use of the electron microprobe did not provide sufficient details on the preparation of samples (1, 2). We would now like to describe a new technique for the elemental analysis of Cl, Na, P, Ca, Mg and K in a sample whose volume is less than one nanoliter. Crystals of the liquid sample are obtained and the characteristic X-rays are analysed by the electron microprobe. In order to avoid evaporation, liquid samples are manipulated under oil with special calibrated micropipettes (50-400 picoliters). The exact volume delivered by the micropipette is determined by measuring the radioactivity of a fraction derived from a labeled sample. Fifteen to thirty samples may be taken up by the same siliconised micropipette with each sample separated from another by an oil droplet. The accuracy of delivery by the micropipette is better than 1 % S.D.

The liquid samples are delivered from the micropipette with stereomicroscopic control, on to a pure beryllium piece that is wetted with paraffin oil. Beryllium was chosen because of its low background properties. After the oil is washed with m-xylene, the liquid samples remaining on beryllium, are quickly frozen in isopentane precooled to  $-150^{\circ}\text{C}$ . The beryllium piece is put on a thermoelectric module and the samples are freeze-dried under vacuum ( $P < 0.05$  Torr,  $T^{\circ} = -40^{\circ}\text{C}$ ). With this technique, very small crystals, less than  $1\text{ }\mu\text{m}$ , are obtained ; they are localised uniformly on a small spot, 50-120 microns in diameter, on the surface of the beryllium piece. One hundred and fifty samples may be easily handled on a beryllium piece of 1 cm in diameter. A liquid sample of 0.2 nanoliter (max. conc. : 20 mg/ml, density  $\approx 1$ ) will give rise to a dry spot of  $100\text{ }\mu\text{m}$  in diameter, and less than  $1\text{ }\mu\text{m}$  in thickness even if only half of the surface is covered by crystals. Samples are not coated because beryllium provides good conductivity

The analysis is done with a CAMECA/C.E.C. microprobe. The electron accelerating potential is 11 Kv. With this potential, excellent electron penetration and good excitation energy in the range of the elements studied are obtained. Specimen current is 500 nA on the beryllium and the beam diameter is 75 to  $150\text{ }\mu$ , in order to excite the entire spot under the probe. Gain is either adjusted depending of the concentration of the element being analysed or kept constant for the highest concentration. K  $K\alpha$  is analysed with a PET crystal, Na  $K\alpha$  and Mg  $K\alpha$  with a KAP, Ca  $K\alpha$  with a 1011 or PET and P  $K\alpha$  with PET or KAP crystal. Two elements are analysed simultaneously.

Reproducibility has been tested on single or mixed salts. Values deviate usually less than 2 % of the standard error as illustrated in Table I ; this depends on the shape of crystals which must be less than 2  $\mu\text{m}$ . No significant difference in measured intensity was obtained for P, Ca, K (0.5 mM/L) either alone or in the presence of NaCl (220 mM/L). There is also no significant difference in counts rate for the same sample no matter what its position under the probe is (checked with a rotating holder). There is no sensible loss by vaporization except for chlorine (loss could be 2 to 3 %/min).

Linearity and sensitivity have been tested with five standard solutions of mixed salts : NaCl,  $\text{MgSO}_4 \cdot 7\text{H}_2\text{O}$ ,  $\text{KH}_2\text{PO}_4$  and  $\text{CaCl}_2$ . Figure 1 shows an example of standard curves ; for all the elements tested correlation coefficient of linear regression is approximately unity.

This method then allows quantitative elemental analysis of biological fluids of less than one nanoliter ; several elements of biological importance (P, Ca, Mg) may be quantitated on the same sample.

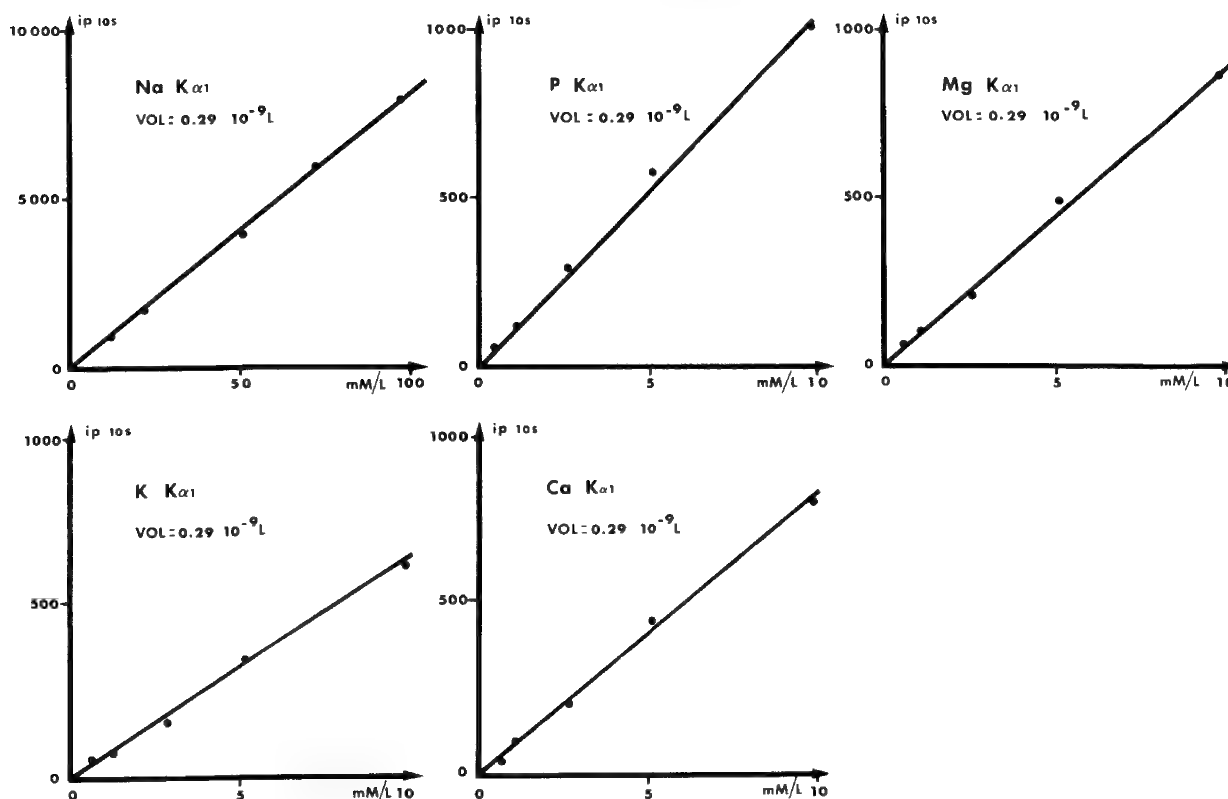
- 1) M.J. INGRAM and C.A.M. HOGBEN. Anal. Biochem., 18 : 54-57, 1967.
- 2) F. MOREL et N. ROINEL. J. Chim. Phys., 66 : 1084-1091, 1969.

TABLE I  
REPRODUCIBILITY

	Salt	mM/L	Q $\times 10^{-10}$ g	Intensity (counts/10sec)			S.E. (% mean)	Beam diameter ( $\mu$ m)
Na	NaCl	145	7.64	1603	57*	(15)#	0.92	150
Cl	NaCl	87	7.08	1844	61	(17)	0.80	150
K	KCl	41	3.69	10630	573	(21)	1.18	100
Ca	CaCl <sub>2</sub>	10	0.92	899	81	(16)	2.25	100
P	Na <sup>2</sup> HPO <sub>4</sub>	64.5	4.60	5590	395	(19)	1.62	70

\*Standard Deviation,      #Number of samples,      Q = Absolute amount of element delivered.

FIGURE 1  
STANDARD CURVES



VOL = volume delivered ; ip 10s = true counts per 10 sec ; mM/L = concentration of the element in the mixed salt solution (200, 140, 100, 40, 20 mM/L in Na and 10, 5, 2.5, 1, 0.5 mM/L in Mg, K, Ca and P). For each point, measured intensity of at least six samples have been averaged.

Correlation coefficient  $r$  = Na : 0.999 ; P : 0.998 ; Mg : 0.998 ;  
K : 0.998 ; Ca : 0.999.

ELECTRON PROBE MICRO-ANALYSIS OF ELECTROLYTES IN KIDNEY SLICES

by

A. P. V. Rosenstiel, H. J. Hohling, J. Schnermann and W. Kriz

The intracellular distribution of the element sodium, potassium and chlorine has been investigated by electron probe analysis in different regions and different tubular segments of rat kidneys. Kidneys of antidiuretic rats were frozen in liquid propane at  $-170^{\circ}\text{C}$ . Sections of 6-7  $\mu\text{m}$  thickness were cut in a cryostat (at  $-20^{\circ}\text{C}$ ), put on a thin nylon foil of an electron probe holder and freeze-dried at  $-40^{\circ}\text{C}$ . In order to keep the slices flat on the foil the edges of the slices were fixed by a drop of methacrylate (910 Eastman Adhesive). The whole procedure could be performed within 12 hours. For improved conductivity and heat dissipation an aluminum layer of  $\pm 400\text{\AA}$  was vacuum coated on both sides of the specimen.

Data were evaluated according to the "relative method" of Hall and coworkers (1966).<sup>(1)</sup> Furthermore data were obtained from thin standards for a quantitative evaluation, according to the "absolute method" of Marshall and Hall (1966).<sup>(2)</sup>

The preparation of the standards was carried out in the following ways:

1. NaCl was pulverized, dried and embedded in methacrylate. Ultra-thin sections were obtained, using an ultramicrotome (without contact with water) and transferred on the nylon foil of a microprobe holder. Both sides of the foil were coated with an aluminum layer of about 400 $\text{\AA}$ .
2. The same procedure was carried out with the mineral Sanidin (85% K and 15% Na).
3. Solutions of different concentrations of  $\text{K}^+$ ,  $\text{Na}^+$  and  $\text{Cl}^-$  were mixed with Agar-Agar. This mixture was frozen and cut on a cryostat, followed by a procedure similar to point 1.

The first two standards were used to get weight-fractions, whereas the third standard served as an additional control for evaluating the elemental concentrations per volume of tissue.

So far the evaluations are carried out only according to the "relative method" (Hall and coworkers 1966); determinations according to the "quantitative method" in co-operation with T. A. Hall are in progress.

---

(1) Hall, T. A., Hale, A. I., and Switsur, V. R., "Some Applications of Microprobe Analysis in Biology and Medicine", in: The Electron Microprobe (Eds. McKinley, Heinrich and Wittry), pp. 805-833, John Wiley & Sons, New York, 1966.

(2) Marshall, D. J. and Hall, T. A., "A Method for the Microanalysis of Thin Films", in: X-ray Optics and Microanalysis (Eds. Castaing, Descamps and Philibert), pp. 374-381, Hermann, Paris, 1966.

Using the "relative method", the following results were obtained in the different regions of the kidney:

1. The intracellular concentrations of sodium and chlorine increases from the superficial layers of the renal cortex towards deeper layers of the cortex.
2. A more pronounced increase of the intracellular concentrations of sodium and chlorine in the outer zone of the renal medulla as compared to the cortex was found.
3. Distinct from sodium and chlorine no cortico-medullary gradient for potassium was observed.
4. Point countings for sodium, potassium and chlorine in the tubular segments of the same renal region showed a strongly heterogenous intracellular distribution in particular for chlorine.

# ELECTRON MICROPROBE CHARACTERIZATION OF THE STOICHIOMETRY AND HOMOGENEITY OF MIXED-CRYSTAL SEMICONDUCTOR MATERIALS.

James P. Smith and Herbert Kraus

Texas Instruments Incorporated, Dallas, Texas

This paper describes a method for characterizing homogeneity and stoichiometry of mixed-crystal systems such as  $\text{Ga}(\text{P}_x\text{As}_{1-x})$ ,  $\text{Pb}(\text{Sn}_x\text{Te}_{1-x})$  and  $(\text{Hg}_{1-x}\text{Cd}_x)\text{Te}$ . Presently, the characterization of the electrical properties and crystallographic variations<sup>1</sup> are used to detect very small electrical inhomogeneities and crystalline imperfections but these techniques are not as applicable to the study of material with gross inhomogeneities. Standard chemical and spectrographic methods cannot be used to determine differences in the material at microscopic points, whereas the electron microprobe analyzer can<sup>2</sup>.

Electron microprobe measurements are made at several random points on the surface of each  $(\text{Hg}_{1-x}\text{Cd}_x)\text{Te}$  sample. Measurements are made of the L-series x-ray radiation from each of the three elements. The x-ray intensities are compared to those from CdTe and HgTe single crystal standards. The electron microprobe data is corrected to yield quantitative compositions using calibration curves calculated by a computer program.

The samples which were analyzed in this study had the compositions,  $\text{Hg}_{.796}\text{Cd}_{.204}\text{Te}$ ,  $\text{Hg}_{.714}\text{Cd}_{.286}\text{Te}$ ,  $\text{Hg}_{.60}\text{Cd}_{.40}\text{Te}$  and  $\text{Hg}_{.83}\text{Cd}_{.17}\text{Te}$ . The  $\text{Hg}_{.83}\text{Cd}_{.17}\text{Te}$  sample was very inhomogeneous because it was cooled from the melt quite slowly allowing some segregation to take place. The method illustrated in Figure 1 is a useful way to display the data. The relative  $\text{CdL}\alpha$  x-ray intensity,  $K_{\text{Cd}}$ , is plotted as a function of the relative  $\text{HgL}\alpha$  intensity,  $K_{\text{Hg}}$ . These relative intensities are the ratios of the intensity of x-rays emitted by the sample to the intensity emitted from CdTe and HgTe respectively. The statistical significance of this type of plot has been discussed by Anderson and Lathe<sup>3</sup>. In Figure 1, the results of the analysis of three  $(\text{Hg}_{1-x}\text{Cd}_x)\text{Te}$  samples of different composition are plotted. The solid line shows the theoretical line on which the data points from stoichiometric  $(\text{Hg}_{1-x}\text{Cd}_x)\text{Te}$  samples would lie. An analysis with a significant deviation from that line would indicate that the sample was not stoichiometric.

The value of  $x$  in the formula  $(\text{Hg}_{1-x}\text{Cd}_x)\text{Te}$  is indicated across the top, thus this value can be quickly determined for the points which lie on the line. The theoretical composition of the three samples is indicated by the dashed vertical line. Each of the three samples were analyzed at more than 25 random points distributed over the entire  $10 \times 3\text{mm}$  surface. The statistical spread in the data must be characterized in order to derive a meaningful indication as to the degree of inhomogeneity. Actually two of the three samples which were used to obtain the data shown in Figure 1 had been shown to be slightly inhomogeneous by the electrical characterization procedures.

An indication of the inhomogeneity of the sample can be obtained by comparing the standard deviation as determined by Poisson statistics to the root mean square deviation of the data points. This comparison clearly indicates that Sample A is inhomogeneous whereas Samples B and C seem homogeneous in mercury from point to point but a possible variation of cadmium from stoichiometry is indicated. Multivariate statistical methods are required for a comprehensive analysis of this data. The data can be used as a test of the theoretical stoichiometry line. Clearly the line does exist and is approximately a straight line in the range studied. The equation for the line is

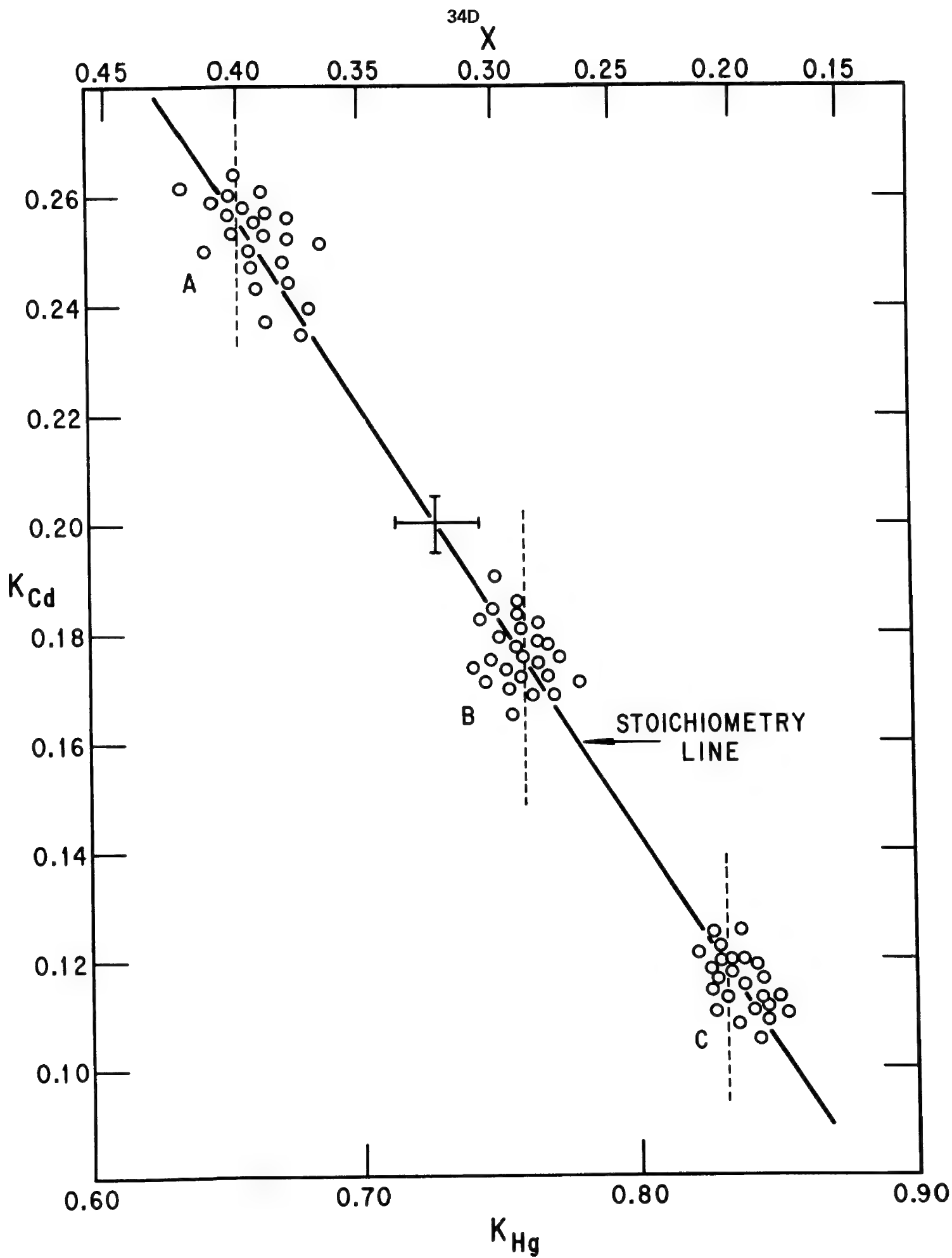
$$K_{\text{Cd}} = -1.30K_{\text{Hg}} + .986$$

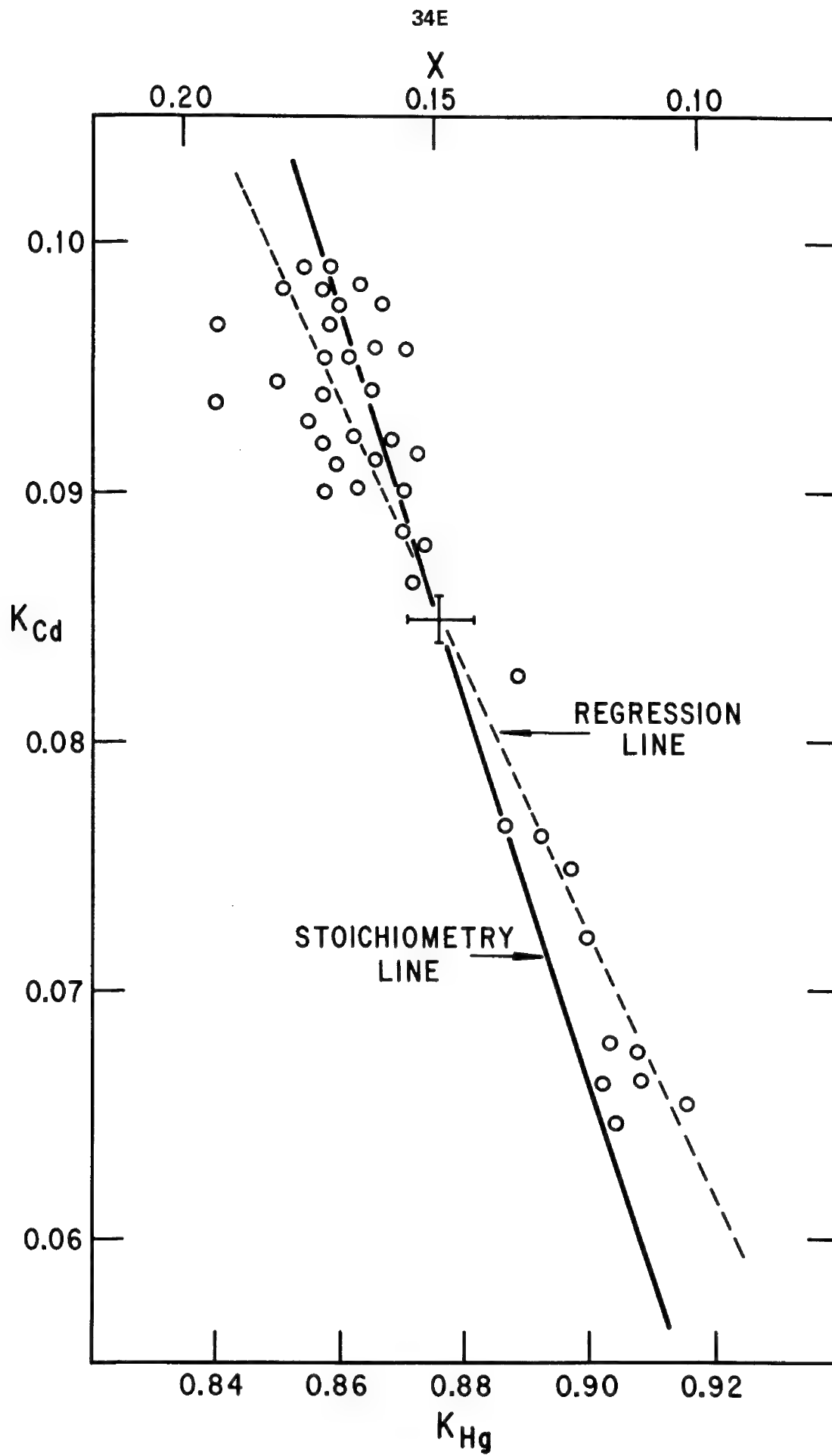
This equation applies only for  $L_{\alpha}$  radiation measurements made by a microprobe with an x-ray take-off angle of  $52.5^\circ$  and a 25 KeV beam potential, using CdTe and HgTe standards.

The data shown in Figure 2 was obtained from the inhomogeneous sample with the composition  $\text{Hg}_{.83}\text{Cd}_{.17}\text{Te}$ . On this plot it is clear that the material is inhomogeneous but that the various compositions remain almost stoichiometric. Thus the composition appears to vary between  $(\text{Hg}_{.80}\text{Cd}_{.20})\text{Te}$  and  $(\text{Hg}_{.90}\text{Cd}_{.10})\text{Te}$ . The dashed regression line was determined using a generalized least-squares calculation in which both dimensions were weighted in accordance with the Poisson standard deviation of the intensity ratio. This regression line was shown to be significantly different from the stoichiometry line. This fact shows that extreme compositions were slightly off-stoichiometry, i.e. when the material is rich in cadmium there is a lesser quantity of mercury than is required by the stoichiometric relationship and vice versa.

- (1) L. N. Swink and M. Brau, Metallurgical Transactions, March (1970).
- (2) H. Kraus, S. Parker and J.P. Smith, J. Electrochem, Soc.: 114, 616 (1967).
- (3) C.A. Anderson and R. F. Lathe, 2nd National Conference on Electron Microprobe Analysis, Boxton (1967).







# APPLICATION OF COMPLEX ANALYSIS OF VARIANCE TO ELECTRON PROBE ANALYSIS

Arthur J. Saffir  
Materials Analysis Company

Gary E. Schwartz  
Harvard University  
Department of Psychiatry

Very frequently in electron microprobe analysis one is concerned only with the detection of a given element. At other times, it is necessary to detect differences in concentration between one specimen and another or between a specimen and a standard. However, it also often occurs that more complex properties must be measured and the statistical differences in these measurements must be ascertained. For example, in studying a welding process one may be interested in measuring several parameters and comparing these among different welding processes. Such a case would be the electron probe measurement of a diffusion gradient as one or more constituents of the material to be welded or of the brazing material are varied in a systematic manner. These factors might have to be correlated with the temperature of the welding process, the time required to weld, the ultimate strength of the weld, the cost of the process, and perhaps other factors as well. We wish to describe a technique for finding the interrelationships of many factors and setting a certainty level on their interactions.

The example that we wish to present is the electron probe measurement of fluorine distributions in the teeth of experimental animals, (see Reference 1). In this study the factors considered were three levels of one dietary factor (F), two levels of another (TMP), the difference between the first molars and the second molars, the difference between right teeth and left teeth, and depth from the surface of the tooth. The experimental design employed was specified as  $S_{60}(F_3TMP_2)M_2P_2D_6$  which instructed an IBM 360 computer (Program BMD 02V, Reference 2) that 60 subjects were randomly placed into six separate groups of 10 subjects each. One of six possible combinations of three levels of F (dietary fluoride) and two levels of TMP (dietary TMP) were fed to each group making a  $3 \times 2$  complete factorial design. Furthermore, every subject had two levels of M (molars), two levels of P (positions), and six levels of D (depth) in a  $2 \times 2 \times 6$  factorial design (4 teeth obtained per animal, each tooth measured at 6 depths by the microprobe.) This design specification coupled with a data format statement enabled the computer to obtain the average fluorine concentrations (interactions) of factors and to calculate a Fischer ratio for each factor and all possible interaction of factors (there were 31 such Fischer ratios). From this we were able to obtain a graph for each and every comparison as well as a probability statement reflecting the reliability of each comparison. A number of complex inter-

actions were found which without this technique would have gone undetected. For example, the analysis revealed that TMP did not affect the overall fluorine concentration of the teeth. The complex analysis of variance revealed that TMP markedly enhanced fluorine accumulation in the teeth at low dietary fluoride levels. It produced little or no effect (or even slightly opposite effect) at high dietary fluoride levels i.e., T x F, the TMP interaction with fluoride levels, was statistically significant at the 0.975 confidence level. This effect was shown to be most prominent near the tooth surface for the T x F x D interaction was also statistically significant.

### Conclusion

The results of this study indicate that the interactions of many factors can be considered at the same time and the interactions of all of these factors can also be determined. Their magnitudes can be measured and the certainty of the observations ascertained. The procedure used is extremely simple in concept for it can be performed with a minimal amount of expertise by the investigator by means of existing computer programs (e.g., Reference 2).

### References

- (1) Saffir et al, Simultaneous Multi-element Analysis with a Single X-ray Spectrometer, Fourth National Conference on Electron Microanalysis, 1969.
- (2) Dixon, W. J., ed. BMD Biomedical Computer Programs, Berkeley and Los Angeles, University of California Press, 1968.

ANALYSIS OF ROCKS BY ELECTRON PROBE  
J.C. Rucklidge and E.L. Gasparrini  
Department of Geology, University of Toronto

Rock analysis remains a tedious process despite the advance of instrumental methods in analytical chemistry. The advantages of electron probe micro-analysis can be seen: (a) in the rapidity with which data may be collected on several elements simultaneously, and (b) in the fact that sophisticated computer programs exist to reduce the raw X-ray intensity data to corrected chemical analysis with accuracy suitable for the geologist's needs. Certain rocks may be conveniently homogenized by direct fusion, and a glass produced. The glass may be analysed by normal electron probe methods, though the 'micro' capability of the probe is no longer needed. In fact a large spot (10 $\mu$ ) is preferable since this serves to further smooth out inhomogeneities in the glass. A method utilizing these ideas has recently been published by Rucklidge et al (1970), and this presentation will describe the same method after experience of a year's routine use.

To test the method five United States Geological Survey rock powders - diabase W-1, basalt BCR-1, andesite, AGV-1, granodiorite GSP-1, and granite G-2 - were heated in graphite crucibles within a platinum furnace containing a hydrogen atmosphere. After fusion, glasses were produced by quenching in cold water. Polished thin sections of the glasses could be checked microscopically for homogeneity before carbon coating. The glasses were analysed for the ten elements. Si, Al, Ti, Fe, Mn, Mg, Ca, Na, K and P on an ARL-EMX microprobe, using 25 kV, 0.04 $\mu$ A sample current and 10 second counting periods. Standards were those routinely used for silicate mineral analysis, namely quartz, rutile, microcline, halite, apatite, anorthite, ferrosilite, tephroite, and diopside, the last four being synthetic. Samples were moved slowly beneath the beam during analysis and ten separate sets of counts were averaged for each glass. Data were processed by the program EMPADR which reduces the manifold readings on standard and sample to a final oxide analysis for direct use by the geologist.

Results for three of the rocks are presented in the table, where they are compared with the preferred analyses for the same rocks, corrected to a volatile free basis. Since these rocks have been analysed extensively by many investigators using a variety of methods, some estimate of the reliability of the probe method may be made. The error indicated for the wet analysis (column b) is that obtained by halving the range of values reported for any element, while the error given for the probe analysis is one standard deviation for the ten sets of readings taken on a sample.

The results show that the technique is good enough for routine analysis

of certain rocks, however there are distinct limitations in the range of rocks from which representative glasses may be made.

Reference

Rucklidge, J.C., F.G.F. Gibb, J.J. Fawcett, and E.L. Gasparriini. 1970.  
Rapid rock analysis by electron probe.  
Geochimica Cosmochimica Acta. 34, pp 243-247

Table 1 Probe and chemical analyses of standard rocks

	W-1		AGV-1		G-2	
	a	b	a	b	a	b
SiO <sub>2</sub>	52.3 ± 1.0	52.90 ± 1.4	60.8 ± 1.6	60.12 ± 1.3	69.0 ± 2.4	69.71 ± 1.2
Al <sub>2</sub> O <sub>3</sub>	15.0 ± 0.7	15.03 ± 0.8	17.5 ± 0.8	17.35 ± 0.9	15.7 ± 1.6	15.46 ± 0.7
TiO <sub>2</sub>	1.01 ± 0.05	1.09 ± 0.12	1.13 ± 0.08	1.10 ± 0.19	0.52 ± 0.20	0.53 ± 0.09
FeO*	9.78 ± 0.75	9.95 ± 0.45	6.34 ± 0.40	6.24 ± 0.21	2.85 ± 0.41	2.51 ± 0.15
MnO	0.18 ± 0.09	0.17 ± 0.09	0.11 ± 0.02	0.10 ± 0.03	0.00 ± 0.04	0.04 ± 0.03
MgO	6.66 ± 0.21	6.52 ± 0.36	1.49 ± 0.10	1.52 ± 0.56	0.92 ± 0.13	0.79 ± 0.37
CaO	10.5 ± 0.2	10.92 ± 0.6	4.93 ± 0.17	5.08 ± 0.81	2.18 ± 0.21	2.00 ± 0.26
K <sub>2</sub> O	0.67 ± 0.11	0.63 ± 0.13	3.04 ± 0.09	2.96 ± 0.24	4.95 ± 0.37	4.54 ± 0.40
Na <sub>2</sub> O	2.37 ± 0.79	2.15 ± 0.17	4.45 ± 0.50	4.42 ± 0.41	4.58 ± 1.00	4.19 ± 0.46
P <sub>2</sub> O <sub>5</sub>	0.14 ± 0.02	0.14 ± 0.03	0.52 ± 0.06	0.50 ± 0.16	0.17 ± 0.05	0.14 ± 0.06
Sum	98.13	99.50	100.31	99.39	100.84	99.91

a Probe results--the indicated error is the standard deviation of ten sets of counts from different points on the sample.

b Preferred values (W-1), average values (AGV-1, G-2) from wet chemical analyses, with deviations (see text).

\* Total Fe calculated as FeO.

## NON-DISPERSIVE X-RAY ANALYSIS

T. C. Loomis  
 Bell Telephone Laboratories, Incorporated  
 Murray Hill, New Jersey 07974

Dispersive x-ray spectrographic systems - even those employing curved crystals - are notoriously inefficient in terms of the fraction of characteristic radiation from the specimen that finally arrives at the detector. In conventional x-ray spectrographs, compensation for this inefficiency is provided by high-powered x-ray tubes. For certain applications (e.g., electron probes and scanning electron microscopes) such intense excitation may not be possible or may involve unacceptable side-effects such as increased beam size or a high excitation voltage. In such a situation, increased intensity at the detector usually can be acquired only at the sacrifice of wavelength resolution.

A possible alternative is to eliminate the analyzing crystal with its inefficient diffraction capability and intensity-consuming slits or collimators. Resolving a polychromatic x-ray beam into a spectrum then requires electronic sorting of the electrical pulses produced by x-ray quanta absorbed by the detector. The average voltage of pulses produced in conventional gas-filled or scintillation counters is proportional to the energy of the absorbed photons. The possible spread in the voltage of pulses that may be produced by photons having the same energy is too large, however, for such measurements to be generally useful.

Lithium-drifted germanium or silicon diode detectors, on the other hand, give much narrower pulse distributions as shown in Figure 1. Note that no hint of resolution of  $K\alpha$  and  $K\beta$  resolution appears in the scintillation counter curves.  $MoK\beta$  is partially resolved from the  $K\alpha$  by the gas proportional counter, but the spectra are complicated by the addition of argon escape peaks on the low-energy side of the main peaks.

The major reason for the improved resolution of the semiconductor detectors is the lower average energy,  $\epsilon$ , needed to produce an electron-hole pair. This quantum efficiency amounts to about 3.6 eV (per electron-hole pair) for silicon. In comparison, each gas ionization event in a proportional counter requires about 30 eV of photon energy and in a scintillation counter approximately 300 eV is needed for each photoelectron produced at the photomultiplier cathode. The number of ion pairs,  $N$ , created in an ionization event helps determine the voltage of the pulse produced by that event. For a photon of energy  $E$ ,  $N$  is equal to  $E/\epsilon$ . The statistical fluctuation in  $N$  is proportional to  $\sqrt{N}$ . The statistical relative deviation in the size of the pulse is thus proportional to  $\sqrt{N}/N$  (or  $1/\sqrt{N}$ ). It is apparent then that a smaller value of  $\epsilon$  leads to a larger value for  $N$  and a smaller statistical fluctuation in pulse voltages.



In actual practice the resolution of semiconductor detectors is limited more by electronic noise than by these statistical fluctuations. The noise that results from leakage current in the silicon detector wafer is reduced (but not eliminated) by maintaining this component at liquid nitrogen temperature. The most likely source of noise is the field-effect transistor (FET) in the input stage of the charge-sensitive preamplifier. These are usually selected for low noise and also operated at low temperature. Recently, Kern and McKenzie (1,2) have reported a very low noise ceramic-encapsulated FET which may eliminate the need for pre-selection. Another major noise source is the feedback resistor in the pre-amplifier. Optical feedback systems omitting this resistor to further reduce noise have been devised (2,3). Such preamplifiers have thus far been operable only at low counting rates, but a pulsed feedback system has been suggested which could permit operation at reasonably high rates with little or no loss in resolution.

Figure 2 shows in block diagram the complete nondispersive analyzer system. Depending on the application, some of the analyzing or display components may be eliminated or substituted for. Probably the most popular applications of these detectors at the present time are in electron probe analysis and scanning electron microscopy. Because of the high detection efficiency it is possible in a matter of minutes or even seconds to acquire a spectrum covering a reasonably large energy range. For such an application a multichannel analyzer with a high speed analog-to-digital converter is used. Careful attention to the selection and adjustment of the various electronic components is required to achieve good energy resolution at reasonably high counting rates. For carrying out quantitative analysis or spatial distribution studies of selected elements, single channel analyzer operation is usually indicated. For simultaneous determination of a few elements, single channel analyzers may be "stacked" together on the same amplifier.

The principal disadvantage of non-dispersive systems for these purposes is that their energy resolution for the x-ray region usually involved in electron probe analysis is much poorer than for dispersive optical systems. This means, of course, that for complex samples, spectral line interference will be a much more likely problem. Other difficulties are introduced if high counting rates are employed. As the x-ray flux at the detector is increased, resolution is usually decreased, energy peaks appear to shift, and counting losses may occur. In addition, line-to-background ratios for non-dispersive optics are significantly lower.

X-ray (fluorescence) milliprobes, on the other hand, are frequently used for higher energy characteristic lines than those used in electron probes. Satisfactory curved-crystal dispersive systems for the short wavelength region are difficult to construct. For wavelengths shorter than about one Angstrom non-dispersive spectrometers show a clear superiority in resolution. Also, their high efficiency permits the use of smaller apertures and lower x-ray tube power. For large samples, this high efficiency makes it possible to use a radioisotope source for primary excitation instead of the conventional x-ray tube. The advantage of such excitation include high stability, low cost, small size, and (in most cases) low background due to the absence of white radiation.

Non-dispersive analyzers do not represent the solution to all the problems of x-ray spectrochemical analysis. They are, however, significantly superior to dispersive systems for certain types of measurements. Very rapid advances are

currently being made in semiconductor detectors and the accompanying electronic circuitry. These improvements will undoubtedly continue to make these systems more useful to the spectroscopist.

---

<sup>1</sup>H. E. Kern and J. M. McKenzie, "Methods of Reducing Noise of Junction Field Effect Transistor (JFET) Amplifiers", IEEE Trans. Nucl. Sci., NS-17, No. 1, February, 1970.

<sup>2</sup>H. E. Kern and J. M. McKenzie, "Noise Studies of Ceramic Encapsulated Junction Field Effect Transistors", to be published in Transactions of the 12th Scintillation and Semiconductor Counter Symposium, Washington, D. C., March, 1970.

<sup>3</sup>F. S. Goulding, J. Walton and D. F. Malone, "An Opto-Electronic Feedback Preamplifier for High Resolution Nuclear Spectroscopy", Lawrence Radiation Laboratory, UCRL-18698 (1969).

## COMPARISON OF X-RAY DETECTORS

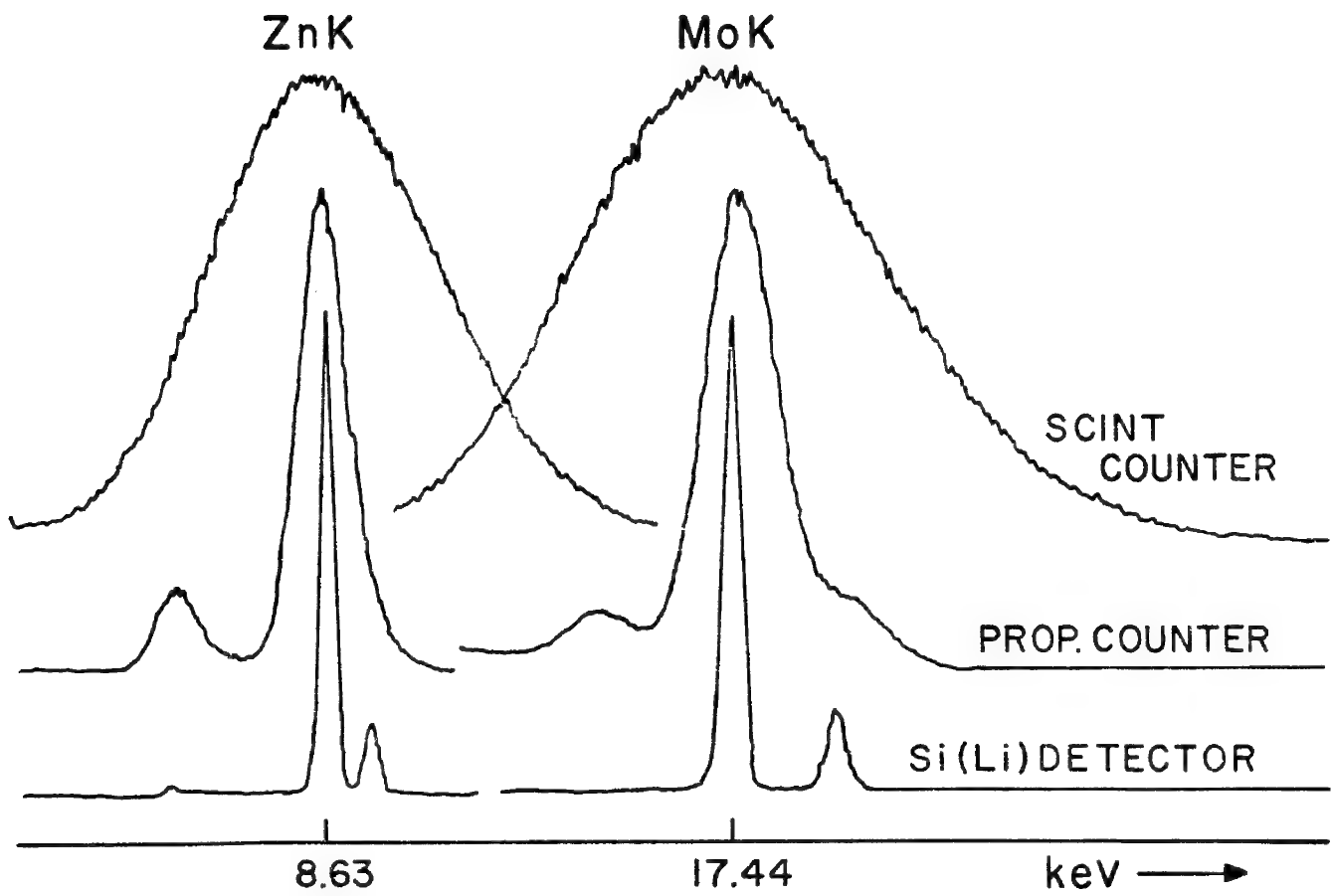


FIGURE 1

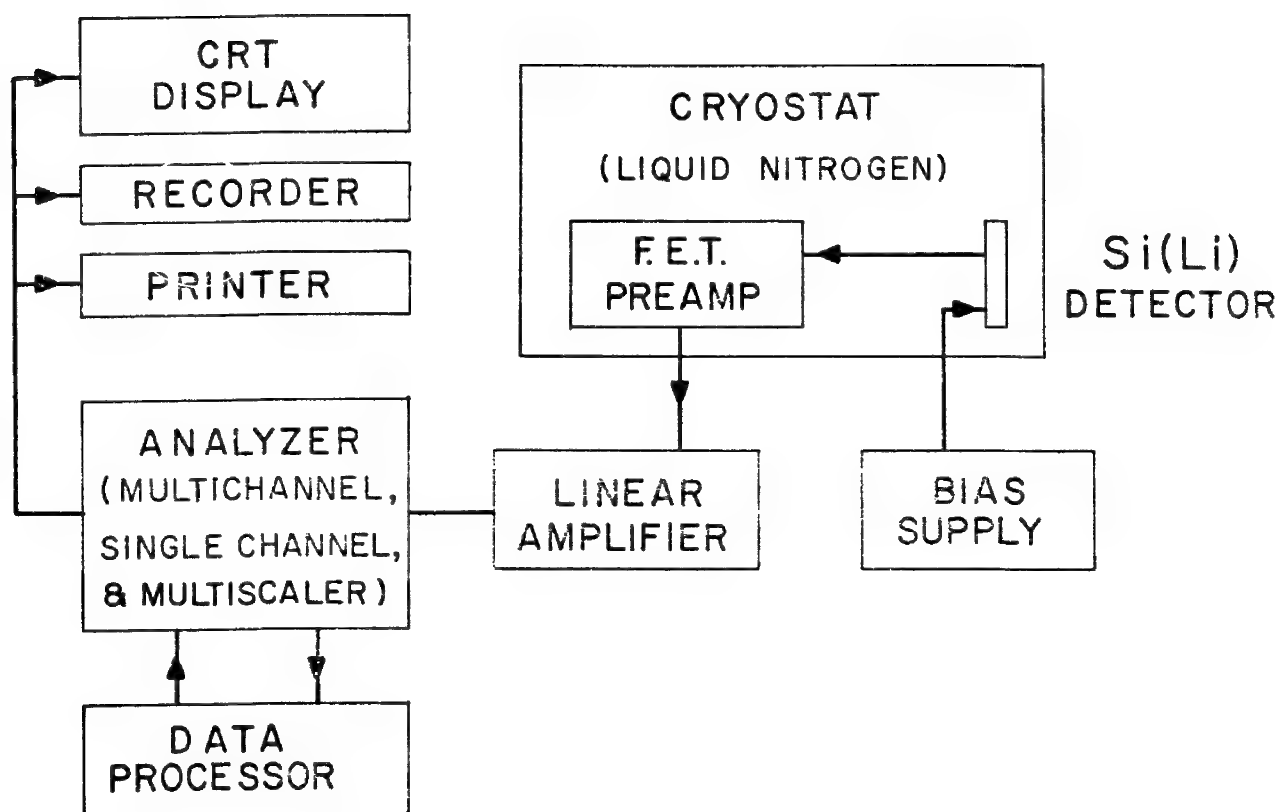


FIGURE 2

AN ANALYTIC METHOD FOR THE ION MICROPROBE  
MASS ANALYZER, PART III

C. A. Andersen  
Hasler Research Center  
Applied Research Laboratories  
Goleta, California

An analytic model has been developed (1,2) for the interpretation of sputtered positive ion emission of samples bombarded with high energy beams of reactive gases. The model proposes that positive ions created in the atomic collisions are subject to electron attachment as they leave the surface of the sample. The number that undergo such attachment is directly proportional to the availability of loosely bound surface electrons. It has been shown quantitatively that positive ion emission from metals increases as the surface barrier and/or the work function of the sample increases. It has been demonstrated that these electronic properties are influenced by the choice of the bombarding gas. Bombardment with highly reactive, electronegative gases, as opposed to inert gases, raises the potential barrier and increases the yield of positive ions.

Studies of the emission of negative ions from metals shows that the yield of these ions is directly proportional to surface electron availability. The yield of negative ions can be increased by reducing the work function of the surface. It has been demonstrated that this can be accomplished by bombarding with an electropositive element such as Cs. It can be shown quantitatively that the yield of negative ions from metals is proportional to the difference between the work function of the surface and the electron affinity of the sputtered atom. For both positive and negative ion emission from metals, electron attachment in the majority of cases is proposed to be a thermionic process governed by the Fermi-Dirac distribution of electrons and the effective electron temperature of the bombarded surface.

The model has been extended to include the emission of positive and negative ions from insulators and semiconductors. These materials differ fundamentally from metals by having an energy gap within the electronic band structure of the solid that is normally forbidden to electron residence. This forbidden gap reduces the number of electrons available for thermionic transfer by effectively increasing the work function of the surface.

Negative ion yields from insulators and semiconductors have been determined and indicate that there are normally enough electrons present in the conduction band of the bombarded sample to permit significant electron attachment to sputtered atoms of sufficient electron affinity. The results of studying stoichiometric compounds of silicates, carbonates, sulfates and phosphates demonstrate that as the effective work function decreases the yield of negative ions increases. The yield of a particular ion being proportional to the atom's electron affinity.

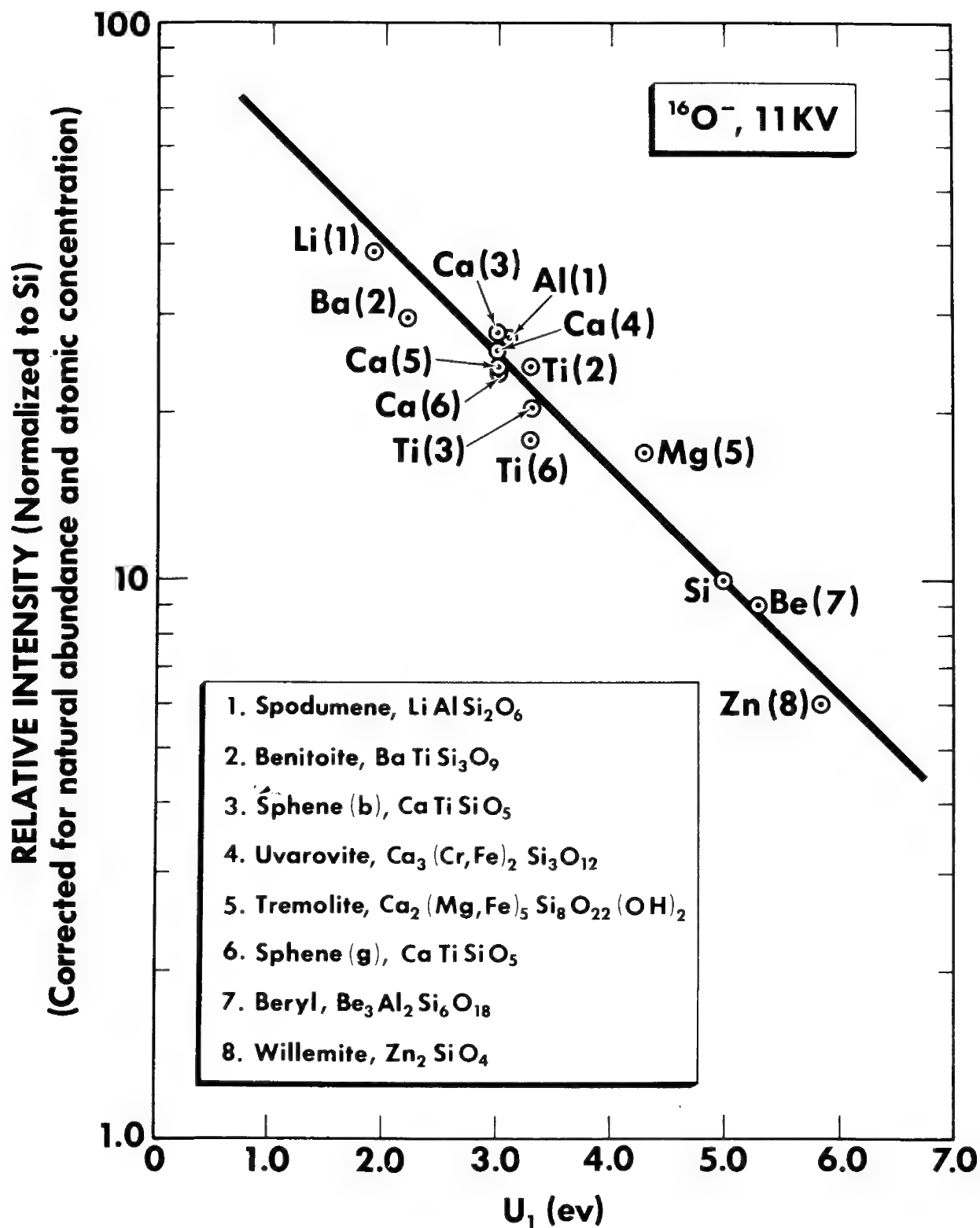
Positive ion yields from insulators and semiconductors have been determined and indicate that as the effective work function increases the yield of positive ions increases. For compounds of high effective work function positive ion neutralization by thermionic electron attachment is minimal. It is proposed, therefore, that the varying positive ion yields observed for different elements from such compounds illustrate the relative degree to which the different atoms are electronically excited in the atomic collisions. It is proposed that the majority of the sputtered positive ions observed in our experiments result from the resonance ionization (3) of such excited atoms. The yields of different elements from some silicate compounds are shown in figure one. In this figure the atomic excitation energy,  $U_1$ , is assumed to be equivalent to that necessary to excite the most intense resonance line in the atom's optical spectra (4). The probability of an electron being excited to a given level being inversely proportional to the height of the level above the ground state of the atom (5).

In insulators and semiconductors resonance ionization processes are limited to rather narrow energy bands resulting in restrictions on the excited atomic levels that can ionize to form positive ions. The slope of the line in figure one therefore is sensitive to the band structure of the sample and can be altered in various ways. Knowing the slope of the line, however,

and the concentration of one component of a compound permits a quantitative analysis to be performed on other elements of the compound using the known as an internal standard (6).

## REFERENCES

1. C. A. Andersen, Third Natl. Electron Microprobe Conf., Chicago, 1968; J. Mass Spect. and Ion Physics, 2 (1969) 61.
2. C. A. Andersen, Fourth Natl. Electron Microprobe Conf., Pasadena, 1969; J. Mass Spect. and Ion Physics (1970) in press.
3. H. D. Hagstrum, Phys. Rev., 96 (1954) 336.
4. W. F. Van der Weg and P. K. Rol, Nuclear Instruments and Methods, 38 (1965) 274.
5. A. Russek, Phys. Rev., 132 (1963) 246.
6. C. A. Andersen, J. R. Hinthorne and K. Fredriksson, Geochimica et Cosmochimica Acta (1970) in press.





AN AUTOMATIC COLOR RECORDING TECHNIQUE  
FOR ELECTRON PROBE X-RAY IMAGES

By:

T. Baum and R. Lewis, Bell and Howell Company

The use of color composite techniques as a method for displaying multi-element X-ray images obtained with the electron probe microanalyzer has been described by a number of authors. These techniques have ranged from the use of a color display computer type oscilloscope adapted to imaging scanning<sup>1</sup>, to the combination of black and white micrographs with a copy camera to obtain color composites<sup>2</sup>. The method used here is a variation of the method described by Heinrich<sup>3</sup> and Ingersoll<sup>4</sup>.

A Bell & Howell/Cameca electron probe equipped with Steinheil Oscillophot Camera using Polaroid color film has been adapted for this study. The objectives of this investigation were to find a simple means of obtaining composite multi-element X-ray image micrographs, to determine if the procedure could be successfully automated, and finally to evaluate the direct CRT color composite image recording technique compared to obtaining a color composite by copying black and white micrographs. In addition, the method had to be easily adapted to the electron probe with its existing instrumentation.

The features of the Steinheil Camera that made it particularly amenable to the automatic color operation were the electronic shutter control and high speed lens. The camera was fitted with an automatic color filter interchange mechanism. The X-ray components that required automating were the X-ray channel selector and the fixed count control. A schematic of the device is shown in Figure 1.

The standard CRT on the electron probe utilizes a P7 phosphor. The use of this phosphor imposed some problems because it is predominately a blue-green rather than a white phosphor. Using this phosphor imposed limitations in the color combinations that could be used.

To utilize the P7 phosphor effectively it was necessary to experiment with a number of color filters. This study was facilitated by selecting a homogeneous specimen and setting up the X-ray input to the CRT to produce a uniform structure-free X-ray raster. Placing filter strips directly in front of the CRT face and using a series of exposure steps produced all the test information needed in one exposure. Of the filters that were tested, red, blue and green provided satisfactory results.

An interference problem causing white bands to appear at the element boundaries was noted. This was most pronounced with large beam diameters. Beam diameters of less than two microns did not exhibit this effect.

The advantages of color composites have been pointed out by other authors<sup>2,4</sup>. However, automation lends an additional advantage of allowing more "operator free" use of the instrument. The cost of one color composite X-ray image versus three or more black and white X-ray images makes the technique competitive in price.

A major advantage of obtaining the color composite directly from the CRT compared to the copy camera technique is the accurate registration capability of the former. This improved registration allows narrow cracks and voids separating two different element boundaries to be observed readily.

#### Bibliography

1. J. F. Ficca, Jr., Electron Probe Multicolor Scanning Images, 1968 National Probe Conference
2. H. Yakowitz, Composite Microprobe Scanning Images in Color, 1968 National Probe Conference
3. K. Heinrich, Advances in X-Ray Analysis, Vol. 7
4. R. M. Ingersoll, Rev. Sci. Inst. 40, 637 (1969)

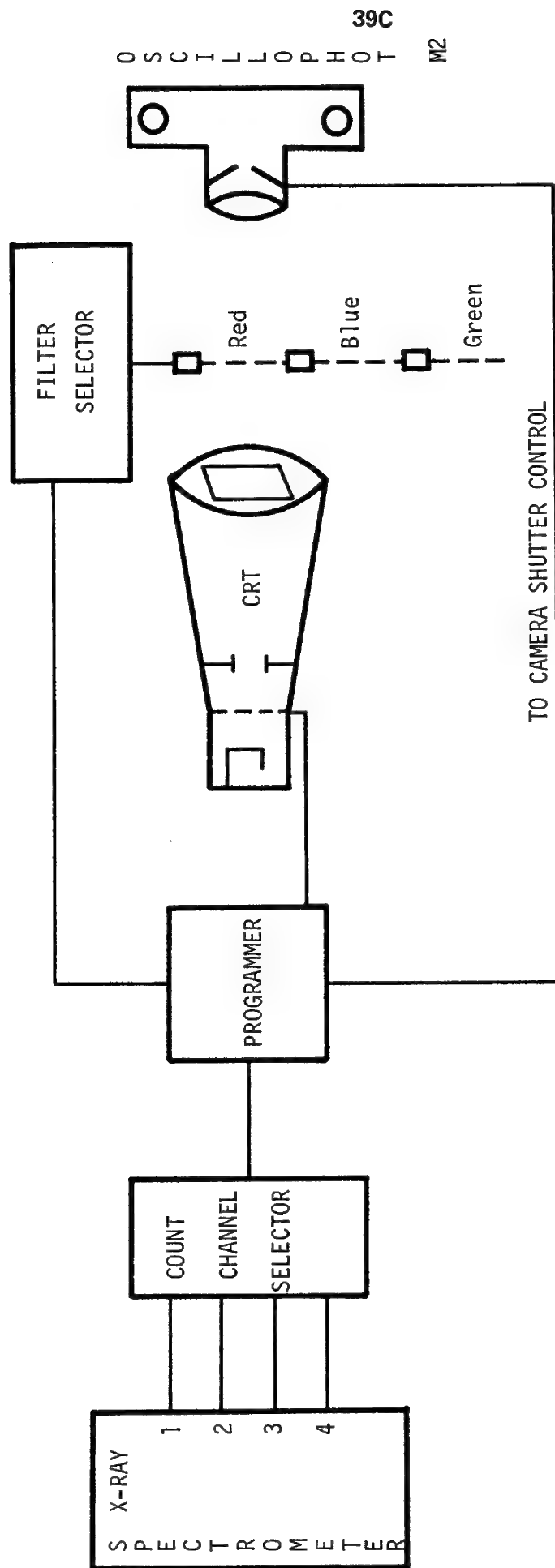


FIGURE 1  
SCHEMATIC DIAGRAM OF AUTOMATED SYSTEM FOR COLOR X-RAY IMAGES



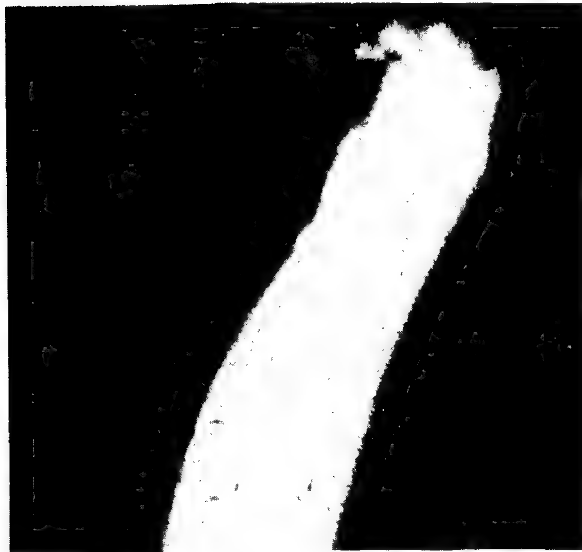
Al

250X



Fe

250X



Cu

250X



Blue

Red

Green

Red

Blue

250X

Color Composite and Black and White X-Ray  
Images obtained on a fractured end of metal laminate specimen.

CHARACTERIZATION OF HOMOEPITAXIAL GaAs USING THE  
DIRECT IMAGING MASS ANALYZER

R. Lewis\*, R. B. Marcust† and J. DiLorenzo†

\* -Bell &amp; Howell Co., Pasadena, California

† -Bell Telephone Laboratories, Inc. Murray Hill, New Jersey

A Bell & Howell/Cameca ion imaging mass analyzer has been used extensively to study a variety of conductive and insulating materials. These studies have been directed towards investigating the applicability of this new analytical technique in characterizing a number of typical specimens encountered in metallurgical, geological, biological and semiconductor device investigations. Some of these specimens have also been studied with the electron probe microanalyzer which provided a valuable comparison of the two techniques.

This ion imaging mass analyzer method was first described by Castaing and Slodzian<sup>1</sup>. The description of the instrument has been published in detail elsewhere<sup>2</sup>.

The instrument produces a beam of positive or negative ions which sputter material from the sample, forming a crater ~300 $\mu$  diameter; only the ionic fraction of material from a region ~150 $\mu$  diameter contributes to the signal, thus avoiding the steeply curved sides of the crater. An instantaneously viewable 300X ion image can be produced which gives the lateral spatial distribution of all isotopes of any element (m/e). In addition, this spatial distribution may be followed in depth since successive layers are removed as the analysis proceeds.

A complete mass spectral analysis also may be obtained from any selected area within the image by suitable aperturing or probe techniques. Distribution in-depth may be found by tuning to a specific m/e peak and monitoring the intensity of this peak as a function of time. Using calibrated known erosion rates gives accurate in-depth measurement of chemical concentration, with a resolution better than 100 Å.

In a study of 2-10 micron thick epitaxial layers of n-type GaAs on bulk n+-type GaAs grown by halide synthesis transport, electrical measurements indicated variation in carrier concentration producing an "i" layer at the film substrate interface. The analysis required was an identification of the impurities which might account for this variation in carrier concentration. An in-depth distribution of silicon and potassium was monitored with the ion analyzer; the traces are shown in Fig. 1 for one sample. The presence of silicon and potassium at the

---

<sup>1</sup>R. Castaing, et al., "Focusing of Charged Particles, "Academic Press, New York, 1967.

<sup>2</sup>J. M. Rouberol, et al., "Transactions of the Third National Conference on Electron Microprobe Analysis", Paper No. 28, 1968.

interface was verified using the direct imaging mode. After burning down to the vicinity of the interface the mass analyzer was carefully tuned through the whole mass range, and the ion image was used as the means of detection. High concentrations of impurities at the interface produced well-defined curved bands in the image; the white band shown in Fig. 2 was produced by silicon at the interface, after moving the specimen slightly to bring a sloped side of the crater (containing this interface) into the viewing area.

Potassium and silicon are concentrated near the i-layer (compare  $N_D-N_A$  curve and silicon, potassium traces in Fig. 1) in particularly large amounts; silicon is present at a level near 1 atom %. A tentative correlation is made between the appearance of silicon near the interface and the appearance of an i-layer.

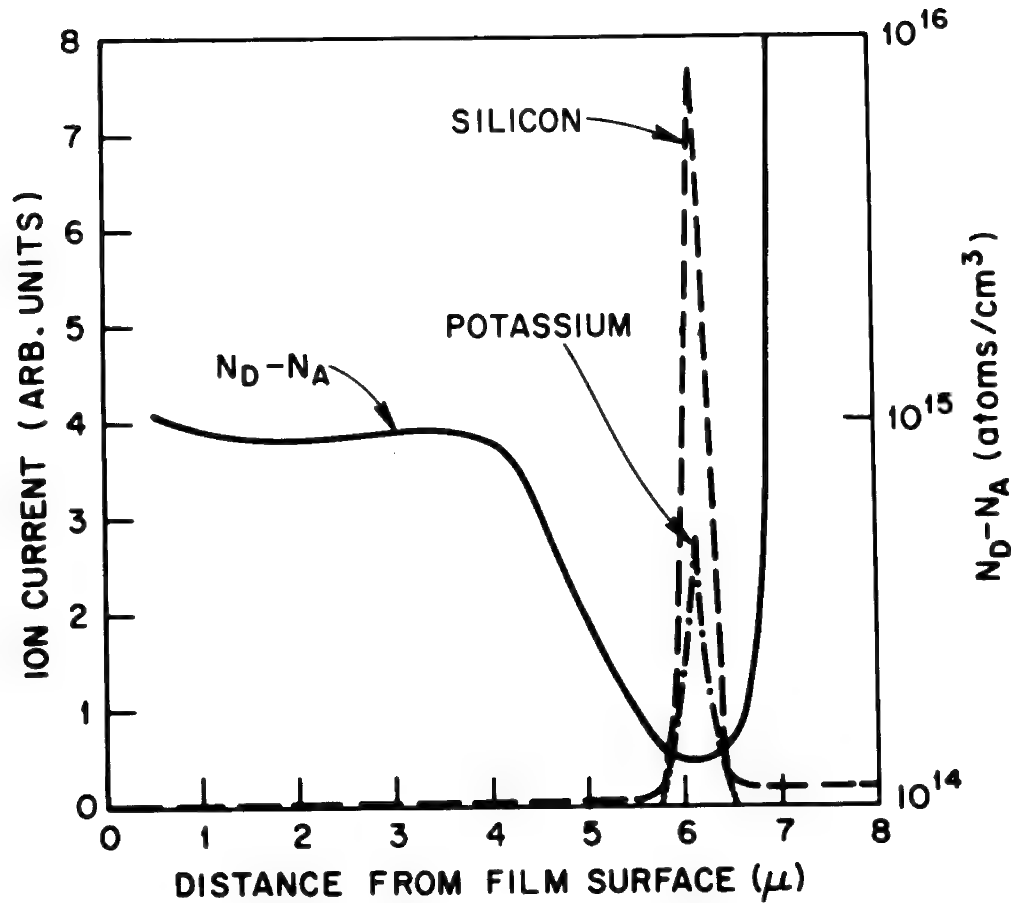


FIG.1 DEPTH PROFILES OF SILICON AND POTASSIUM, AND DEPTH PROFILE OF NET DONOR CONCENTRATION IN HOMOEPITAXIAL FILM OF GaAs; THE INTERFACE IS 6-7 $\mu$  BELOW THE SURFACE.



FIG.2 SILICON ION IMAGE ( $^{28}\text{Si}^+$ ) FROM ABOVE SAMPLE. THE LIGHT BAND SHOWS THAT SILICON IS HEAVILY CONCENTRATED NEAR THE INTERFACE.

## ION PROBE MASS SPECTROMETER: CONCENTRATION AND DIFFUSION PROFILING

J. M. Hollerbach

IBM Components Division  
East Fishkill Facility  
Hopewell Junction, N.Y. 12533

EXTENDED ABSTRACT

The GCA ion probe mass spectrometer is a new type of mass spectrometer used to analyze solid materials. A primary ion beam of argon ions bombards a solid surface and sputters off secondary particles. Of these, the positive ions are accelerated into a mass analyzer where they are sorted according to their mass: charge ratio and are detected. The magnetic field in the analyzer may be preset to allow only ions of a certain mass: charge ratio to reach the detector, thereby producing a concentration profile with depth as the ion beam peels layer after layer of atoms from the surface of the solid.

This latter capability, unique to the instrument, is further discussed by considering aspects of the sputtering process that may influence concentration profiling. A first consideration is the production of a high energy primary ion beam that has a low energy spread and that has a constant current density throughout a cross section of the beam. The duoplasmatron ion source satisfies well the former condition, whereas space charge effects in the einzel lens cause the ions to congregate more heavily near the perimeter of the beam. Moreover, the gas used as primary ion source is important with regard to sensitivity for different elements and complexity of the mass spectrum.

A high energy primary ion has both potential and kinetic energy. The potential energy can be lost by the processes of resonance neutralization and Auger de-excitation or neutralization near the target surface. The kinetic energy is dissipated by collisions with target atoms, which may subsequently become ionized by kinetic ejection mechanisms.



Sputtering of surface atoms occurs when sufficient energy is propagated to the surface from collision sequences in the bulk due to the primary atoms and struck atoms. There is yet some disagreement in the literature with regard to the mechanism of this energy propagation in the case of single crystals, but the trend seems to favor random collision cascades over focused collision sequences.

Channeling in single crystals gives rise to deeper penetration into the bulk and a concomitant decrease in sputtering rates due to the absence of collisions near enough to the surface. This effect, plus differences in binding energy for surface atoms in different crystal orientations, will cause difficulties in analyzing polycrystalline materials. Moreover, grain boundary areas will also sputter more easily, so that concentration profiling in polycrystals will only yield averaged concentration readings with depth. This problem does not exist for amorphous and crystalline materials.

The secondary ion current readings obtained on the instrument are dependent on sputtering yields and secondary ion yields. Sputtering yields depend on a large number of factors, such as target atom mass, primary ion mass, primary ion energy, target temperature, angle of incidence of the ion beam, lattice type and surface binding energy. The secondary ion yields, in addition, are dependent on factors such as work function, ionization potential, partial pressure of oxygen in the target chamber and lattice structure. The secondary ion yield for an impurity element will differ from that of the pure element in its solid matrix due to differences in bond type. Calibration of the instrument must take into account all these factors when converting ion current readings into concentration readings. It is, however, unnecessary to measure directly sputtering yields and secondary ion yields, if readings are compared to those from standard samples.

Ions sputter with varying amounts of energy; in particular, at higher energies molecular ions are unstable and cease to contribute to the spectrum. The energy window feature on the instrument permits selection of secondary ions that are in a narrow energy band at any energy level. Thus, it is possible to decouple some peaks, such as  $^{56}\text{Fe}^+$  and  $^{28}\text{Si}_2^+$ . Moreover, surface contaminants such as adsorbed gases sputter with

low energies, and their influence on the spectrum can be diminished by higher energy window settings.

Finally, sputtering of insulators is made possible by bathing the target surface with electrons from a nearby tungsten filament.

The space charge effect was first noticed when tally surf measurements of craters produced during ion bombardment indicated greater sputtering near the periphery. Consequently, different techniques were sought to produce flat craters that would render depth determination of concentrations meaningful. Three have been found:

1. masking the sample to select the center of the beam;
2. grounding the einzel lens; and
3. introducing a nearly transparent gold gauze in the einzel lens.

Diffusion profiles have been obtained for boron in silicon, and show agreement with electrical measurements. The sensitivity for boron at present is around  $1 \times 10^{16}$  atoms/cc, which has been obtained with special techniques such as the addition of oxygen into the target chamber. Modifications to the detector system will further increase the sensitivity to around  $10^{14}$  atoms/cc. A problem in determining concentration profiles is the procurement of suitable standards, since methods of calibrating the standards are often no more accurate than the ion probe mass spectrometer.

EXPANDED WAVELENGTH COVERAGE WITH  
DIGITALLY CONTROLLED X-RAY SPECTROMETERS

E. Davidson, A. J. Hartwick, J. M. Taylor

Applied Research Laboratories  
Sunland, California

---

The development of various crystal materials and their fabrication into fully or semi-focusing x-ray diffraction elements during the past twenty years made it possible to equip electron microprobe instruments with appropriate spectrometers for the analysis of specimens containing elements with high and low atomic numbers. However, the wavelength range covered by each diffraction crystal is severely limited by its own 2d planar spacing and the efficiency of crystals for the long x-ray wavelength region is decreased severely due to internal absorption. A concave diffraction grating used at a grazing incidence angle does not suffer from these disadvantages. Successful ruling and replication techniques have made it possible to consider the application of grazing incidence grating spectrometers for practical x-ray fluorescence analysis in recent years.

The work to be described in this paper is based on the earlier development work of Nicholson and Hasler, who reported on the experimental use of a blazed grating scanning monochromator in an electron microprobe.<sup>(1)</sup> More recent engineering development was carried out leading to the practical evaluation of a blazed grating spectrometer in a commercially available Electron Microprobe X-Ray Analyzer. Partial results of that evaluation are shown in Figure 1 and compared to those obtainable with appropriate crystal spectrometers. The spectrometer can cover the wavelength range from 8Å to 200Å encompassing the AlK $\alpha$  and AlL $\alpha$  lines. The advantages of the grating over crystal spectrometers are the following:

1. Wavelength coverage of at least three crystals.
2. Analytical results essentially equal or better.
3. Outstanding sensitivity for oxygen.
4. Long wavelength capability not at all attainable with available crystals.

The spectrometer is operated on a focal circle of 0.5m radius and uses a Bausch & Lomb gold coated concave diffraction grating with 1200 grooves/mm, blazed at an angle of 1°.

In order to operate the spectrometer with the highest degree of efficiency over the expanded wavelength range from 8Å to 200Å, which could not be covered even by three diffraction crystals, a versatile scanning system was designed, constructed, and evaluated. While manual operation of the detector or wavelength scanning drive and adjustment of the incidence angle or grating drive have not been eliminated, front panel control of these two drives should be considered the normal mode of operation. Additional sophistication is added through the application of a digital

control system shown in Figure 2. It provides automatic operation of the grating spectrometer as well as other dispersive x-ray spectrometers disposed radially in a multiple array around the central electron beam column. The digital controller or an optional, remotely located, computer replaces the operator in this mode since not only the spectrometers but also the pulse height analyzers, the sample stage, and the electron beam deflection can be automatically set. A special feature of the digital drive control unit is its ability to accelerate or decelerate the stepping motors for smooth and precise positioning action. Coordinate electron beam deflection and window widths as well as baseline adjustments of three pulse height analyzers are controlled by the D/A Converter. The multiplexer and the voltage to frequency converter permit selection of sample or beam current output to the associated scaler unit. The Scaler/Timer System receives information from the Digital Controller to determine whether pre-set time or counts will terminate data acquisition and serves to transfer analytical data back to the Digital Controller.

It has become apparent that the application of digital control devices and computers to the functional operation of electron microprobes and scanning electron microscopes can increase the effectiveness of many laboratories where repetitive analyses must be performed on a routine basis. The development of more versatile dispersive spectrometer arrays combining fixed wavelength monochromators and crystal as well as grating spectrometers for expanded wavelength coverage makes it even more desirable to use digital drive systems under software control for the achievement of greater efficiency not only in the service, but also in the research laboratory.

1. J. B. Nicholson and M. F. Hasler, "A Blazed Grating Scanning Monochromator Suitable for Use in an Electron Microprobe," Advances in X-Ray Analysis, 9, p. 420 (1966).

ELEMENT	GRATING		CRYSTAL (3)	
	C/S	L/B	C/S	L/B
F K $\alpha$	51,000 (1) 190,000 (2)	178 72	48,000 (4)	500
O K $\alpha$	34,000 (1) 116,000 (2)	243 70	9,500 (4)	500
C K $\alpha$	35,000 (1) 115,000 (2)	170 105	60,000 (5)	100
Be K $\alpha$	2,500 (2)	123	4,200 (6)	200
Si L $\alpha$	700 (2)	42	NOT ATTAINABLE	
Al L $\alpha$	63 (2)	25		

EXIT SLIT WIDTH	CRYSTAL
(1) 0.05 mm	(4) RAP
(2) 0.25 mm	(5) Pb SD
(3) 0.50 mm	(6) LIGNOCERATE

DATA @ 10KV 1.0  $\mu$ A  
& NORMALIZED TO 100 %

Figure 1

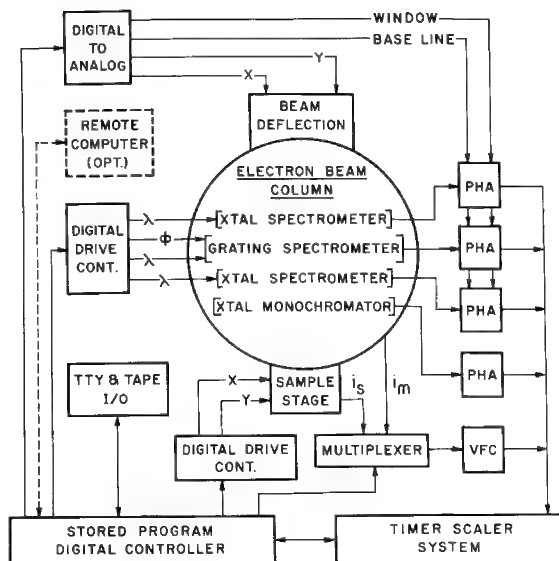


Figure 2

AN IMPROVED TARGET CURRENT AMPLIFIER FOR THE  
ELECTRON MICROPROBE AND THE SCANNING ELECTRON MICROSCOPE

by

K. F. J. Heinrich, C. E. Fiori, and L. A. Marzetta  
National Bureau of Standards  
Washington, D. C. 20234

We have constructed a novel amplifier for the formation of scanning target current images of improved versatility and quality. The device consists of two basic units, called the linear amplifier and the derivative signal modulator.

By using low-noise operational amplifiers of recent availability, and by eliminating ground-loops and other sources of noise, we have obtained a linear amplifier which yields images of satisfactory quality with target currents as low as  $10^{-9}$  A. The output of the linear amplifier is modified in the derivative signal modulator.

The derivative signal modulator contains the following components:

1. An inversion stage, which permits inverting the polarity of the signal if so desired.
2. A derivative signal generator, which produces the first derivative with respect to time of the amplified signal.
3. A signal mixer, which mixes the original signal and its first derivative in adjustable proportions.
4. An output amplifier which provides the signal level required to drive the cathode ray oscilloscope tube.

If the output signal is entirely derivative, all areas of uniform target current, regardless of level, are depicted in the same gray tone. Therefore, the derivative signal provides images containing mainly topographic information, while the linear amplification of the signal yields an image which also reflects differences in atomic number. Both signals can be inverted and combined in any proportion (Figure 1). The adjustment of conditions of operation is easily controlled if both the original signal and the output signal are monitored by means of an oscilloscope.

The same amplifier can also be used with advantage to provide secondary electron images and has been employed for this purpose on a scanning electron microscope.

When used to amplify target current, this amplifier, in a totally or partially derivative mode, is capable of yielding images which closely resemble secondary electron images. Experiments with a scanning electron microscope showed that up to 10,000X the spatial resolution of target current images is comparable to that

of secondary electron images. This amplifier should therefore be particularly useful in connection with microprobes which are not provided with secondary electron detectors. In particular, it will be demonstrated that with proper signal modulation, very satisfactory images of the interior of cracks and recesses can be obtained. The device also yields greatly improved images of three-dimensional microscopic objects.

The modulated target current images can be used to advantage to improve the spatial resolution of composite color images based on x-ray area scans.<sup>(1)</sup> These composites are obtained by superposing, in primary colors, up to three x-ray area scans. We have modified this technique by further adding, in neutral (gray) tone, a modulated target current scan. This adds topographic information to the image, and, at high magnifications, it delineates more sharply the phases present, the composition of which is represented by local color. The method, which will be illustrated with several examples, including material of lunar origin, constitutes a novel microscopic technique for the study of distribution of chemical elements.

---

(1) Yakowitz, H. and Heinrich, K. F. J., J. Res. NBS, 73A, p. 113-120 (1969).



Figure 1. Ilmenite grains and iron particles (in center) imbedded in diallylphthalate. Excitation voltage: 20 keV. Target current: 4.10 A. Magnification: 500 X. left: linear target current signal (inverted). center: differential signal. right: mixed signal.

## A CLEAN VACUUM ELECTRON BEAM COLUMN FOR CATHODOLUMINESCENCE INVESTIGATIONS\*

H. C. Marciniak and D. B. Wittry

Departments of Materials Science and Electrical Engineering  
University of Southern California, Los Angeles, California 90007

Due to contamination of specimens at low temperatures, it has been virtually impossible to study the temperature dependence of cathodoluminescence in conventional electron beam instruments. For this reason, a special electron beam column has been constructed.

To minimize the partial pressure of organic vapors in the system oil-free pumps were used. An oil-free carbon vane pump is used for roughing the system down to a pressure of 1000 Torr. The main pump assembly is a commercially available table-top UHV system. It consists of a liquid nitrogen cooled sorption pump which brings the system's pressure down to 5 Torr, and a combination of titanium sublimator and ion pumps capable of pumping to  $10^{-9}$  Torr or less.

The system is shown in Figure 1. The walls of the vacuum chamber are heliarc welded from plates of 304 stainless steel. Vacuum seals use either copper gaskets or Viton-A O-rings. Since some components used in the electron and light optical systems are not constructed according to UHV practices, the specimen chamber is partially isolated by a T-shaped tube located just below the electron lens. This tube has a small hole for the electron beam on top and a large outlet on the bottom communicating directly with the high vacuum pumps. A liquid nitrogen cooled copper cone is located at this outlet to reduce back diffusion of organic vapors to the specimen from the lower portion of the vacuum chamber. The system uses a single flat objective electron lens which is liquid nitrogen cooled<sup>1</sup> and located on top of the T-shaped tube. The liquid nitrogen flows first through the cold trap and then through this lens. Cooling of the lens along with the liquid nitrogen cold trap at the outlet of the T-shaped tube further reduces the partial pressure of organic vapors in the sample region.

The sample is mounted at the end of a cryo-tip refrigerator. This refrigerator unit is mounted on a bellows to provide specimen motion. The cryo-

---

\* Research sponsored by the Air Force Office of Scientific Research, Office of Aerospace Research, United States Air Force, under grant # AF-AFOSR-68-1414.



tip refrigerator uses Joule-Thomson expansion of high pressure nitrogen and hydrogen gas and is capable of achieving temperatures of  $25^{\circ}\text{K}$ . A small resistor is mounted in the sample holder so that studies of cathodoluminescence can be made above room temperature. The sample holder is electrically insulated by a thin mica disk from the cryo-tip refrigerator so that sample current can be monitored. A copper-constantan thermocouple which is in thermal but not in electrical contact with the specimen is used to measure sample temperature.

In preliminary tests pressures of only  $10^{-6}$  Torr have been achieved. Lower pressures are expected when some of the small leaks have been repaired and the system is pumped continuously for longer periods. Sample currents up to  $1\text{ }\mu\text{A}$ , with a spot size of about  $5\text{-}10\text{ }\mu\text{m}$  at an accelerating voltage of  $20\text{ kV}$  have been obtained. Sample temperatures of approximately  $30^{\circ}\text{K}$  have also been achieved.

In spite of the rather high pressure, no contamination of a GaAs specimen could be seen with an optical microscope after irradiation of a  $5\text{-}10\text{ }\mu\text{m}$  spot at a temperature of  $30^{\circ}\text{K}$  for 30 minutes with a sample current of  $0.18\text{ }\mu\text{A}$  and an accelerating voltage of  $20\text{ kV}$ .

Luminescence is collected by a reflecting objective. This system has a numerical aperture of 0.40, a magnification of 28.0 and a focal length of  $10.2\text{ mm}$ . The emerging light is mechanically chopped at  $11\text{ Hz}$  and is focused on the entrance slit of a spectrometer whose numerical aperture is 6.6. A lens in front of the entrance slit serves to reduce the image size so that a smaller slit can be used without reducing the amount of light entering the spectrometer. Light emerging from the exit slit falls on a photomultiplier whose signal is amplified and recorded by a synchronous amplifier.

The initial experiments to be made with this system involve temperature dependence of cathodoluminescence in  $\text{GaAs}_{1-x}\text{P}_x$  alloys and attempts to observe electron beam excited donor-acceptor pair recombination.

---

<sup>1</sup> Hermann Neuhaus, "Reduction of Contamination Effects in Electron Microprobe Analysis", Third National Conference on Electron Microprobe Analysis; No. 19, 1968.

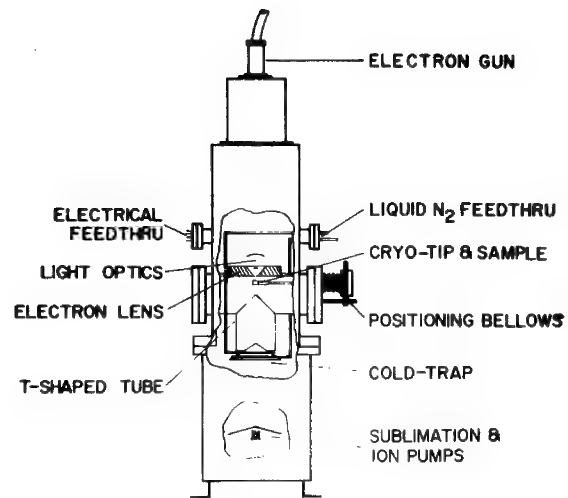


Figure 1 : Schematic Diagram of  
Electron Beam Column

# CHANGES IN THE FINE FEATURES OF X-RAY EMISSION SPECTRA FROM Al-Cu ALLOYS USING THE ELECTRON MICROBEAM PROBE

J. S. Solomon  
University of Dayton Research Institute  
Dayton, Ohio 45409

W. L. Baun  
Air Force Materials Laboratory (MAYA)  
Wright-Patterson AFB, Ohio 45433

Characterization of alloy phases by usual quantitative electron microprobe methods is usually a lengthy and complex process requiring accurate corrections or standards that are very near the composition of the unknown. Further, a standard quantitative analysis does not indicate whether chemical combination has occurred or if there is just an elemental mixture. Of course if the surface conditions are not ideal, quantitative analysis becomes extremely difficult.

Another approach to alloy characterization is to examine the effects of alloying on the X-ray emission spectra. Baun and Fischer have shown these effects in the Al-Cu system<sup>1</sup>. One effect of alloying on X-ray emission spectra in this system is the splitting of the Al K band into two components. Figure 1 is a plot of the energy difference between these two components versus the atomic % concentration

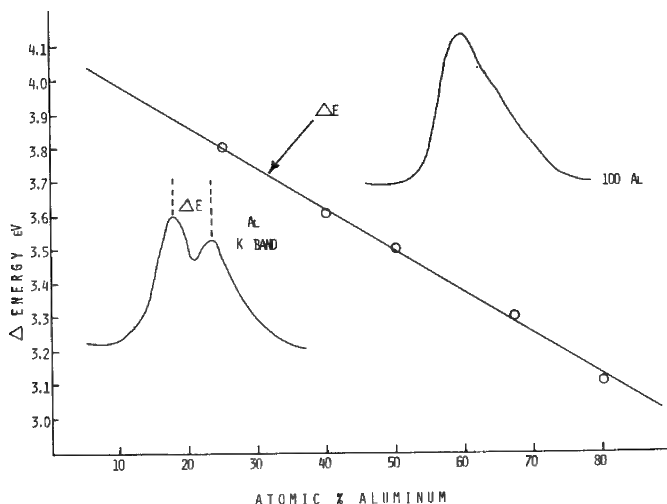


Figure 1

of the Al. Inserted in Figure 1 are the shapes of the Al K band from pure Al and an Al-Cu alloy. The energy difference between the two components,  $\Delta E$ , is nearly a linear function of the alloy composition and may be used to determine the composition of unknown Al-Cu alloys. Since the energy difference for a given composition is a constant it may be used in much the same way as a lattice parameter to determine the composition of an unknown alloy. Therefore, once the curve of  $\Delta E$  versus concentration for the entire composition range has been made it is not necessary to run standards each time an analysis is to be performed. In addition, surface conditions will have no effect on the value of  $\Delta E$ .

Changes in the features of the Cu La band are more subtle than in the Al K band. As the Cu content is decreased the band shifts to a slightly lower energy and features on the short wavelength edge become more prominent. The energy shift of Cu La is linear with Alloy Composition in the Al-Cu system and can also be used for alloy identification. However, since Cu La is so highly influenced by self absorption effects, sample and excitation conditions must be controlled carefully in order to use this band for chemical combination studies.

Measurement of the changes in the fine features of the Al K and Cu L X-ray emission spectra is a very tedious task that requires a high degree of precision in data collection. To guarantee precision and lessen the tedium in measuring these small spectral changes, automatic data acquisition and handling systems are used. The X-ray spectrometers are advanced in steps by precision stepping motors which are interconnected with a stepper control, printing timer-scaler, teletype interface, and teletype with paper tape output. The paper tape is fed into a computer and a data sheet for each spectrum along with normalized and smoothed plots of the spectrum are prepared by the computer. The measurements are taken directly from these data sheets and plots.

Three model Al-Cu systems have been studied. They include a diffusion couple, thin film, and hypervelocity impact specimens. Figure 2 shows the cross sections of two hypervelocity impact specimens. A is a cross section of the impact crater in a Cu target made by a 0.125 inch diameter Al projectile and B is a cross section of the impact crater in an Al target made by a 0.125 inch diameter Cu projectile. In both cases the projectile struck the target at a velocity of approximately 22,000 ft./sec.

The physical appearance of the crater walls is different in both targets. The crater in the Cu block A, in addition to being smaller, has fairly smooth sides and what appears to be an even coating of Al throughout the crater. The sides of the crater in the Al target, B, are very rough and irregular and a coating of the projectile material, Cu, is not evident in the crater. Electron microprobe analysis of the cross sectional edge of the crater in B shows Cu along the walls of the crater and isolated masses of Cu below the crater surface. X-ray emission spectra of the Al K band at points along the edge and in the Cu rich areas away from the edge show that chemical combination has occurred and the composition of the Al-Cu alloys were identified.

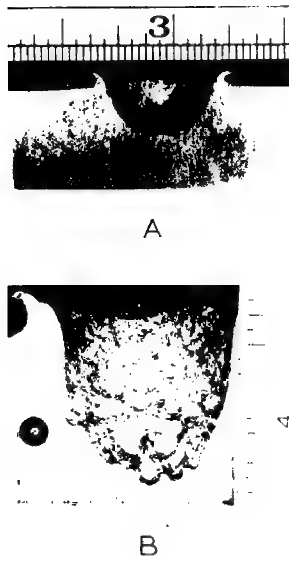


Figure 2

Likewise, the emission spectra from points along the edge of the crater in A show that alloying between the Cu target and Al projectile has occurred. Unlike the Al target B, there was no evidence of isolated masses of projectile material away from the crater's edge.

1. W. L. Baun & D. W. Fischer, J. Appl. Phys. 38, 2092 (1967).

# THE INTERACTION OF SELF PROLONGING AND NON SELF PROLONGING COUNTING COMPONENTS

D. R. Beaman, The Dow Chemical Company, Midland, Michigan  
 J. A. Isasi, Westinghouse Electric Company, Lester, Pennsylvania  
 H. K. Birnbaum, University of Illinois, Urbana, Illinois

---

Last year(1) it was reported that the efficiency of a commercial counting system depended upon the nature of the counting components comprising the counting channel. In this report the expressions governing the possible conditions of interaction in a two component counting channel are presented. When activation of a device results in the loss of any additional pulses arriving during a fixed time with no affect on the initial pulse, the deadtime is non self prolonging (nsp) or non extendable. The efficiency of a nsp device is  $m/n=1/1+n\tau$  where  $m$  and  $n$  are the measured and true intensities respectively and  $\tau$  is the deadtime. When incoming pulses to the device interact to create a single output pulse of increased pulse width (sometimes also increased pulse amplitude) with consequent loss of all interacting pulses, except the extended initial pulse to the counting system, the deadtime is self prolonging (sp) or extendable. The efficiency of a nsp device is  $m/n=e^{-n\tau}$  where  $\tau$  is the pulse duration associated with a single uninterrupted event in the device. The deadtime in the sp device was found to be(1)  $\tau'=(e^{n\tau}-1)/n$ . Experimental measurements revealed that preamplifiers and amplifiers were sp, while pulse height analyzers and scalers were nsp.

In the practical counting environment there are several components in a counting system and the problem is one of predicting losses when components of like or different nature interact serially. The effect of each component upon a random x-ray distribution entering a counter will depend upon its own characteristics and those of the preceding components in the circuit. In the figure, the following pulse configurations for two component systems are illustrated: a nsp component followed by another nsp component, sp followed by sp, sp followed by nsp, and nsp followed by sp for the conditions of  $\tau>\lambda$  and  $\lambda>\tau$  where  $\tau$  and  $\lambda$  are the pulse durations (not necessarily the deadtime) of the first and second components respectively. The triggering or driving of the second component is also considered since triggering can occur on the leading or trailing edge of the incoming pulse. The first and second component pulse outputs are schematically represented by sine and square waves respectively. In each case the deadtime ( $T$ ) and counting efficiency ( $m/n$ ) for the binary chain is given.

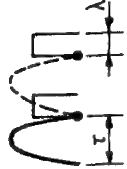
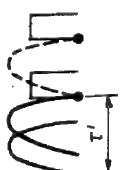







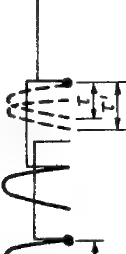
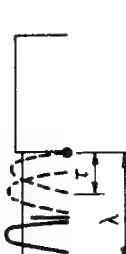

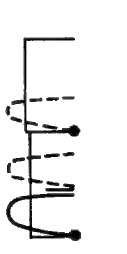
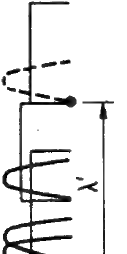
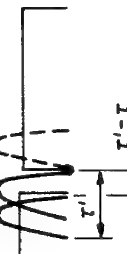

The procedure generally used to obtain these expressions was to establish the deadtime,  $T$ , of the binary chain and then use  $T$  to calculate the counting efficiency. When triggering of the second

component is on the leading edge of the pulse, the deadtime is the minimum time between two counted events. If  $\lambda > \tau$  and triggering of the second component is on the trailing edge, it is necessary to take into account the fact that the first component can begin to process a second pulse during the initial operation of the second component. In this case, the deadtime is the minimum time between the leading edge of the first pulse and the release of the second pulse minus the minimum pulse duration,  $\tau$ , characteristic of the first device. Once  $T$  is known, the number of pulses lost per second ( $n-m$ ) can be calculated, since the counts lost per counted event are  $nT$  and there are  $m$  counted events per second. Thus,  $n-m=mnT$  and the efficiency is given by  $m/n=1/(1+nT)$ . The derivation of the expressions shown in the figure will be discussed.

Some of these configurations are encountered in practice and the expressions for efficiencies are needed to accurately correct for counting losses. The limits of the expressions also provide guidance in understanding a real counting chain often containing five components. Measurements of the triggering sequence, the pulse duration characteristics of each component, and the component nature coupled with the expressions governing component interaction indicate that the reduction of commercial counting channels to binary systems is valid.

- 
1. D. R. Beaman, J. A. Isasi and R. Lewis, Proceedings Fourth National Conference on Electron Microprobe Analysis, July 16-18, 1969, Pasadena, California, Paper No. 13.

**POSSIBLE PULSE CONFIGURATIONS IN TWO COMPONENT SYSTEMS**  
**THE NATURE OF THE LEADING COMPONENT FOLLOWED BY (→) THE NATURE OF THE TRAILING COMPONENT**

$\tau$ vs $\lambda$	PULSE RE-LEASE			
	$nsp \rightarrow nsp$	$sp \rightarrow sp$	$sp \rightarrow nsp$	$nsp \rightarrow sp$
$\tau > \lambda$	 <p><math>T = \tau</math>  <math>m/n = 1/1 + n\tau</math>; Elmore, Blackman</p>	 <p><math>T = \tau'</math>  <math>m/n = e^{-n\tau}</math></p>	 <p><math>T = \tau'</math>  <math>m/n = e^{-n\tau}</math></p>	 <p><math>T = \tau'</math>  <math>m/n = 1/1 + n\tau</math>; Elmore</p>
	 <p><math>T = \tau</math>  <math>m/n = 1/1 + n\tau</math>; Elmore</p>	 <p><math>T = \tau'</math>  <math>m/n = e^{-n\tau}</math></p>	 <p><math>T = \tau'</math>  <math>m/n = e^{-n\tau}</math></p>	 <p><math>T = \tau</math>  <math>m/n = 1/1 + n\tau</math>; Elmore</p>
$\lambda > \tau$ or $\lambda > \tau'$	 <p><math>T = \lambda</math>  <math>m/n = 1/1 + n\lambda</math>; Elmore</p>	 <p><math>T = \tau' + (\{e^{n(\lambda-\tau)} - 1\} / n)</math>  <math>m/n = 1/\{e^{n\tau} + e^{n(\lambda-\tau)} - 1\}</math></p>	 <p><math>T = \tau' + (\lambda - \tau)</math>  <math>m/n = 1/\{e^{n\tau} + n(\lambda - \tau)\}</math></p>	 <p><math>T = \tau + (\{e^{n(\lambda-\tau)} - 1\} / n)</math>  <math>m/n = 1/\{n\tau + e^{n(\lambda-\tau)}\}</math>  <math>m/n = \text{Eq. 7; Elmore, Ruark}</math></p>
	 <p><math>T = \lambda</math>  <math>m/n = 1/1 + n\lambda</math>; Elmore</p>	 <p><math>T = \lambda' = (e^{n\lambda} - 1) / n</math>  <math>m/n = e^{-n\lambda}</math></p>	 <p><math>T = \lambda + (\tau' - \tau)</math>  <math>m/n = 1/\{e^{n\tau} + n(\lambda - \tau)\}</math></p>	 <p><math>T = \tau + (\{e^{n(\lambda-\tau)} - 1\} / n)</math>  <math>m/n = 1/\{n\tau + e^{n(\lambda-\tau)}\}</math>  <math>m/n = \text{Eq. 7; Elmore, Ruark, Blackman, Alaoglu}</math></p>



## IMPROVED LOW CARBON ANALYSIS OF Fe-BASE ALLOYS

E. Eichen, K. R. Kinsman, and J. Tabock  
Ford Motor Company, Dearborn, Michigan

The principles of design for adding a light element detection capability to an existing electron microprobe analyzer are well recognized. The factors involved for achieving good quantitative results in the long wavelength region of the light element x-ray spectrum are essentially the same as that for the heavier elements, namely, the availability of good crystals of the proper "d" spacing, the availability of good standards, and the ability to analyze the sample without contaminating it. It is in the last two areas where major difficulties of analysis reside since good crystals for detecting carbon are now readily available. The main technological factor which establishes the lower limits of the detectability range for carbon is the effective control of sample contamination during analysis. Realizing that optimum control can rarely be established in practice we present here a simple yet practical design for installing an effective anti-contamination device in a probe which may also serve the daily needs for other than light element detection. The detectability limit for carbon in iron has been lowered to the point (about 0.03% C) where the classical problems in ferrous physical metallurgy are now accessible.

Standard microprobe equipment and techniques were employed for analysis which included a new lead stearate decanoate crystal in conjunction with a thin window flow proportional counter using P-10 gas. The significant innovation in our experiment was the use of a cold finger, the design of which is shown in Figure 1. Anti-contamination devices in general are conceptually simple in design; however, the differences in efficiency seem to depend more on how much cooling surface is within the vacuum tank of the probe rather than on the complexity of the geometric configuration. Thus, the anti-contamination efficiency of this design is directly related to the fact that a significant amount of the liquid nitrogen reservoir (in the form of the long tube) lies within the probe tank. In the design of any anti-contamination device based upon the use of liquid nitrogen, it is important not to cool the specimen or its holder since as they approach the temperature of the anti-contamination device, the ability to prevent the specimen from contaminating rapidly decreases. Thus a design which cools the objective lens can defeat the initial purpose unless the specimen is fitted with a compensatory heater to keep the sample temperature close to ambient. With the above apparatus and employing a baffled, liquid nitrogen trapped, oil diffusion vacuum system, it is possible to operate on one spot of the sample for six and one half minutes (6 1/2) before the onset of detectable contamination. Actual counting times in practice were controlled by the counting statistics required and ran a little over 2 minutes for the metallurgical evaluation reported below. The useful detectability limit was established as always being less than 0.03%.

An improved set of Fe-C standard specimens were prepared, with special precautions as to metallurgical procedure, which supersede the set which was previously available.

This improved carbon detection unit was critically evaluated through application to a metallurgical problem of classical importance previously outside the range of electron microprobe analysis. The

requirements of the technique were both chemical and spatial. They are chemical in the sense that it is necessary to analyze in the range of solubility of carbon in ferrite which is in the order of 0.025%, and they are spatial because of the necessity of analyzing extremely small plates (in the order of 2-3 microns thick). In the example shown in Figure 2, the spatial distribution has been relaxed for demonstration purposes. A large second phase article was traversed, as indicated by a retrace performed after the actual analyses under conditions which led to rapid contamination thereby marking the path of carbon content evaluation. The requirement, metallurgically, was to establish significant, and scientifically meaningful deviations in carbon content between ferrite and the surrounding austenite matrix (appearing here at room temperature as martensite) in an alloy which contains only 0.11% C, the previously accepted detectability limit for carbon analysis using this microprobe technique. The results are illustrated in Figure 2a by the carbon concentration profile across the ferrite grain boundary precipitate shown metallographically in Figure 2b. The carbon content of the ferrite lies below the new detectability limit of approximately 0.03% C, the metallurgically expected result.

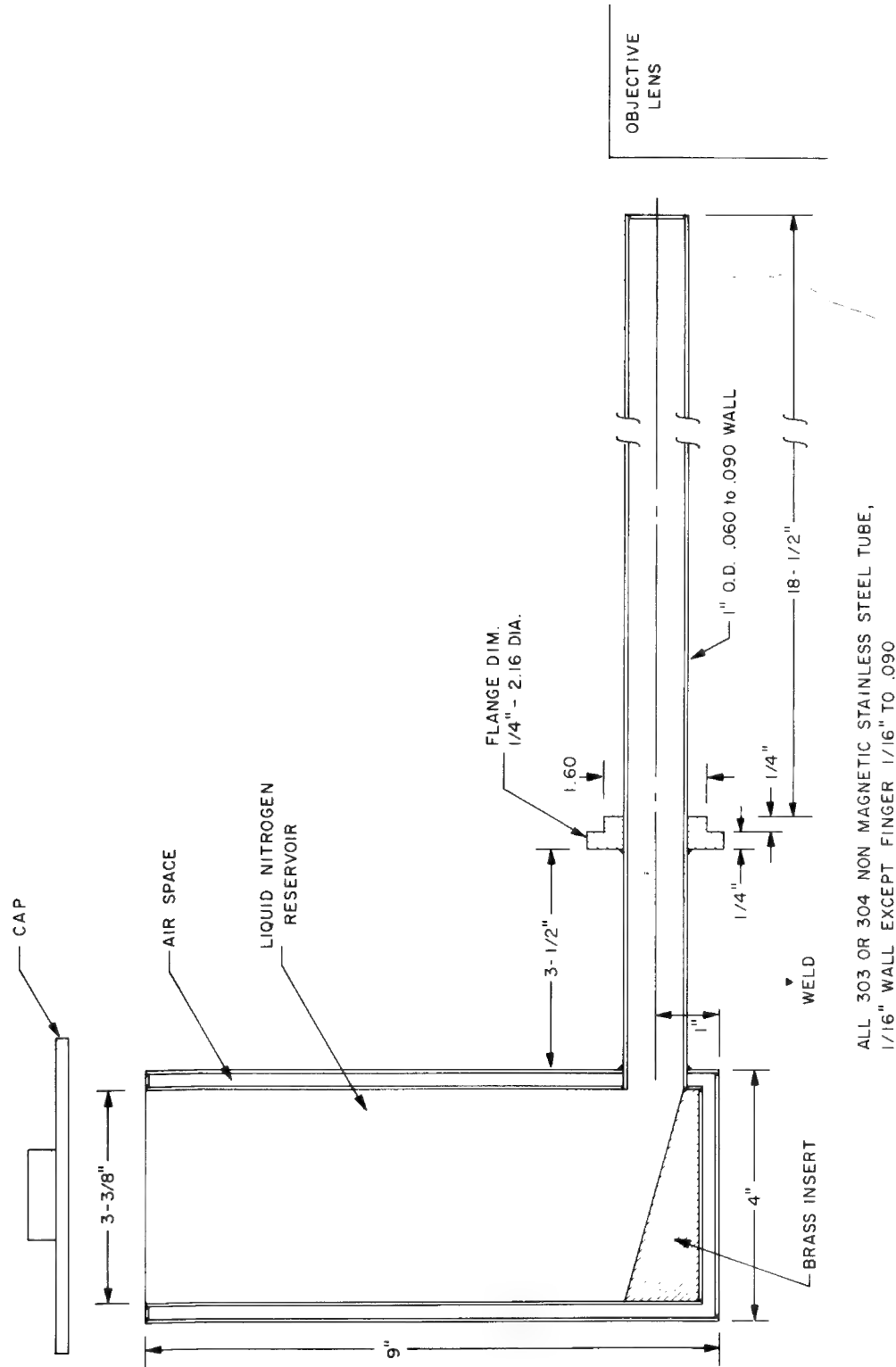


Figure 1 - Engineering drawing of the decontamination device adapted to the A.R.L. -E.M.X. electron microprobe analyzer.

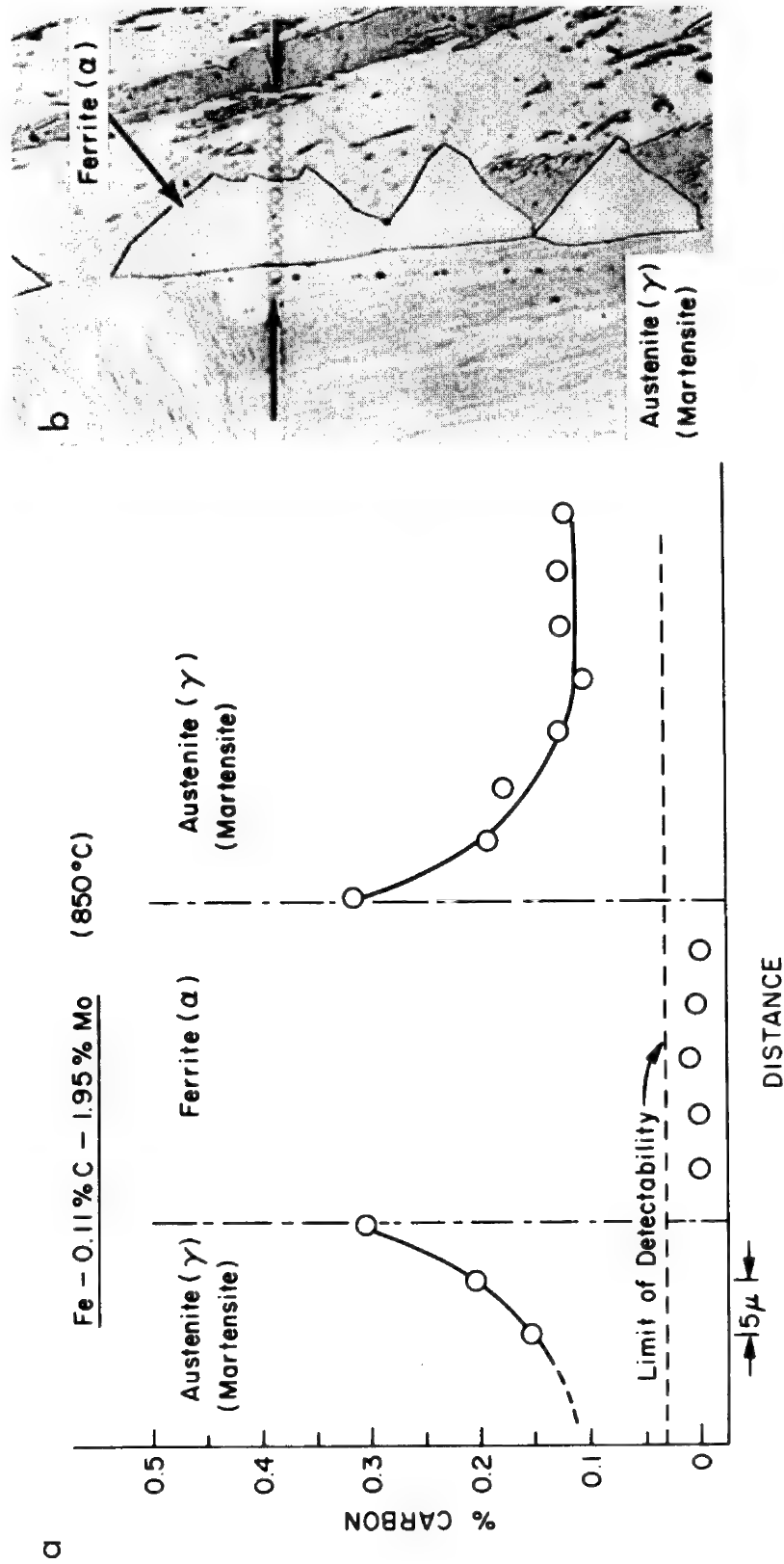


Figure 2 - (a) Chemical resolution of the improved technique as demonstrated via the carbon content profile across grain boundary ferrite precipitated from an austenite (here transformed to martensite) matrix at 850°C. (b) Etched and retrace (contaminated condition) microstructure of the profile plotted in (a).

# HIGH RESOLUTION SCANNING ELECTRON MICROSCOPY WITH AN ELECTRON MICROPROBE

C. H. Anderson, J. W. Leitner, J. M. Taylor

Applied Research Laboratories  
Sunland, California

---

The advantages of carrying out an elemental analysis on a sample whose morphological features have been characterized by scanning electron microscopy are generally recognized. Two separate approaches have been made to date: (1) scanning electron microscopes have been fitted with dispersive or non-dispersive x-ray detectors, or (2) electron microprobes have been equipped with secondary electron detectors and beam scanning capabilities. While it appears that it will be difficult to achieve the analytical capabilities of a microprobe by further modifications to a scanning electron microscope, it would seem that reductions in beam size are possible in an instrument whose design is optimized for electron probe microanalysis. As a result, its performance in a SEM mode would be equivalent to that achieved in all but the very highest resolution scanning electron microscope. It was the objective of this investigation to achieve routinely with the EMX-SM, 500Å resolution with a possible resolution of 250Å when operated in the SEM mode. In addition, it was a further requirement that there be no degradation of present beam size-sample current relationships of the ARL EMX-SM when the probe was operated at the higher sample currents (5-100 nanoamps) necessary for x-ray microanalysis.

Preliminary estimates of the spherical aberration coefficient of the inverted objective lens in the EMX-SM indicated that the contribution of this aberration to spot size was of negligible proportions ( $\sim 50\text{\AA}$ ), and allowed further consideration of modifications to achieve a small (250Å) beam size. If the beam size were to be reduced by a factor of 4-8 (with a two lens system) it was necessary to: (1) reduce the size of the cross-over point in the electron gun, and (2) increase the total demagnification by decreasing the focal length of the condenser lens. At the same time, since very low beam currents are associated with minimum spot size, a more efficient secondary electron detection system would be required. Other factors to be considered, which become more critical at high resolution, were: (1) the effect of magnetic fields, and (2) vibration effects.

Initial experiments were carried out to improve the secondary electron signal detection capabilities. Improved geometry and scintillation detectors resulted in a 20-30 fold increase in detection efficiency. Vibration effects were readily eliminated with a vibration dampening device and shielding of the high voltage power supply together with the shielding already present in the instrument reduces magnetic effects to negligible proportions.

In order to determine the best conditions for minimum source size (cross-over diameter) the probe was operated as a one lens system, using the objective lens only to demagnify the source. Since the total demagnification is known, the relatively large beam sizes (1-2  $\mu\text{m}$ ) can be readily measured and the effective cross-over size determined

under a variety of experimental conditions. With the conventional grid cap operating at low emission currents, the source size was reduced from approximately 100 microns to 60 microns. Resolution tests confirmed that corresponding improvement in resolution from .18 microns to .10 microns was obtained. Experiments with modified grid caps were carried out and under optimum conditions it was found that a source size of 25 microns was achieved. Confirming resolution studies showed the predicted resolution to be observed ( $500\text{\AA}$ ).

In order to further demagnify the source, the condenser lens focal length was decreased by a factor of approximately 2.2 by the addition of a lens insert thus furnishing a predicted (approximately)  $220\text{\AA}$  beam size. Confirming resolution tests show approximately  $250\text{\AA}$  resolution attainable with this system. Figure 1 illustrates a typical example of resolution which can be obtained.

Measurements of beam size versus sample current show no degradation of spot size at 5-100 nanoamps sample current; thus no compromise of x-ray performance has been observed. Furthermore, SEM pictures obtained using the liquid nitrogen cooled lens as an anticontamination device, are equivalent to those obtained at ambient temperatures.

In summary, it has been shown that by relatively simple modifications to a two lens microprobe, high resolution scanning electron microscopy can be accomplished with no loss in performance in the x-ray microanalytical mode.



FIGURE 1 GUPPY SCALE 20,000X

A UNIVERSAL HEATING STAGE MODULE FOR USE IN  
ELECTRON MICROPROBE ANALYZERS AND SCANNING ELECTRON MICROSCOPES

William D. Donnelly

Materials Analysis Company  
Palo Alto, California

This paper describes the nature and application of a universal heating stage module for use in electron microprobe analyzers and scanning electron microscopes.

The heating stage module consists of two major parts, the heating stage and its power and coolant supply. The heating stage is composed of two parts in one package, a furnace body that holds the specimen to be heated and a subminiature electron source.

The furnace body, specimen and secondary electron source will fit in any specimen stage that will accomodate a one inch diameter by three-quarter inch high specimen. The heating stage will handle samples up to .20 inches in diameter by .15 inches high. The electron source used for heating is a triod mounted directly beneath the sample and capable of supplying up to 30 watts to heat the specimen. Specimen temperature is controlled by a time-proportioning on-off controller that senses a Pt-Pt, 13% Rh thermocouple that is in contact with the sample. The controller desaturates the hot tungsten filament during the controller's off cycle by lowering the filament heater current about 200°C, as a result there is virtually no emission from the electron gun during the off cycle.

Application of the heating stage module is demonstrated by showing scanning micrographs of several steel samples. These micrographs include the following modes: x-ray, specimen current and secondary electrons. The specimens shown include AISI 1040 steel, AISI 1020 steel and a .06% C steel. All three steels are observed to have a eutectoid transformation at 725°C and the .06% C steel is shown during the transformation  $\gamma \rightarrow \delta$  (1475°C).

Other solid transformations are shown at elevated temperatures up to 1600°C.

## Enzymatic Destruction of Bone

Arthur Saffir, Stephen Kreitzman and Michael Fritz

It has recently been reported that the enzyme phosphoprotein phosphatase is able to catalyze the rapid demineralization of tooth enamel. This enzyme, which has no apparent proteolytic activity and does not appear to hydrolyze synthetic hydroxyapatite, is thought to act by dephosphorlating the mineralized phosphoprotein matrix of the enamel.

Recent data from this laboratory have demonstrated bone destruction in vitro by phosphoprotein phosphatase, and have suggested a possible role for this enzyme in the resorption of bone in pathological and physiological conditions. The bone specimens after treatment with the enzyme however demonstrated a protein-like coagulum. As the major protein constituent of bone has been shown to be collagen, experiments were designed to investigate the possible additive effect of collagenase plus phosphoprotein phosphatase on bone specimens.

Fragments of bone from the mandibles of twenty-one-day-old COBS rats were dissected, defleshed and enclosed in dental wax so that an area of bone of approximately 3 X 3 mm was exposed to the test solutions.

The specimens were incubated for either 3 or 6 hours at 37° in two milliliters of one of the following solutions: 1) Deionized water, 2) 0.1 percent trypsin, 3) 0.1 molar sodium acetate buffer pH 6.0, 4) 0.01 percent phosphoprotein phosphatase, 5) Autoclaved, heat inactivated, 0.01 percent phosphoprotein phosphatase, 6) 0.1 percent collagenase, 7) Combination of 0.1 percent collagenase and 0.01 percent phosphoprotein phosphatase. All enzymes were prepared in the acetate buffer.

Following incubation all specimens were observed through a dissecting microscope and photographed. Selected specimens were subsequently prepared for scanning electron microscopic study.



The scanning electron microscopic examination of the treated mandibles revealed the three dimensional morphology of the in vitro lesions. The surfaces of the mandibles exposed to buffer alone, water, trypsin, or heat inactivated phosphatase, revealed no change from untreated mandibles. Treatment of the mandibles with collagenase produced a surface with irregular holes; these holes were either elongated or circular and their dimension often exceeded two-hundred microns. Phosphoprotein phosphatase produced changes in the bone surface considerably different from that seen with collagenase. A combination of the two enzymes produced the most marked result, large craters and gross destruction of osseous tissue. The extent of destruction varied directly with the time of exposure to the enzymes.

The scanning electron microscope has provided evidence that bone destruction can be simulated in vitro by the use of enzymes. These enzymes which are known to be present in vivo at sites of bone destruction, may conceivably be involved in the normal bone destructive mechanisms in vivo.

We wish to thank Mr. James Webber of Materials Analysis Company for providing a scanning electron microscope and electron microprobe for this study, and for his personal interest and discussions.

This study was supported in part by Grant #2879 from National Institute of Dental Research and by Bowman's Children's Dentistry Research Fund.

FIGURE 1 - CONTROL

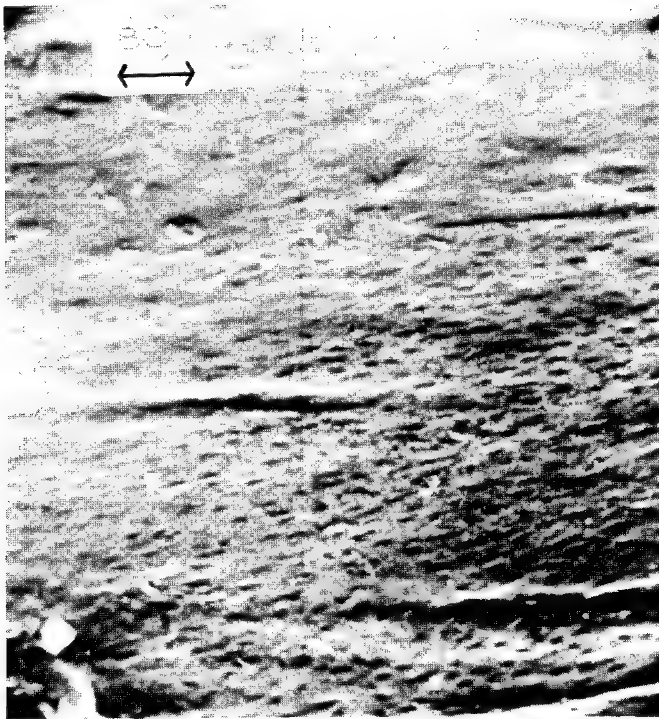
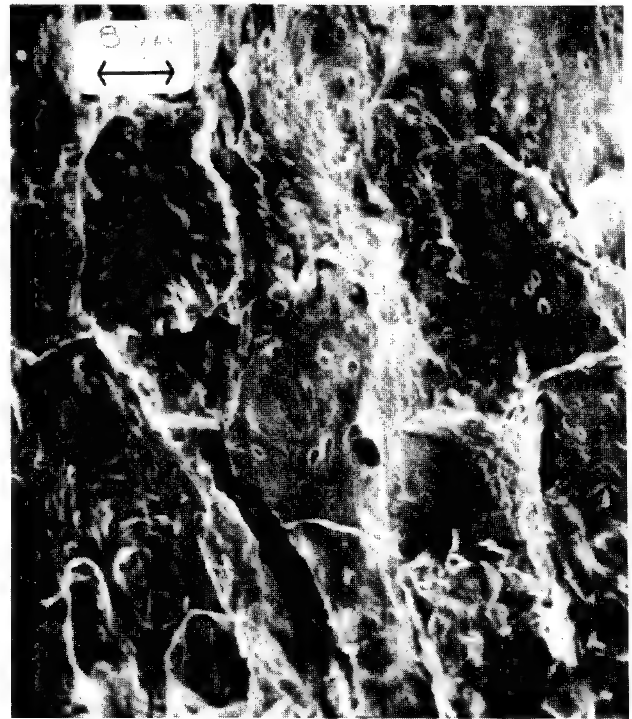
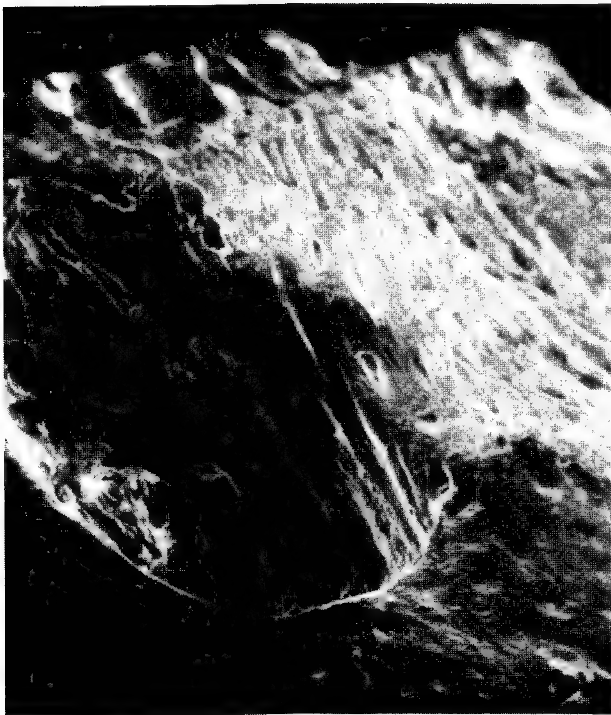


FIGURE 2 - COLLAGENASE

FIGURE 3 - COLLAGENASE  
AND PHOSPHOPROTEIN PHOSPHATASE

The untreated surface of bone is shown to be smooth by the SEM (Fig. 1). Six hours incubation with collagenase produced many small areas of destruction (Fig. 2). The combination of collagenase and phosphoprotein phosphatase produced craters several hundred microns in diameter (Fig. 3). The magnifications of Figures 1, 2 and 3 are identical.

## DISPERSIVE X-RAY SPECTROMETER FOR SCANNING ELECTRON MICROSCOPE

S. Kimoto, H. Hashimoto and S. Tagata  
Japan Electron Optics Lab. Co., Ltd., Tokyo, Japan

Recent scanning electron microscopes have the capability of x-ray microanalysis when used together with a non-dispersive spectrometer.<sup>1)</sup> As this spectrometer is superior in sensitivity to the dispersive spectrometer, it is used with a scanning electron microscope. But as the spectral resolution of the non-dispersive spectrometer is not enough yet for the electron probe microanalysis, the dispersive spectrometer is required for this purpose.

A fully focusing linear scanning spectrometer equal in performance to an electron probe microanalyzer has been developed for the JSM-U3 Scanning Electron Microscope. For its primary purpose, this scanning electron microscope is operated at a working distance of 13mm to obtain a probe diameter of below 100Å and for the purpose of microanalysis it is operated at a working distance of 32mm to reduce the probe diameter to 500Å or less. The electron probe bombards the specimen at a normal incidence angle. The take-off angle of x-rays is 30 degrees. The spectrometer has a Rowland circle 140mm in radius. Such a combined system poses a problem on the critical probe current for microanalysis which depends upon the efficiency on the spectrometer.

Figure 1 shows the relation between the probe diameter and current under a typical operational condition of the system for the purpose of microanalysis. At a probe current of  $10^{-9}$ A, a probe diameter of 1000Å can be obtained. The typical count rates of x-rays at this probe current are shown along with comparative data<sup>1)</sup> of the non-dispersive spectrometer in Table 1. In the region of light elements including Mg and Al, this spectrometer shows a higher count rate than the non-dispersive one. In the region of heavy elements, the count rate of the latter is several times higher. However, inconsideration of the peak intensity to background ratio, the overall sensitivity of the dispersive spectrometer is far better for most elements.

If an optimum count rate of the x-ray intensity to produce an x-ray image of good quality in reasonable exposure time is defined as  $10^4$ /sec,<sup>2)</sup> a probe current of  $10^{-8}$ A or less is sufficient for most elements. For example, at 25kV,  $4 \times 10^{-9}$ A for Al or Cr, and  $10^{-8}$ A for Cu are enough to obtain  $10^4$ /sec. Usually a count rate below  $10^3$ /sec is used in line scanning analysis and  $10^2$ /sec is sufficient for point analysis. Therefore, a probe current of  $5 \times 10^{-10}$ A to  $5 \times 10^{-8}$ A is effectively used and a probe diameter of 1,000Å to 5,000Å can be obtained with a sufficient x-ray intensity.

The practical spatial resolution of x-ray analysis is no better than 3,000Å due to a beam spread in the specimen under usual operational

conditions even if the probe diameter is substantially reduced.<sup>2), 3)</sup> Nevertheless, there is some merit in reducing the probe diameter when an object to be analyzed is as small as the spread beam. As the resolution of an electron image is far better than that of an x-rays image, the contour details of the object can be surveyed more clearly on the specimen surface. An x-ray image and a line scanning profile of Mn distribution in a tool steel are shown with a secondary electron image in Figure 2.

- 1) J. C. Russ and A. Kabaya; Scanning Electron Microscopy, P59(1969)
- 2) P. Duncumb; X-ray Microscopy and Microanalysis, Elsevier, P365(1960)
- 3) S. J. P. Read; X-ray Optics and Microanalysis, Hermann, P339(1966)

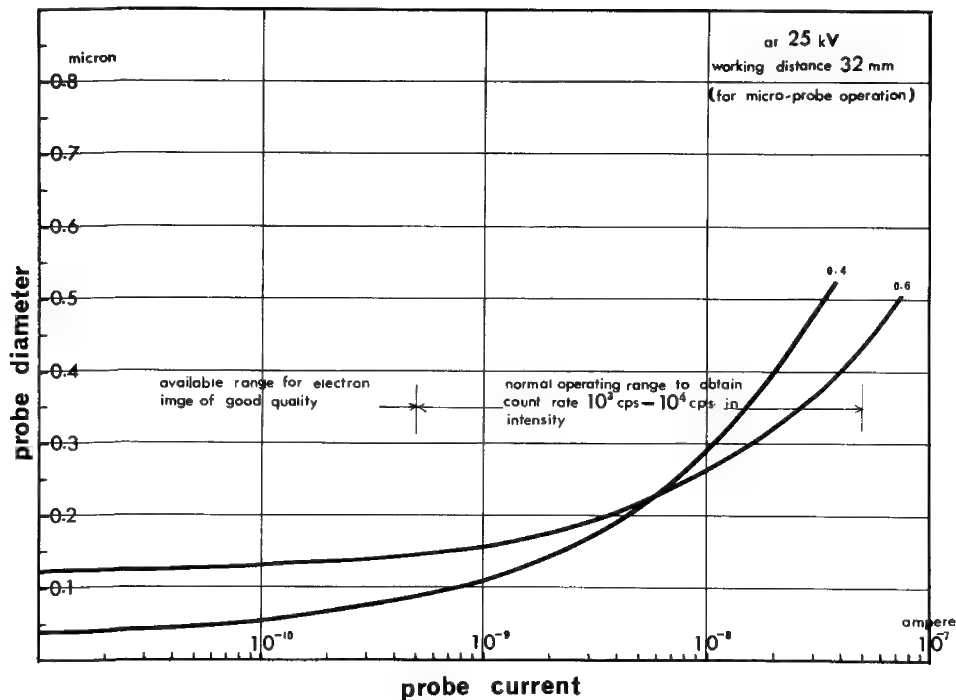
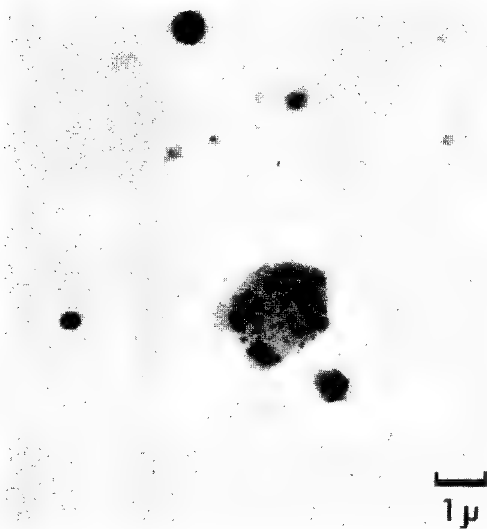


Fig. 1

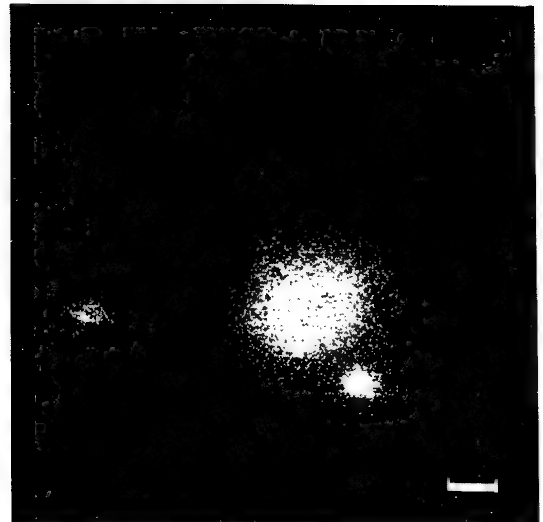
Line (Ka)	Typical Efficiency of Dispersive Spectrometer		Comparative Efficiency of <sup>11</sup> Non-dispersive Spectrometer	
	Peak Intensity (c.p.s./nA)	P/B Ratio	Peak Intensity (c.p.s./nA)	P/B Ratio
C	90	70		
Mg	2 000	2 000	800	7
Al	2 400	1 500	1 300	11
Si	1 800	850	2 000	16
Ti	1 800	700	10 000	22
Mn	1 800	300	.....	...
Fe	800	500	.....	...
Cu	1 000	300	14 000	16

Table 1

at 25kV (10 kV for Carbon)



(a)



(b)

(a) Secondary electron image  
exposure 50 sec.

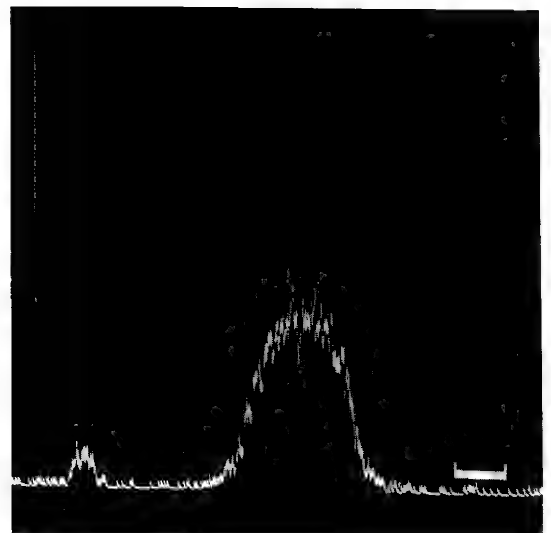
(b) Mn-K $\alpha$  X-ray image  
exposure 7,000 counts

(c) Mn-K $\alpha$  line profile  
exposure 500 sec.

$E = 25\text{kV}$

$i = 8 \times 10^{-10}\text{A}$

$d = 1,000\text{\AA}$



(c)

Fig. 2. Mn-distribution in Tool Steel

# THE USE OF BACKSCATTERED ELECTRONS IN HIGH RESOLUTION SCANNING ELECTRON MICROSCOPY

P.S. Ong

Philips Electronic Instruments

The electron energy spectrum emitted by a sample under electron bombardment consists mainly of two parts:

1. The "true secondary" electrons with an energy range of between 0 and 20eV.
2. The primary backscattered electrons with an energy range from 0 up to the primary electron energy.

Of these, only the secondary electrons are generally used for high resolution electron scanning microscopy. The reason for this is that in the past, various authors<sup>1,2</sup>, have successfully convinced the microscopists (and microscope manufacturers) that the only way to obtain good spatial resolution is to use the secondary electrons, which basically are emitted from the uppermost top surface of the sample. Backscattered electrons are emitted from a greater depth, and therefore result in poor resolution. Using 30kV electrons, the resolution would be no better than say  $0.5\mu^3$ . Combined with the low backscatter yield for low atomic number specimens, these electrons proved to be unsuitable for the study of biological samples.

In this paper I will show that with a gold coated sample, resolution below 250Å can be obtained with backscattered electrons using primary electron energy of 60kV. Moreover, resolution is expected to be better for low atomic number samples, which opens some interesting possibilities for the study of biological samples. This is true because in a uniformly coated sample, of which the coating is of much higher atomic number than the sample itself, the bulk of the backscattered electrons come from the coating. If the coating is made very thin, i.e., 200-500Å, the resolution limit will be set by the probe size, rather than by the diffusion of the beam. The coating must however, be thick enough to give a backscatter yield reasonably higher than that of the bulk sample. Experiments show that resolution below 250Å can be obtained on biological samples as well as various mineralogical and metal samples using gold palladium as a coating metal. The following pictures will illustrate some of the results. The voltage used was 60kV and the detector a Si diode. The instrument used here was the EM 300 electron microscope, provided with an SEM attachment. Figures 1a and 1b, show the difference in resolution between an uncoated and a coated Cu foil sample. The magnification is indicated by the 10μ bar.

Figure 1a, is uncoated while the same sample shown in 1b, gives more surface structure even at high magnification. In an earlier experiment we were limited by cracking of the gold layer as shown by the insert of Figure 1b,

(5x larger magnification). Excellent results are obtained by a better control of coating material (gold palladium 60-40) and thickness as shown in Figures 2, 3, 4 and 5.

Figure 2, is sponged copper as prepared by acid cyanide process. Figure 3, is a particle in a lunar dust sample from Apollo 11 flight. Figure 4, is a meteorite sample and Figure 5, red blood cells.

Finally, it is worthwhile to mention here that the coating thickness can be selected to yield a backscatter factor comparable to that of the bulk sample. In that case, variations in atomic numbers of the latter would "shine through" the high resolution surface structure, in various shades of density.

#### Acknowledgement:

The author wishes to acknowledge the competent assistance of Irene Piscopo in obtaining the pictures and the following persons and institutions who supplied the samples:

Treadwell Corporation, New York, New York, Figure 2.

Dr. G. Mueller, University of Miami, Florida, Figures 3 and 4.

Dr. P. Farnsworth, Barnard College, New York, New York, Figure 5.

#### Reference:

1. R.F.W. Pease and W.C. Nixon  
J. Sci. Instruments. 42, 81, (1965)
2. R.F.W. Pease  
J. Sci. Instruments. 42, 158 (1965)
3. P.R. Thornton  
Scanning Electron Microscopy, p. 209  
Chapman and Hall Ltd, 1968

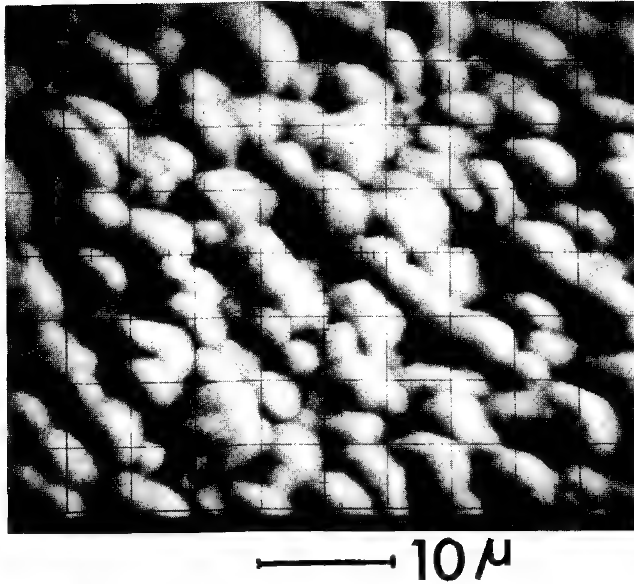


Fig. 1a, uncoated copper foil, 60kV backscattered electrons.

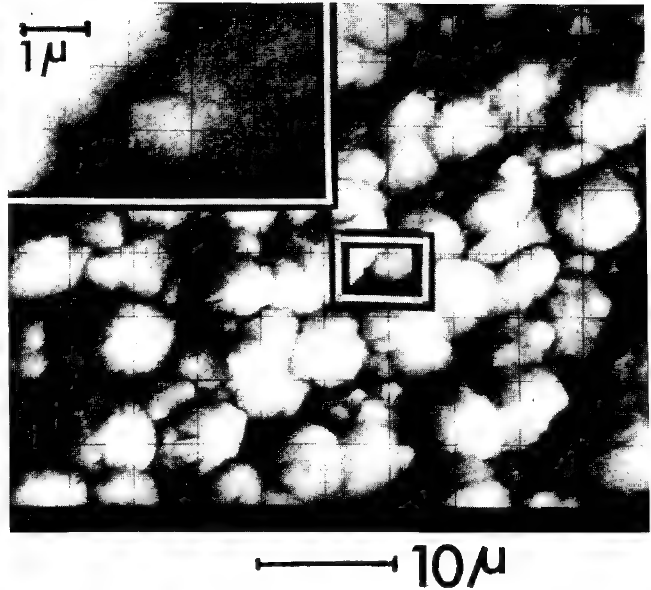


Fig. 1b, gold-coated copper foil, 60kV backscattered electrons. Insert 5x larger magnification shows cracks in gold layer.



Fig. 2, sponged copper-Treadwell acid cyanide process, gold palladium coating, 60kV backscattered electrons.

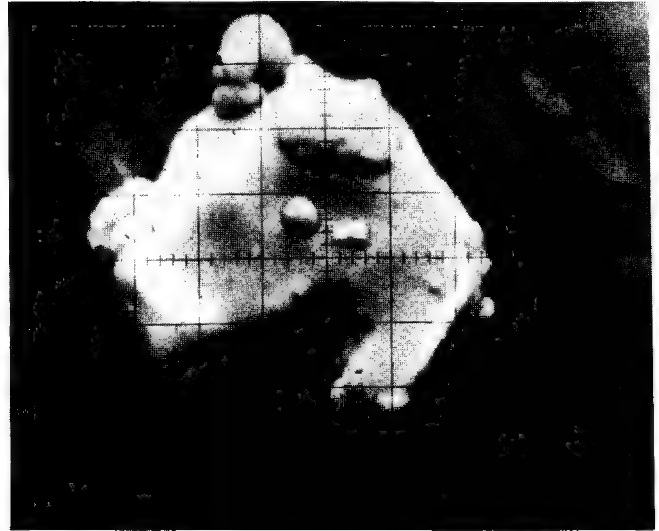


Fig. 3, Particle in lunar dust sample from Apollo 11 flight. Gold coating 60kV backscattered electrons.



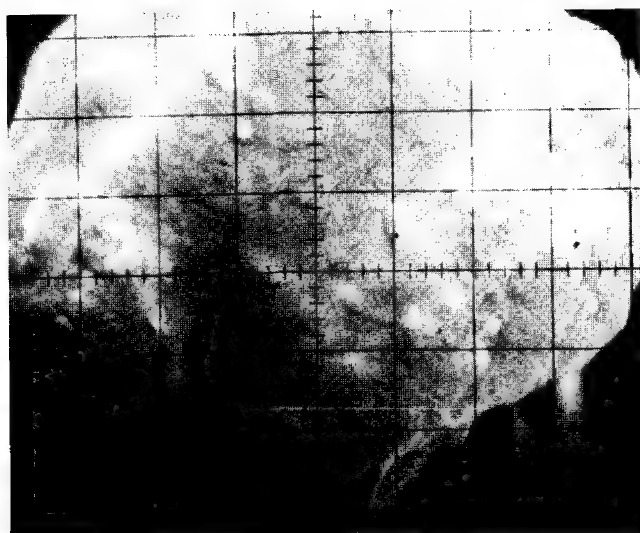


Fig. 4, Meteorite sample, gold coating, 60kV, backscattered electrons.

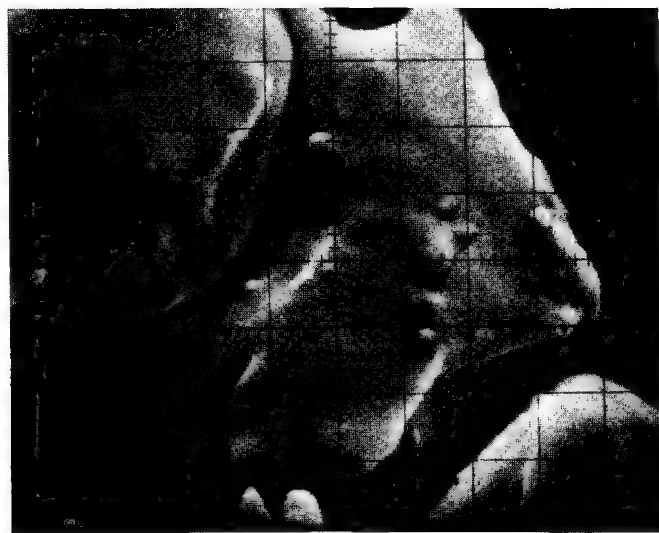


Fig. 5, human red blood cells, gold coated, 60kV backscattered electrons.

THE NEW AMR/PHILIPS HIGH RESOLUTION  
SCANNING ELECTRON MICROSCOPE

S. Moll, M. Schippert, R. Ogilvie\*, J. T. Norton, D. Koffman  
Advanced Metals Research Corporation  
\*Massachusetts Institute of Technology

The new AMR Model 900 High Resolution Scanning Electron Microscope (Fig's. 1,2) represents a new generation of commercially available instruments. Incorporating many modern design features in the electron optics, specimen chamber, electron detection and display systems, the AMR instrument provides a range of technical performance, ease of operation and convenience of maintenance never before available in Scanning Electron Microscopes.

The Electron Optical Column consists of an externally adjustable electron gun, electromagnetic beam alignment unit, two independent lenses, a final objective lens, stigmator, scanning coils, electron detector assembly, and finally, a large specimen chamber and specimen stage.

Each of the three magnetic lenses is contained in a modular cylindrical assembly which can rapidly be removed from the electron optical column as a unit. Each of the lenses may be mechanically aligned with the electron optical axis, during operation, with externally provided adjustments. Each lens contains its own aperture assembly with three disc type apertures. This holder can rapidly be interchanged and/or centered during operation. Thus it is possible to quickly align the lenses, insert clean apertures or change the illuminating conditions without disassembling the column. The aperture assemblies are easily withdrawn from the column for aperture cleaning. A fluorescent screen below the condenser lenses acts as an alignment aid and also permits inspection of the aperture cleanliness without their removal.

The specimen chamber allows incorporation of various types of specimen stages, experimental apparatus, bulky samples, etc. The internal dimensions of the chamber are approximately: 10 inches high, 14 inches long and 10 inches wide. Access is provided through the open front end and large ports are provided on both sides of the chamber. Multi-lead electrical connectors are provided to facilitate the operation of various microelectronic devices.

The eucentric goniometer stage (Fig. 4) will accept a specimen as large as five inches diameter and two inches thick and will analyze an area which is 1 1/4 inches square. One can mount any kind of sample holder but the standard unit holds five 5/8 inch diameter stubs. All of the X, Y, Z, rotation and tilt motions of the stage are centered with respect to the electron optical axis.

The tilt motion is  $-5^{\circ}$  to  $+60^{\circ}$  about an axis perpendicular to and intersecting the electron optical axis. The specimen may be rotated  $180^{\circ}$  in its own plane, about the electron optical axis, at any tilt angle. Lateral motion is  $1\frac{1}{4}$  inches in both the x and y direction, and always in the plane of the specimen surface regardless of rotation or tilt angle. The rotation and tilt motions are maintained with respect to the electron optical axis and the x-y motions are within the plane of the specimen surface, regardless of the working distance (Z motion). The working distance (specimen height) is externally adjustable so as to allow working distances which are continuously variable from zero to two inches. The specimen stage is mounted to the front door of the specimen chamber and may be removed as a unit after the chamber is vacuum isolated from the rest of the column.

All electronics are solid state and use integrated circuits on plug in boards for ease of service and trouble free operation. The cathode ray tube drives and the scan coils in the electron optical column are optionally programmed with either a standard solid stage analog, or a unique, solid state, digital scanning system.

The standard, analog scan system offers selection of almost any scanning speed ranging from 120 milliseconds per full picture frame to 2,000 seconds per frame. Simple push-button switches select single frame mode (for photography), line scan mode, point mode, or reduced or partial frame mode. A deflection modulation mode is also standard. The reduced or partial frame mode of operation is extremely important for fine focusing, stigmating, and gun and column alignment. The line scan and fixed point may be positioned anywhere within the scan field. The scanning rate is independently adjusted for both the display and record oscilloscopes. This allows the record scope to remain properly adjusted for perfect photography while the display scope is operated over a wide performance range. A TV scan rate monitor is also available.

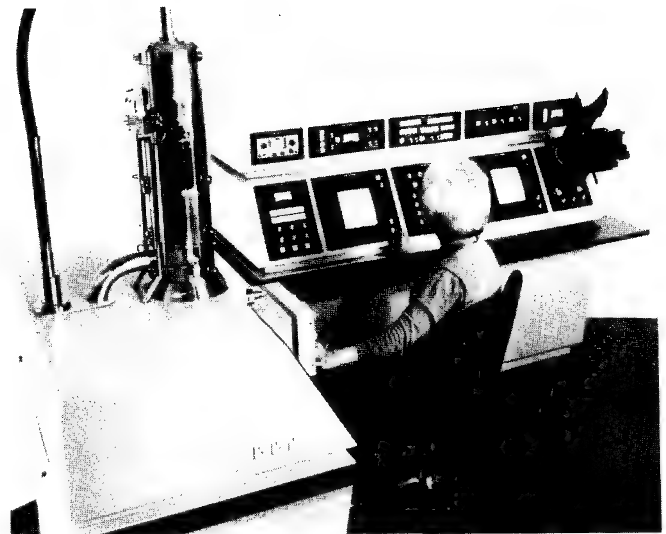
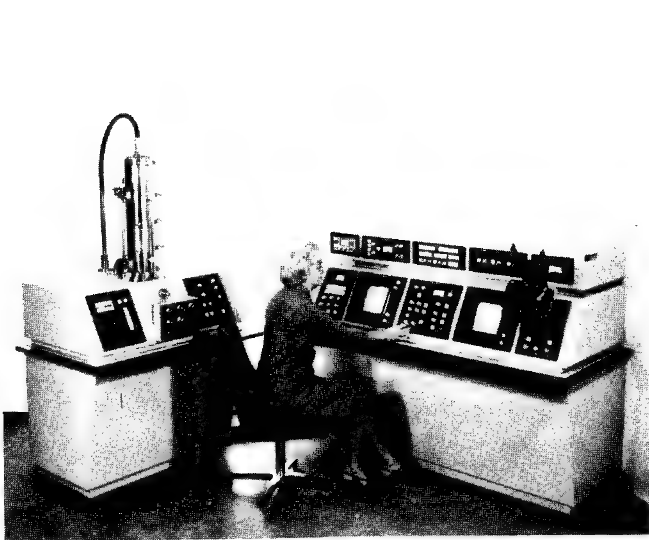
At a specimen working distance of 12 mm and an acceleration potential of 20 KV, the scanning coils in the column are capable of forming a distortion free raster as large as 5 mm square. The resulting magnification on the record scope is 20X. At a working distance of 50 mm, magnifications as low as 5X provide the operator a maximum in convenience in specimen searching. Magnifications up to 200,000X are obtained when the scan raster size is reduced to  $0.5\mu$  square.

The display oscilloscopes used in the Electronics and Display Console are a full 10 inches in diameter with P-7 phosphors and 800 lines resolution. The display scopes are mounted at an angle of  $30^{\circ}$  on the tilted console face. These large, tilted screens allow a convenience and ease in operator viewing. The record oscilloscope provides a fast response (P-11 phosphor) in a high resolution (1500 lines), 7 inch diameter CRT.

Two sets of signal processing amplifiers each allowing linear or non-linear gain corrections to be applied to the signal in order to improve the sensitivity to the fine low signal level detail are standard. In addition, the signal may be inverted so as to vary the sense of the black to white contrast obtained in the image.

The varying signal which is led from the signal processing amplifiers to the display or record scopes is also presented on both a signal monitor oscilloscope and signal level panel meter. The monitor scope displays a line scan which helps the operator to reproducibly adjust the signal contrast while the panel meter is used as an integrating device to allow proper adjustment of the average signal or gray scale brightness for perfect photography.

The AMR/Philips Model 900 also provides many other features which are new in scanning electron microscopy including an optional Scanning Electron Mirror Microscopy attachment. Applications and performance features will be discussed.



Fig's 1, 2 AMR/Philips Model 900  
High Resolution Scanning Electron Microscope

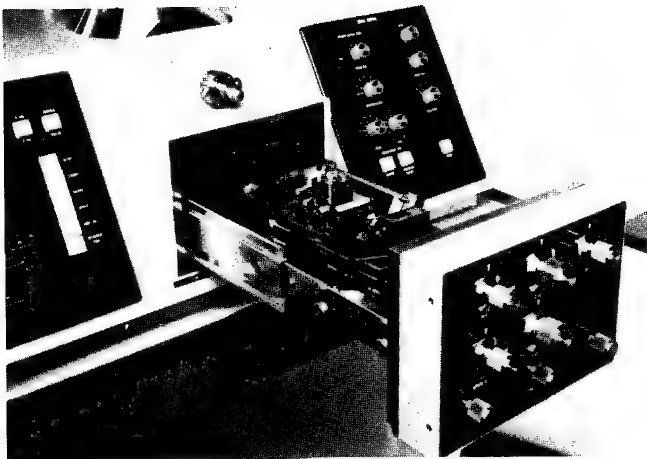


Fig. 3 Specimen Chamber & Stage  
Drawer

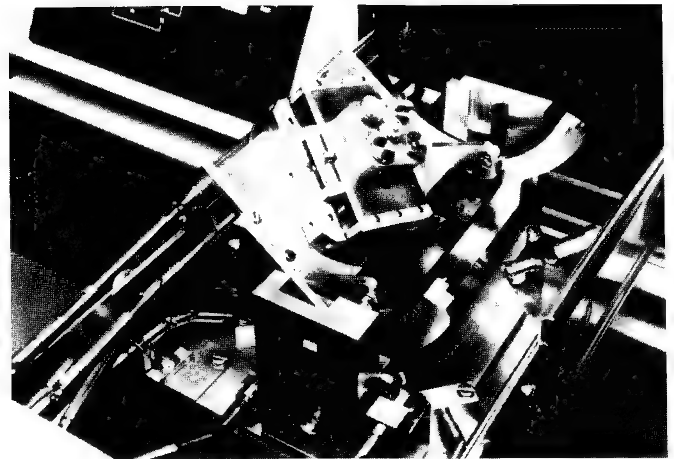


Fig. 4 Eucentric Goniometer  
Five Specimen Stage

## A NEW SCANNING ELECTRON MICROSCOPE

by J. GUERNET, M. TONG and C. CONTY

Société CAMECA - 103 Boulevard Saint-Denis  
92 - COURBEVOIE

A new SEM has been designed by CAMECA and is being exhibited in the U.S. for the first time at this conference. This instrument features the following :

- 1) complete goniometric capability for the sample stage with high mechanical reproducibility.
- 2) remote operation of the electron column specimen stage section.
- 3) very high operating vacuum.
- 4) a very high speed pumping system.
- 5) a wide variety of display modes.
- 6) a large specimen chamber readily adaptable to a variety of accessories.
- 7) versatile simple operation.

The SEM consists of three main sections, namely : an electron column, a remote control console and a power supply cabinet. The first two sections are shown in Fig. 1.

Classical electron optics have been utilized. The electron column employs a hot tungsten filament gun with three electromagnetic lenses. The high voltage is adjustable from 2 - 50 kV.

The large specimen chamber at the base of the column has been designed to accept a variety of accessories. In addition to the standard electron detection systems, the chamber will accept one energy dispersive X ray spectrometer, two fully focussing X ray spectrometers, a transmission electron detector, and a cathodoluminescence detector. The chamber can also be readily adapted with hot, cold or wet stages.

Particular attention has been given to the specimen stage design, which is shown schematically in Fig. 2. Complete goniometric capability and integrated X-Y controls allow tilt and rotation motions to be made without loss of focus or field of view. The mechanical reproducibility of the X-Y motions is better than one micron. The Z focussing adjustment is coupled with the electron optical focussing to facilitate maintaining focussing when changing specimen height.

A schematic of the pumping system is shown in Fig. 3. The secondary vacuum pump is a 1200 l/s oil pump with low back diffusion. Connection to the main chamber is made through a high conductance manifold which contains a LN<sub>2</sub> baffle. The primary vacuum pumps are isolated with zeolite traps. All vacuum seals are either metal, viton gasket or bellows. The specimen interchange is made through an air interlock system. The typical operating vacuum achieved is  $2 \times 10^{-7}$  Torr.



# INDEX OF AUTHORS AND THEIR AFFILIATIONS

		<u>Paper Number</u>
Andersen, C. A.	Hassler Research Center, Applied Research Laboratories, Goleta, California, 93017	38
Anderson, C. H.	Applied Research Laboratories, 9545 Wentworth Ave., Sunland, California, 91040	48
Aronstein, J.	I. B. M. Components Division, Hopewell Junction, New York, 12533	22
Baum, T.	Bell and Howell Company, 360 Sierra Madre Villa, Pasadena, California, 91109	39
Baun, W. L.	Air Force Materials Laboratory, Wright Patterson Air Force Base, Ohio, 45433	45
Beaman, D. R.	Dow Chemical Company, Midland, Michigan, 48640	17,46
Berkley, C.	Mount Sinai School of Medicine, 5th Avenue at 100th Street, New York, New York, 10029	29
Bhalla, R. J.	Pennsylvania State University, University Park, Pennsylvania, 16802	30
Birnbaum, H. K.	Dow Chemical Company, Midland, Michigan, 48640	46
Bloxom, H. L.	NASA Langley Research Center, Hampton, Virginia, 23365	28
Borile, F.	Laboratorio per la Tecnologia dei Materiali Metallici Tradizionali, Via Induno, 10 - 20092-CINISELLO B. Milan, Italy	14
Brown, D. B.	U. S. Naval Research Laboratory, Washington, D. C., 20390	4
Campbell, W. E.	Rensselaer Polytechnic Institute, Materials Division, Troy, New York, 12181	22
Campot, M.	Harvard University, 24 Oxford Street, Cambridge, Massachusetts, 02138	31
Chambers, W. F.	Sandia Laboratories, P. O. Box 5800, Albuquerque, New Mexico, 87115	7



		<u>Paper Number</u>
Colby, J. W.	Bell Telephone Laboratories, 555 Union Boulevard, Allentown, Pennsylvania, 18103	19
Conty, C.	CAMECA, 103 Boulevard Saint-Dennis, 92 Courbevoie, France	54
Davidson, E.	Applied Research Laboratories, P. O. Box 129, Sunland, California, 91040	42
DiLorenzo, J.	Bell Telephone Laboratories, Mountain Avenue, Murray Hill, New Jersey, 07974	40
Donnelly, W. D.	Materials Analysis Company, 1060 East Meadow Circle, Palo Alto, California, 94303	49
Drake, J. C.	Harvard University, 24 Oxford Street, Cambridge, Massachusetts, 02138	31
Duncumb, P.	Tube Investments Research Laboratories, Hinxton Hall, Cambridge, England	1
Eichen, E.	Ford Motor Company, P. O. Box 2053, Dearborn, Michigan, 48181	5,47
Elliot, J. F.	Massachusetts Institute of Technology, 77 Massachusetts Avenue, Cambridge, Massachusetts, 02139	26
Fiori, C. E.	National Bureau of Standards, Washington, D. C., 20234	43
Fisher, G. L.	International Nickel Company, Sterling Forest, New York, 10901	18
Fritz, M.	Emory University School of Dentistry, 1462 Clifton Road, Atlanta, Georgia, 30322	50
Gasparrini, E. L.	University of Toronto, Toronto 5, Ontario, Canada	36
Gorz, H.	Pennsylvania State University, University Park, Pennsylvania, 16802	10
Guernet, J.	CAMECA, 103 Boulevard Saint-Dennis, 92 Courbevoie, France	54
Hartwick, A. J.	Applied Research Laboratories, P. O. Box 129, Sunland, California, 91040	42
Hashimoto, H.	Japan Electron Optics Laboratory Company, 1418 Nakagami-cho, Akishima-shi, Tokyo, Japan	51

		<u>Paper Number</u>
Heinrich, K. F. J.	National Bureau of Standards, Washington, D. C., 20234	2,11, 43
Hohling, H. J.	Institut fur Medizinische Physik, Hufferstrasse 68, 44 Munster, Germany	33
Hollerbach, J. M.	I. B. M. Components Division, East Fishkill Facility, Hopewell Junction, New York, 12533	41
Isasi, J. A.	Westinghouse Electric Company, P. O. Box 9175, Philadelphia, Pennsylvania, 19113	46
Judd, G.	Rensselaer Polytechnic Institute, Troy, New York, 12181	22,23
Kimoto, S.	Japan Electron Optics Laboratory Company, 1418 Nakagami-cho, Akishima-shi, Tokyo, Japan	51
Kinsman, K. R.	Ford Motor Company, P. O. Box 2053, Dearborn, Michigan, 48121	47
Klein, C., Jr.	Harvard University, 24 Oxford Street, Cambridge, Massachusetts, 02138	31
Klimpel, R.	Dow Chemical Company, Midland, Michigan, 48640	17
Koffman, D.	Advanced Metals Research Corporation, 149 Middlesex Turnpike, Burlington, Massachusetts, 01803	53
Kraus, H.	Texas Instruments, P. O. Box 5936, Dallas, Texas, 75222	34
Kreitzman, S.	Emory University School of Dentistry, 1462 Clifton Road, Atlanta, Georgia, 30322	50
Kriz, W.	Anatomisches Institut der Westf. Wilhelms Universitat, Vesaliusweg 2-4, 44 Munster, Germany	33
Kunz, F.	Ford Motor Company, P. O. Box 2053, Dearborn, Michigan, 48181	5
Kyser, D. F.	I. B. M. Research Laboratory, Monterey and Cottle Roads, San Jose, California, 95114	12
Langer, A.	Mount Sinai Hospital, 5th Avenue at 100th Street, New York, New York,	29
Lannin, T. E.	General Electric Company, Vallecitos Road, Pleasanton, California, 94566	25

		<u>Paper Number</u>
Lebiedzki, J.	Pennsylvania State University, University Park, Pennsylvania, 16802	10
Lechene, C.	Universite de Sherbrooke, Sherbrooke, Quebec, Canada	32
Leitner, J. W.	Applied Research Laboratories, 9545 Wentworth Avenue, Sunland, California, 91040	48
Lewis, B. W.	National Aeronautics and Space Administration, Hampton, Virginia, 23365	27
Lewis, R.	Bell and Howell Company, 360 Sierra Madre Villa, Pasadena, California, 91109	39,40
Lifshin, E.	General Electric Research and Development Center, Schenectady, New York, 12301	8
Lisagor, W. B.	NASA Langley Research Center, Hampton Virginia, 23365	28
Loomis, T. C.	Bell Telephone Laboratories, Mountain Avenue, Murray Hill, New Jersey, 07974	37
Marciniak, H. C.	University of Southern California, Los Angeles, California, 90007	44
Marcus, R. B.	Bell Telephone Laboratories, Mountain Avenue, Murray Hill, New Jersey, 07974	40
Marzetta, L. A.	National Bureau of Standards, Washington, D. C., 20234	43
Matthews, H. G.	Canberra Industries, 45 Gracey Avenue, Meriden, Connecticut, 06450	5
McMillan, R. E.	University of Pennsylvania, University Park, Pennsylvania, 16802	10
Melde, G. F.	General Electric Company, Sunnyvale, California, 94086	25
Moll, S.	Advanced Metals Research Corporation, 149 Middlesex Turnpike, Burlington, Massachusetts, 01803	53
Murata, K.	Osaka University, Suita, Osaka, Japan	3
Myklebust, R.	National Bureau of Standards, Washington, D. C., 20234	11

Paper Number

Norton, J. T.	Advanced Metals Research Corporation, 149 Middlesex Turnpike, Burlington, Massachusetts, 01803	53
Ogilvie, R. E.	Massachusetts Institute of Technology, Cambridge, Massachusetts, 02139	21,53
Ong, P. S.	Phillips Electronic Instruments, 750 Fulton Avenue, Mount Vernon, New York, 10550	52
O'Nions, R. K.	University of Alberta, Edmonton 7, Alberta, Canada	16
Pielet, H. M.	Massachusetts Institute of Technology, Cambridge, Massachusetts, 02139	26
Rao-Sahib, T. S.	University of Southern California, Los Angeles, California, 90007	13
Reuter, W.	I. B. M. Watson Research Center, Yorktown Heights, New York, 10598	15
Rosenbaum, H. S.	General Electric Company, Vallecitos Road, Pleasanton, California, 94566	25
Rubin, I.	Mount Sinai School of Medicine, 5th Avenue at 100th street, New York, New York, 10029	29
Rucklidge, J. C.	University of Toronto, Toronto 5, Ontario, Canada	36
Russ, J. C.	Japan Electron Optics Laboratory Company, 477 Riverside Avenue, Medford, Massachusetts, 02155	9
Saffir, A. J.	Materials Analysis Company, 1060 East Meadow Circle, Palo Alto, California, 94303	6,26, 35,50
Schippert, M.	Advanced Metals Research Corporation, 149 Middlesex Turnpike, Burlington, Massachusetts, 01803	53
Schnermann, J.	Physiologisches Institut der Universitat Munchen, 8000 Munchen, Pettenkoferstrasse 12, Germany	33
Schwartz, G. E.	Harvard University, 74 Finwood Road, Boston, Massachusetts, 02115	35
Shastri, C. R.	Rensselaer Polytechnic Institute, Troy, New York, 12181	23
Shimizu, R.	Osaka University, Suita, Osaka, Japan	3

		<u>Paper Number</u>
Smith, D. G. W.	University of Alberta, Edmonton 7, Alberta, Canada	16
Smith, J. P.	Texas Instruments, P. O. Box 5936, Dallas, Texas, 75222	34
Solomon, J. S.	University of Dayton Research Institute, Dayton, Ohio, 45409	45
Tabock, J.	Ford Motor Company, P. O. Box 2053, Dearborn, Michigan, 48121	47
Tagata, S.	Japan Electron Optics Laboratory Company, 1418 Nakagami-cho, Akishima-shi, Tokyo, Japan	51
Taylor, J. M.	Applied Research Laboratories, 9545 Wentworth Avenue, Sunland, California, 91040	42,48
Tong, M.	CAMECA, 103 Boulevard Saint-Dennis, 92 Courbevoie, France	54
Trueb, L. F.	Denver Research Institute, University of Denver, Denver, Colorado, 80210	24
vonRosenstiel, A.	Metaalinstituut TNO, P. O. Box 52, Delft, The Netherlands	33
Walitsky, P. J.	Westinghouse Electric Company, 1 Westinghouse Square, Bloomfield, New Jersey, 07003	19
Walker, G. H.	National Aeronautics and Space Administration, Hampton, Virginia, 23365	27
White, E. W.	Pennsylvania State University, University Park, Pennsylvania, 16802	10,30
Wittry, D. B.	University of Southern California, Los Angeles, California, 90007	13,20, 44
Wolf, R. C.	Materials Analysis Company, 1060 East Meadow Circle, Palo Alto, California, 94303	6
Yakowitz, H.	National Bureau of Standards, Washington, D. C., 20234	11

